

April 2020

## Understanding the Role of Cereblon in Hematopoiesis Through Structural and Functional Analyses

Afua Adutwumwa Akuffo  
University of South Florida

Follow this and additional works at: <https://digitalcommons.usf.edu/etd>



Part of the [Biology Commons](#), and the [Immunology and Infectious Disease Commons](#)

### Scholar Commons Citation

Akuffo, Afua Adutwumwa, "Understanding the Role of Cereblon in Hematopoiesis Through Structural and Functional Analyses" (2020). *Graduate Theses and Dissertations*.  
<https://digitalcommons.usf.edu/etd/8911>

This Dissertation is brought to you for free and open access by the Graduate School at Digital Commons @ University of South Florida. It has been accepted for inclusion in Graduate Theses and Dissertations by an authorized administrator of Digital Commons @ University of South Florida. For more information, please contact [scholarcommons@usf.edu](mailto:scholarcommons@usf.edu).

Understanding the Role of Cereblon in Hematopoiesis Through Structural and  
Functional Analyses

by:

Afua Adutwumwa Akuffo

A dissertation submitted in partial fulfillment  
of requirements for the degree of  
Doctor of Philosophy  
Department of Cell Biology, Microbiology, and Molecular Biology  
College of Arts and Sciences  
University of South Florida

Major Professor: Gary W. Reuther, Ph.D.  
Committee: Daniel Abate-Daga, Ph.D.  
Amer Beg, Ph.D.  
Shari Pilon-Thomas, Ph.D.  
Pearlie K. Epling-Burnette, PharmD., Ph.D.  
H. Leighton Grimes, Ph.D.

Date of Approval:  
March 31<sup>st</sup> 2020

Keywords: cereblon, E3 ubiquitin ligase receptor, functional conservation,  
hematopoietic stem cell regulation

Copyright © 2020, Afua A. Akuffo

## DEDICATION

I dedicate this dissertation to...

...my grandmother, Elizabeth Naa Kai Afful Darko. I miss you. You are my inspiration. You taught me many lessons. You taught me to abandon materialism and avarice but value God, culture, tradition, relationships and family. I remember watching you sweat over coal pots (never a fancy stove) to make an assortment of dishes you would then distribute to all of us weekly. Our freezers were always full of your gourmet cooking. You taught me the importance of "spare the rod, spoil the child!" A true disciplinarian fueled by your faith, generosity and compassion. You taught me to work hard and give my all in everything. I watched you manage a household and farm while facilitating a successful *gari* business and supporting your children and grandchildren. Finally, you taught me the essential traits of motherhood: unconditional love, sacrifice, provision, protection and discipline. Our bums were tender, our bellies were full, and we know right from wrong. Thank you Maa. Thank you for our toothy-smile FaceTime conversations that always brightened up my day. Thank you for instilling a piece of you in me so I carry you with me always. Thank you for being a formidable pillar of our family. Above all thank you for loving me unconditionally. Maa, *meda wo ase*.

...my heartbeat, Mummy, Caroline Bekoe Darko. The epitome of grace and kindness, you love me unreservedly, support me unendingly, teach me

continuously, bring me joy eternally, make me mad occasionally, encourage me perpetually and pray for me unceasingly. Without you there is no me. Thank you.

... my family and friends. For providing me with love, laughs and motivation during the tough times, thank you.

...the patients, survivors and fallen soldiers. May you continue to fuel me as I press ahead in the battle to cure cancer. May your strength and courage constantly inspire others. May you always be remembered in our hearts. Thank you.

...my Creator. For keeping me, for guiding me, for healing me, for comforting me and for strengthening me, thank you.



## ACKNOWLEDGMENTS

Firstly, I would like to recognize my mentor, Dr. PK Epling-Burnette without whom this work would not have been possible. Dr. Burnette's perseverance, support, encouragement and teachings over these past six years have molded me into the resilient and meticulous scientist that I am. The collaborative and friendly atmosphere of her lab was a perfect fit for my bold personality. I am forever grateful for being allowed to be a part of such a strong work family. To the rest of the Burnette lab, both past and present I would like to extend my deepest gratitude. Aileen Alontaga, Nathan Horvat, Rebecca Hesterberg, Lanzhu Yue, Christelle Colin, Julia Billington, Aya Elmarsafawi, Bill Goodheart, Chris Dukes, Shiun Chang, Xiao Tian, Matt Beatty, Jeff Painter Cem Murdun, and Sharon McKnight, thank you for all the laughs and memories we've created. Thank you for your assistance in making this project come together. I have learnt so much from everyone.

Next, I would like to thank my current mentor, Dr. Gary W Reuther, for stepping in and being a pillar during a difficult and taxing transition. I couldn't have asked for a more supportive, sympathetic and learned new mentor.

To my committee, Dr. Daniel Abate-Daga, Dr. Amer Beg, Dr. Shari Pilon-Thomas, and Dr. Lee Grimes, thank you for your training, guidance, direction and instrumental feedback. I am honored to have had you impact and influence my journey to becoming a scientist.

To my collaborators David Muench, Rainer Metcalf, Wayne Guida, Daniel Kenyon, Andreas Becker, Muhammad Ayaz, Harshani Lawrence, Nicholas Lawrence, Steven Gunawan, Elli Chatzopoulou, Xueke She, Shuai Meng, Dana Rollison, Shalaka Hampras, Rossybelle Amorrortu, Yayi Zhao, Ling Zhang, Derek Park and Alexander Anderson, thank you for all the lessons in interdisciplinary teamwork. Multi-disciplinary collaboration is a fundamental part of scientific discovery.

To the Lynch, Pinilla, Pilon-Thomas, Smalley, Padron, Shain, Beg, Wei, List, Schonbrunn, & Cleveland labs, thank you for all the technical assistance and kind-hearted encouragement over the years. I will treasure the memories.

To the remarkable core facilities especially the flow cytometry, vivarium, chemical biology, bioinformatics, microscopy, and genomics cores, thank you for your excellent services. Special thanks to Jodi Kroger, John Robinson, Johana, Neel, Peter, Hayley, Kristen, DeVon, Kia, Tiffany, Tricia, Michael, Emily, Christine Perry, Crystal Reed, Crystal Rivera, Ling Cen, Sean Yoder, Laura, & Chaomei.

Next I want to acknowledge the Cancer Biology PhD program for embracing me and making Moffitt a home away from home for the last six years. Thank you to the students, Dr. Ken Wright, Cathy Gaffney and Janet Opel who helped facilitate my successful completion of the program.

To my best friends Adetutu Egunsola and Daniela Zarbo, thank you for keeping me sane through the successes and failures both in and out of lab. To my church family without whom my spiritual journey would have plummeted, thank you! Lastly, to my entire family, *ayekoo* we've done it!

## TABLE OF CONTENTS

List of Tables .....	iv
List of Figures .....	v
Abstract .....	vii
Chapter One: Introduction .....	1
The history of immunomodulatory drugs .....	1
Mechanism of IMiD®s in hematological malignancies .....	3
Cereblon's structural features .....	4
IMiD®-mediated effects in humans versus mouse .....	7
Drugging the undruggable with PROTACs .....	8
Cereblon's endogenous role .....	13
Introduction to Hematopoiesis .....	14
Hematopoietic stem cell origin .....	17
Cellular components of the bone marrow niche .....	20
Signaling pathways involved in HSC regulation .....	23
Abnormal hematopoiesis and hematological disorders .....	25
Chapter Two: Ligand-mediated protein degradation reveals functional conservation among sequence variants of the CUL4-type E3 ligase substrate receptor cereblon .....	26
Introduction .....	26
Results .....	
Thalidomide binding domain of CRBN has a conserved immunomodulatory compound binding motif .....	28
Immunomodulatory compound binding is conserved in CRBN sequence variants. ....	34
N-terminal stabilization of CRBN-immunomodulatory compound interactions .....	39
Resistance of mouse cells to immunomodulatory compounds .....	41
Acquired ubiquitin-proximity ligation in mouse cells establishes conserved ligase functions of mouse and human CRBN variants .....	45
Discussion .....	53
Experimental Procedures .....	58
Animals and cell lines .....	58
T-cell isolation, activation and drug treatments .....	58
qRT-PCR .....	60

Treatment of multiple myeloma cells .....	60
General chemistry information.....	60
Cloning, protein expression and purification.....	61
Isothermal titration calorimetry (ITC) .....	63
Intrinsic tryptophan fluorescence assay .....	64
Theoretical calculations .....	64
Detailed chemical methods .....	65
Detailed protein production of wild-type and mutant CRBN .....	68
 Chapter Three: Cereblon E3 ubiquitin ligase receptor control	
of hematopoiesis .....	70
Introduction.....	70
Results.....	73
CRBN expression in adult hematopoietic stem and progenitor cells .....	73
CRBN regulates the frequency of adult hematopoietic stem and non-committed progenitor cells .....	75
Age-related hematopoiesis.....	77
CRBN expression is required for normal embryonic HSC development .....	79
CRBN controls HSC stemness associated molecules and stimulates quiescence .....	80
CRBN's role in differentiation in homeostatic and transplant models .....	83
CRBN ablation does not impair fitness and reconstitution capabilities in adult mice.....	86
Long-term reconstitution potential is enhanced by CRBN depletion in LT-HSC .....	90
CRBN reduces HSC's response to transcription and translation arrest.....	95
Control of CXCR4 is associated with LT-HSC regulation.....	98
CRBN loss in niche cells does not alter hematopoiesis .....	100
Discussion .....	103
Experimental Procedures .....	108
Animal husbandry .....	108
Flow Cytometry analysis of BM populations.....	108
Bone Marrow Colony Formation Assay .....	109
Apoptosis, BrdU & hypoxia assays.....	109
BM homing assay .....	110
Competitive & Non-competitive BM transplants .....	110
<i>In vivo</i> 5-FU challenge .....	111
Fetal Liver harvest and culture .....	111
RNA-sequencing and pathway analysis .....	112
Quantitative real time PCR analysis .....	113
Statistical analyses .....	113

Chapter Four: Summary, Future Perspectives and Clinical Implications .....	119
References .....	124
Appendix A: Institutional Board Approval.....	136
Appendix B: Institutional Animal Care & Use Committee Approvals.....	148
Appendix C: Copyright Permission of Previously Published Materials .....	140
About the Author .....	END PAGE

## LIST OF TABLES

Table 1	“Neo” substrate recruitment by IMiD®s and their clinical use .....	8
Table 2	PROTACs: the advantages and disadvantages of their use.....	10
Table 3	Characterization of hematopoietic lineages .....	16
Table 4	RMSD calculations.....	32
Table 5	Binding affinity (KD, (μM)) of immunomodulatory compounds to WT and mutant human CRBN-TBD determined using ITC and Fluorescence intensity (FI) assay.....	37
Table 6	IC50 (μM) of Multiple Myeloma Cell Lines .....	43
Table 7	Statistical analysis of human T cells treated with IMiD®s, JQ1 and dBET1 .....	48
Table 8	Statistical analysis of <i>Crbn</i> <sup>+/+</sup> and <i>Crbn</i> <sup>-/-</sup> mouse T cells treated with IMiD®s, JQ1 and dBET1.....	52
Table 9	Cell intrinsic and extrinsic regulators of HSC quiescence.....	71
Table 10	Cereblon Genotyping Primers.....	108
Table 11	List of Taqman primers .....	113
Table 12	Flow cytometry instrument settings.....	114
Table 13	Flow cytometry antibodies and panel design .....	116

## LIST OF FIGURES

Figure 1	The historical timeline of IMiD®s .....	2
Figure 2	Structure of CRBN and IMiD®s .....	5
Figure 3	Schematic of CRBN's degron properties .....	6
Figure 4	Proteolysis targeting chimera (PROTAC) modular structure and mechanism of action .....	11
Figure 5	Summary of IMiD®-dependent and independent functions of CRBN.....	13
Figure 6	Classical versus revised mouse and human hematopoietic cell hierarchy. ....	17
Figure 7	Hematopoietic stem cell niches during development.....	19
Figure 8	Summary of niche cells and their contribution to HSC maintenance .....	22
Figure 9	Consequences of abnormal hematopoiesis.....	25
Figure 10	Structure of cereblon is conserved across different species.....	29
Figure 11	RMSD profiles of hCRBN, mCRBN, gCRBN & hmCRBN.....	33
Figure 12	Human and mouse CRBN binds IMiD®s with similar affinities .....	36
Figure 13	Binding affinity of IMiD®s to TBD variants by ITC .....	38
Figure 14	Lenalidomide binds to the TBD and CRBN-DDB1 protein complex .....	40
Figure 15	Lenalidomide treatment induces IL-2 production and proliferation in human T cells .....	42
Figure 16	Mouse cells are resistant to immunomodulatory drugs.....	44
Figure 17	Functional activity of lenalidomide, JQ1 and dBET1 in human T cells and binding affinities of JQ1, dBET1 and Len to human CRBN .....	46

Figure 18 Functional activity of lenalidomide, pomalidomide, JQ1 and dBET1 in mouse T cells .....	50
Figure 19 Drug Treatment of human and mouse multiple myeloma cell lines .....	53
Figure 20 CRBN deletion does not lead to gross abnormalities or birth defects .....	74
Figure 21 CRBN deletion causes a reduction in absolute hematopoietic stem and progenitor counts .....	76
Figure 22 Loss of HSC pool persists in aged <i>Crbn</i> <sup>-/-</sup> mice.....	78
Figure 23 CRBN deficiency provokes loss of HSC in fetal liver .....	80
Figure 24 CRBN deficiency leads to increased HSC proliferation .....	81
Figure 25 CRBN-deficient HSC have increased differentiation capacity both <i>in vivo</i> & <i>in vitro</i> .....	84
Figure 26 CRBN ablation does not impair HSPC homing to BM .....	87
Figure 27 CRBN-deficient HSCs do not outcompete control HSC in 3:1 ratio in competitive primary bone marrow transplant .....	88
Figure 28 CRBN-deficient HSCs do not outcompete control HSC in 3:1 ratio in competitive secondary bone marrow transplant.....	89
Figure 29 CRBN deficiency does not impair reconstitution potential in non-competitive serial transplants. ....	91
Figure 30 Long-term reconstitution capacity is enhanced by CRBN ablation in HSCs .....	93
Figure 31 CRBN deficiency modestly increases vasculature.....	95
Figure 32 Increased HSC proliferation sensitizes CRBN-deficient HSCs to 5-FU treatment.....	97
Figure 33 CRBN deletion alters transcription factor profiles of HSPCs .....	99
Figure 34 CRBN deficiency in niche cells does not impact hematopoiesis.....	101
Figure 35 CRBN deficiency in niche cells does not alter stress hematopoiesis .....	102



Figure 36 Visual abstract..... 102

## ABSTRACT

The discovery and implementation of immunomodulatory drugs (IMiD®s) has revolutionized the treatment of many hematological malignancies due to the plethora of IMiD®-induced clinical responses that include anti-angiogenesis, anti-inflammation, and anti-tumor effects, as well as enhanced erythropoiesis, immune modulation and improved metabolism. More ground-breaking was the identification of cereblon as the target of IMiD®s. Upon binding to thalidomide and other immunomodulatory drugs, the E3 ligase substrate receptor cereblon (CRBN) promotes proteosomal destruction of neo-substrates by engaging the DDB1-CUL4A-Roc1-RBX1 E3-ubiquitin ligase in human cells but not in mouse cells suggesting that sequence variations in CRBN may cause its inactivation. Therapeutically, CRBN engagers have the potential for broad applications in cancer and immune therapy by specifically reducing protein expression through targeted ubiquitin-mediated degradation. To examine the effects of defined sequence changes on CRBN's activity, we performed a comprehensive study using complementary theoretical, biophysical, and biological assays aimed at understanding CRBN's non-primate sequence variations. With a series of recombinant thalidomide-binding domain (TBD) proteins, we show that CRBN sequence variants of different species retain their drug binding properties to both classical immunomodulatory drugs and to dBET1, a chemical compound and targeting ligand (i.e. a PROTAC) designed to degrade bromodomain-containing 4 (BRD4) via a CRBN-dependent mechanism. We further show that dBET1 stimulates CRBN's E3 ubiquitin-conjugating function and degrades BRD4 in both mouse

and human cells. This insight provides evidence that mouse CRBN is functional and provides a new avenue of exploring CRBN's endogenous substrate recruiting function in hematopoietic cells.

Hematopoietic stem cell (HSC) ontogeny is governed by extrinsic and intrinsic programs to control proliferation, localization, differentiation and self-renewal. The E3 ubiquitin ligase substrate receptor CRBN is expressed in hematopoietic lineages, including long-term HSCs (CD48-CD150+Lineage-Sca-1+c-Kit+ (LSK)), but plays an undefined role in hematopoiesis. As CRBN is the only confirmed target of IMiD®s and since IMiD®s have substantial clinical activity in a number of hematological malignancies, CRBN's involvement in hematopoiesis was investigated. In these diseases, the IMiD®-CRBN interaction is associated with tumor cell death and other cellular responses through at least two major proposed mechanisms including, 1) drug-induced activation of neomorphic protein degradation, and 2) inhibition of endogenous substrate recruitment leading to toxic protein accumulation[3]. To gain insights into the role of CRBN in hematopoiesis, we assessed adult steady state and transplant-associated hematopoiesis and evaluated HSC development during embryogenesis using germline *Crbn*<sup>-/-</sup> mice. Compared to *Crbn*<sup>+/+</sup> mice, CRBN deficiency was associated with a 2-3-fold reduction in stem cells in adult bone marrow and a similar reduction in HSCs in the fetal liver at embryonic stage 14.5 when the HSC pool is initiated from several anatomical sites including the yolk sac, aorta gonad mesonephros and fetal liver. Postnatal bone marrow HSCs are maintained throughout life by a process of self-renewal and differentiation. Interestingly, mature lymphoid and myeloid progeny were moderately expanded in peripheral blood of *Crbn*<sup>-/-</sup> mice under homeostatic conditions and following serial bone

marrow transplantation suggesting that CRBN is critical for stem cell maintenance. RNA-seq analyses and qRT-PCR validation of BM-derived *Crbn*<sup>-/-</sup> LSKs and HSCs showed a marked suppression in a “stemness”-related gene signature consisting of *Tie2*, *Hif1α*, and *Notch1* suggesting that CRBN is required to maintain HSCs in the undifferentiated state. Moreover, high amounts of proliferation within the LT-HSCs at steady-state, increased mature cells at steady-state and following serial transplantation, and increased lethality to repeated 5-fluorouracil (5-FU) challenge in *Crbn*<sup>-/-</sup> mice indicate that CRBN maintains HSC quiescence. Collectively our data suggest CRBN functions to maintain HSC quiescence required to maintain the undifferentiated properties of the HSC cells in the adult bone marrow. HSCs reside in highly specialized bone marrow niches where multiple cooperative networks of intrinsic and extrinsic factors are required for HSC homeostasis. Transplantation of *Crbn*<sup>+/+</sup> HSCs into *Crbn*<sup>-/-</sup> recipients failed to generate a defined phenotype. However, HSC adhesion (*Vcam1*, *Cxcr4*)-associated genes were significantly suppressed. Particularly, the G protein-coupled chemokine receptor CXCR4-CXCL12 interaction which controls fetal and mature BM colonization and regulates homeostatic and regenerative HSC maintenance. These results indicate that CRBN is a functional protein in rodents and demonstrates a novel role for CRBN in the control of hematopoiesis with important implications in understanding how IMiD@s exert their therapeutic actions in hematological cancers.

Our results demonstrate a novel role for CRBN in the control of hemopoiesis with important implications in understanding how IMiD@s exert their therapeutic actions in hematological cancers.

## CHAPTER ONE

### INTRODUCTION

**A note to the reader:** Portions of this chapter have been previously published in a review article in *Integrated Cancer Science Therapy*, Akuffo et al<sup>[4]</sup> and has been reproduced here with permission from the publisher.

#### **The history of immunomodulatory (IMiD®s) compounds**

Thalidomide, first developed in Germany in 1956, is infamously known for its teratogenic properties when used to treat hyperemesis gravidarum and for sedation [5]. From the late 1950s until 1962, use of this drug rapidly expanded to 48 countries where it was responsible for birth defects ranging from congenital heart disease, malformations in limb development and ocular abnormalities in thousands of children. While initial preclinical data suggested that thalidomide had an acceptable safety profile in rodents, testing in pregnant animals was not a mandated practice at the time [6]. The tragedy of thalidomide rapidly led to significant changes in the processes required for medical product development throughout the world with enactment of an amendment to the United States Federal Food, Drug and Cosmetic Act in 1962 requiring more rigorous preclinical testing for new pharmaceuticals[7].

In the early 2000s, thalidomide was repurposed in the clinic as a potent anti-angiogenic[8] and immunomodulatory compound for the treatment of multiple myeloma (MM), myelodysplastic syndrome harboring a chromosomal deletion in

5q (del (5q) MDS) and other hematological malignancies [9-11](Figure 1). The drug was approved for cancer treatment under an FDA directive requiring routine pregnancy testing with distribution of written and verbal warnings to inform patients of the detrimental impact of thalidomide on fetal development[12]. Many studies have confirmed the relationship between thalidomide, and its related class of compounds (also known as immunomodulatory drugs, IMiD®) and teratogenicity in humans, zebrafish, chickens and in rodents when given during specific periods of gestation [5, 13-15].

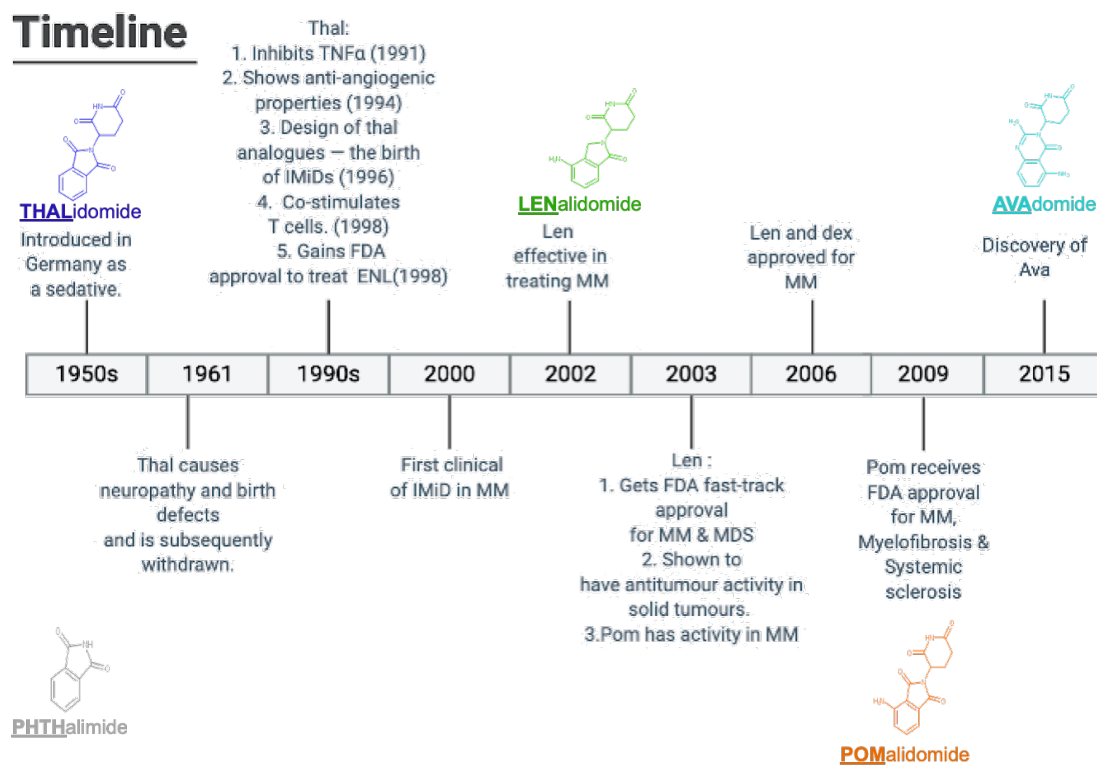


**Figure 1. The history of IMiD®s.** Timeline showing the discovery, development and application of immunomodulatory compounds. pthalimide (PHTH, grey, an inactive derivative), thalidomide (THAL, blue), lenalidomide (LEN, green), pomalidomide (POM, orange) & avadomide (AVA/CC-122, cyan)

## Mechanism of IMiD®s in Hematological Malignancies

Despite its infamous history, over the past decade, the discovery, development, and approval of IMiD®s (thalidomide (Thalomid®), lenalidomide (Revlimid®), pomalidomide (Pomalyst®) and avadomide) in combination with proteasome inhibitors (e.g., bortezomib (Velcade®) and carfilzomib (Kyprolis®) and anti-inflammatory compounds (e.g., dexamethasone ) have revolutionized the treatment of hematological malignancies. Many pharmacological studies have demonstrated that IMiD®s act both to modulate immune function and to directly kill tumor cells by inducing the expression of pro-apoptotic molecules and by severing interactions between tumor cells and their microenvironment [8, 9, 16, 17]. In del5q MDS, lenalidomide was shown to induce cell death through synthetic lethality caused by haplo-insufficient genes on chromosome 5[18].

Malignant hematological disorders give rise to cells that evade immune surveillance, impair normal immune cell function and have enhanced metastatic colonization potential. For example, in multiple myeloma (MM), aberrant plasma cells (PC) secrete immunosuppressive factors such as interleukin 10 (IL-10), IL-6, transforming growth factor beta (TGF- $\beta$ ) and vascular endothelial growth factor (VEGF) that ultimately lead to weak antigen presentation, dysfunctional innate and adaptive immunity and suboptimal tumor-specific immune response[19-23]. Furthermore, MM-bone marrow stromal cell (BMSC) and -extracellular matrix (ECM) interactions promote tumor survival through:

1. Amplification of a myriad of adhesion molecules such as chemokine receptor 4 (CXCR4), very late antigen 4 (VLA-4), leukocyte function-

associated antigen (LFA -1), and syndecan-1 (CD138) on tumor cells, vascular cell adhesion molecule (VCAM-1) and intercellular adhesion molecule (ICAM-1) on BMSC.

2. Activation of NF- $\kappa$ B, a transcription factor that promotes growth and survival in both normal and malignant cells)[24] and secretion of TNF $\alpha$ , a potent mediator of inflammation and osteoclastogenesis [25].
3. Stimulation of signaling pathways critical to tumor growth including mitogen-activated protein kinase (MAPK), Janus kinase (JAK)/ signal transducers and activators of transcription (STAT), I $\kappa$ B kinase (IKK)- $\alpha$ /NF- $\kappa$  $\beta$  and phosphatidylinositol-3 kinase (PI-3K)/Akt pathways).

IMiD® treatment disrupts MM–BMSC-dependent survival advantages through several mechanisms including blocking VEGF production (anti-angiogenesis)[26, 27], limiting TNF $\alpha$  secretion (anti-inflammatory effects) [25], modulation of IL-6 and other crucial cytokines and chemokines production and downregulation of adhesion molecules[19-23].

### **Cereblon's structural features**

The mechanisms underlying the adverse effects and pleiotropic therapeutic responses of IMiD®s remained unclear, due to a lack of known targets, until Takumi Ito and colleagues revealed the molecular mechanism of these compounds through elegant studies conducted in zebrafish and chickens [28]. In the study, Ito and colleagues identified cereblon (CRBN) as the direct target of immunomodulatory compounds and one of many DDB1 and CUL4-associated



factors (DCAFs) that directs protein turnover by ubiquitination and subsequent proteasome recognition. Cereblon is 442 residues long with a disordered region in the N-terminal, two LON domains, (N-terminal LON and C-terminal LON), connected by DDB1-binding region and a thalidomide-binding motif (TBD) in the C-terminal [29] (Figure 2A).

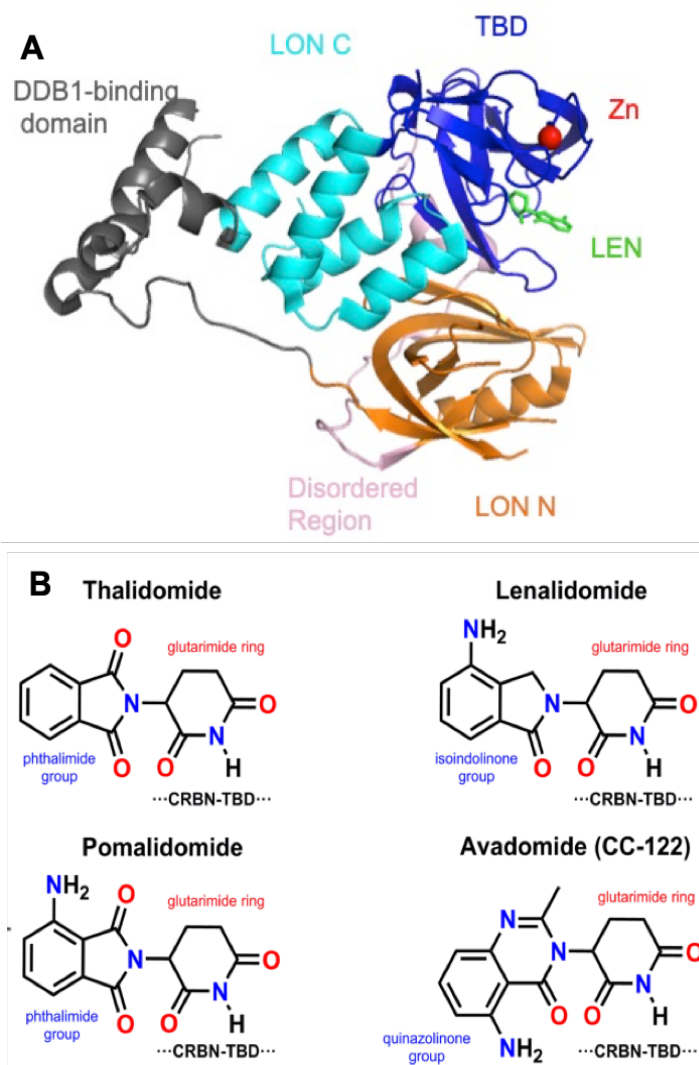


**Figure 2. Structure of CRBN and IMiDs.** (A) Ribbon structure of CRBN showing LON domains (LON-N orange, LON-C cyan), DDB1-binding domain (grey), disordered region (pink), zinc (red), lenalidomide (Len)(green) interacting in TBD. (B) The region of the thalidomide-binding domain (TBD) indicated (red) interacts with the glutarimide ring of the IMiDs, whilst the second ring (phthalimide, isoindolinone and quinazolinone) interacts with the CRBN TBD and its substrates (Ikaros, Aiolos, CK1 $\alpha$ , and unknown proteins), respectively.

Cereblon acts as a substrate recruiting module for the DDB1–CUL4A–Roc1–RBX1 E3 ubiquitin ligase complex and the immunomodulatory compounds thalidomide, lenalidomide, pomalidomide, and avadomide (Figure 2B) alter its recruiting functions by attracting various “neo” protein substrates including Ikaros, Aiolos, [14] and casein kinase 1α (CK1α) to [15, 30] the DDB1-CUL4A-Rbx1 complex (Figure 3). This drug class is characterized by a common structural feature, the glutarimide ring (Figure 2B) which interacts directly in the hydrophobic pocket of cereblon’s TBD. The remainder of the molecule, the solvent exposed portion, is also quite similar among the four drugs, with only the presence or absence of an amino group or a carbonyl group rounding out the structural differences (Figure 2B). This portion of the compound is also responsible for “neo” substrate recruitment and has been shown to reinforce interactions between substrate and the TBD[31].

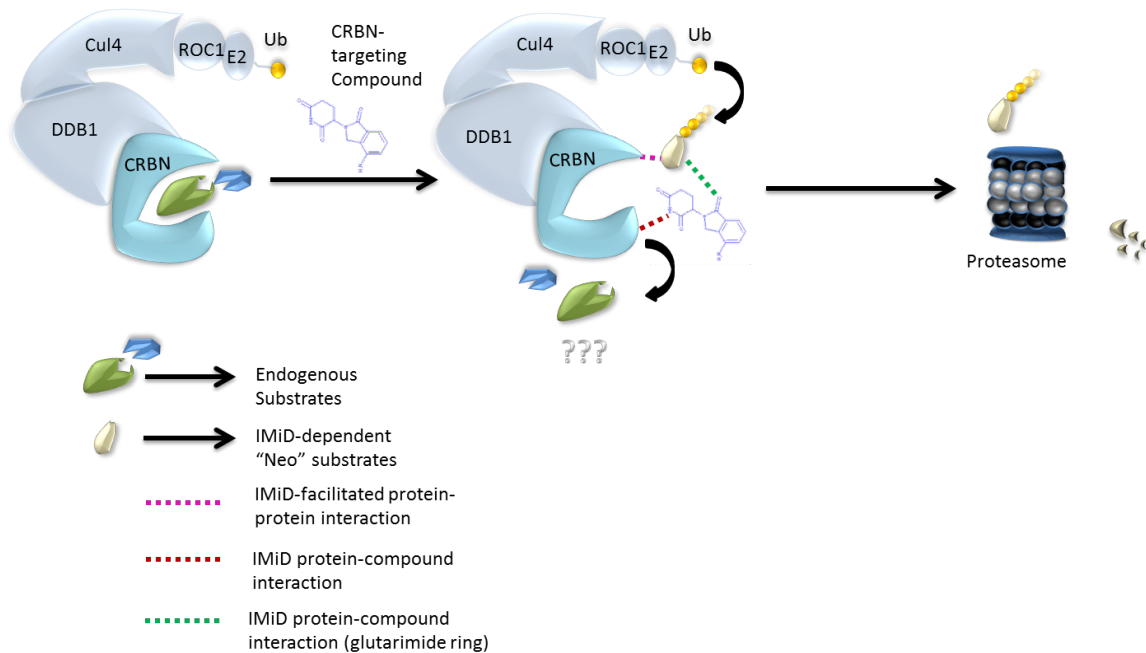


**Figure 3. Schematic of CRBN's degron properties**

## **IMiD®-mediated effects in humans versus mouse**

It is now well established that immunomodulatory drug-dependent degradation of Ikaros and Aiolos encoded by *IKZF1* and *IKZF3* respectively, potentiates human T cells [32-34] and is partially responsible for the cytotoxicity of human MM cells [14]. CK1 $\alpha$  degradation is selectively targeted by lenalidomide which garners an apoptotic phenotype that is uniquely associated with clinical responses in del(5q) MDS [15, 35] and MM [36]. A complete list of identified IMiD®-dependent “neo” substrates can be found in Table 1 below.

Despite advances in our understanding of immunomodulatory drugs and their molecular mechanism, the notion that mice and other rodents are “resistant” to immunomodulatory compounds has been widely circulated due to the initial reports concluding that pups born from thalidomide-treated pregnant dams had no limb abnormalities[37]. This observation was also followed by several studies showing species-dependent differences in thalidomide metabolism[38, 39]. Follow up studies conducted with extremely higher concentrations of thalidomide [40] or mutant mice that are deficient in antioxidant enzyme showed mice can be made sensitive to thalidomide embryopathy under specific conditions[41].

Few medical disasters have reached the level of thalidomide-associated teratogenicity and have had such prevailing consequences in its aftermath. Moreover, as most preclinical compounds are tested in mice, it has become imperative to thoroughly investigate the mechanism of action of preclinical compounds to uncover any divergent clinical responses between humans and mice to prevent teratogenic disasters.

**Table 1.** “Neo” substrate recruitment by IMiD@s and their clinical use

Compound	Compound-Specific Target	Target-specific Effect	Clinical use
All IMiD@s	IKZF1&3	IRF4↓	↑T, B, & NK cell function, Anti-myeloma Anti-angiogenesis Anti-inflammatory ↓Cell-adhesion-mediated drug resistance[42]
Lenalidomide	Ck1 $\alpha$	↑p53 ↓Myc	Anti-MDS (non & del(5))[43] Anti-Myeloma[36]
Avadomide (CC-122)	Currently unknown	↑IFN- $\beta$	Anti-DLBCL[44] (In Clinical Trials)
Iberdomide (CC-220)	Currently unknown	Currently unknown	Treats pomalidomide resistant myeloma[45]
CC-885	GSPT1		None (Toxic to healthy cells)

### Drugging the undruggable with PROTACs

Nearly two decades ago Sakamoto, Crews and Deshaies sought to artificially direct intracellular protein degradation by synthesizing a heterobifunctional molecule, Protac-1, which tethers I $\kappa$ B $\alpha$  phosphopeptide that is recognized by Skp1-Cullin-F box complex containing Hrt1 (SCF) complex substrate receptor F-box protein  $\beta$ -TRCP[46] to ovaclin inhibitor, MetAP-2. Protac-1 successfully bound MetAP-2 to SCF $\beta$ -TRCP and promoted MetAP-2 ubiquitination and degradation. Though a gamechanger in drug design, this technology, dubbed proteolysis targeting chimera (PROTAC), did not gain widespread traction due to poor cellular permeability and the lack of specificity of the peptide moiety of the molecule. Several years later with the discovery of compounds with improved affinity and specificity to various E3 ubiquitin ligase

substrate receptors and exceptional cell permeability, PROTAC has emerged as a robust method to “*drug the undruggable proteome*[47]”.

Currently, four E3 ligases (MDM2, cIAP1, CRBN (cereblon) and von Hippel-Lindau (VHL)) are being used as the basis for PROTAC compound design. See Table 2 for summary of developed PROTACs and some advantages and limitations of PROTACs. IMiD®-based PROTAC compounds dramatically improved affinity and specificity of the high order three dimensional complexes that is required for function including a stable E3 ubiquitin ligase interaction, substrate receptor engagement, and protein target complex. These features along with excellent medicinal properties, including exceptional cell permeability, has led to clinical testing of IMiD®-based PROTACs.

**Table 2.** PROTACs: the advantages and disadvantages of their use<sup>[48, 49]</sup>

<b>E3 Ligase Receptor</b>	<b>Targets</b>			
MDM2	SARM (2008)			
IAP (Otherwise known as Specific and Nongenetic IAP-dependent Protein ERasers (SNIPERs) ) XIAP (SNIPER(ER))	targets include CRABP-I, CRABP-II, ER $\alpha$ , TACC3, BCR-ABL (2010 - )			
VHL	targets include GFP-HaloTag fusions, ERR $\alpha$ , RIPK2, BCR-ABL, BRD4, TBK1, EGFR, HER2, c-Met and TRIM24 (2015 - )			
CRBN	targets include BET proteins (BRD2/3/4), FKBP12, BCR-ABL, BRD9, Sirt2, CDK9, FLT3, BTK, and ALK (2015 - )			
<b>Advantages</b>	Potent and profound degradation of target proteins (most degrade target protein at nanomolar concentrations)	Rapid and sustained depletion of target proteins	Rapid, sustained, and robust inhibition of downstream signaling cascades	Overcome drug resistance due to mutations Enhanced target selectivity
<b>Limitations</b>	The hook effect	Relatively large, may limit it becoming orally active drugs in humans	off-targets were still detected in some studies	

Thalidomide-related/IMiD®-based compounds are key components of PROTAC technology due their fidelity in hijacking the CRBN/DDB1/CuI4A/ Rbx1 E3 ubiquitin ligase complex [50]. Given that thalidomide and its derivatives selectively bind CRBN, dBET1 was one of the first synthesized IMiD®-based PROTAC to induce the degradation of BRD4, a BET-family protein[51] (Figure 4). Using dBET1, a thalidomide-JQ1 PROTAC, Winter et al observed a >85% decrease in BRD4 expression (at nanomolar concentrations), subsequent decrease in oncoproteins c-Myc and PIM-1 that collectively led to superior apoptosis induction both *in vitro* AML cell-based assays and in an *in vivo* murine xenograft model of AML than JQ1 [51].

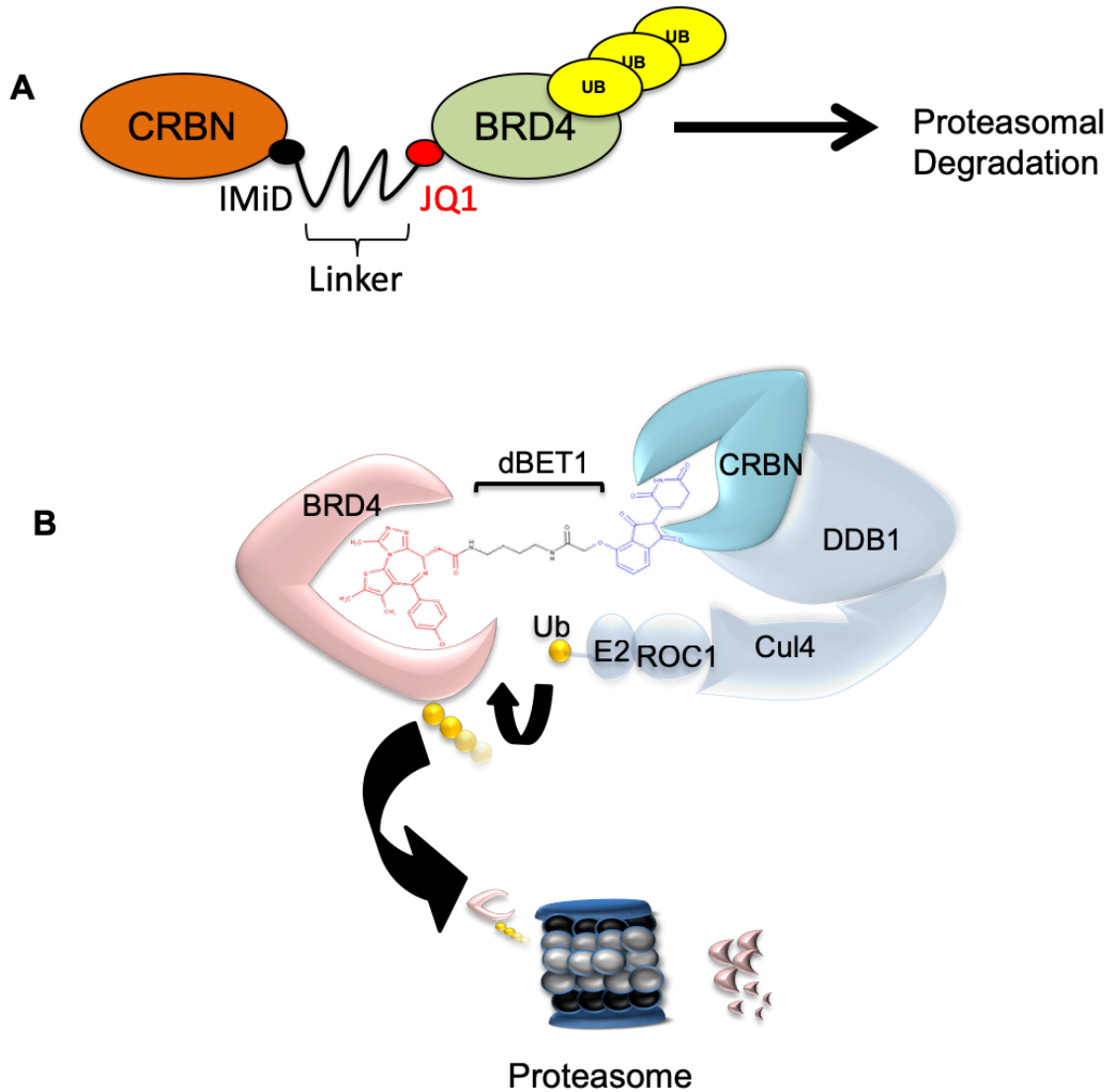


**Figure 4. Proteolysis targeting chimera (PROTAC) modular structure and mechanism of action. (A)** Schematic of structure of BET bromodomain-targeting PROTAC, dBET1<sup>[51]</sup>. **(B)** Chemical structure and modality of dBET1; thalidomide (CRBN-specific compound) linked to JQ1 (BET family-specific compound) is able to recruit BRD4 to cereblon E3 ubiquitin ligase complex. dBET1 is highly selective cereblon-dependent BET protein degrader.

Other IMiD®-based PROTACs have shown superior inhibition of protein function and more potent anti-tumor effects than their parent compound[52, 53]. One in particular, PROTAC P13I, which adopts ibrutinib as a warhead and pomalidomide to recruit CRBN, was synthesized to target BTK degradation and was observed to target both wild-type and mutant forms of BTK [54, 55]. PROTAC P13I elicited better therapeutic responses and limited drug-resistant mechanism employed by human DLBCL cell line.

A study conducted by Zhu et al demonstrated that CRBN suppression via *CRBN* shRNA lentiviral expression constructs is cytotoxic to human MM cell lines[56]. These results reveal an IMiD®-independent role of cereblon in MM survival which prompted the development of homo-PROTAC molecules designed to self-degrade CRBN[57]. Chemical knockout down of CRBN had a modest effect on the viability of MM cell line (↓20%) in comparison to parental compound pomalidomide (↓90%). Though chemical CRBN degradation did not have superior anti-tumor effects as predicted, CRBN degraders will be useful tools for unraveling endogenous substrates and physiological roles of CRBN and providing additional insights into the molecular mechanism of IMiD®s.



## Cereblon's endogenous role

Our understanding of IMiD®-dependent and independent roles of CRBN is still poorly understood due to its innately promiscuous function. Currently, IMiD®-independent functions have been shown to include the modulation of AMPK[58], AGO2[59], glutamine synthase[60], MEIS2[13], CD147-MCT1 complex formation[61]. Although the aforementioned targets have not been crystalized with CRBN in X-ray crystallography, they all share the characteristic  $\beta$ -hairpin loop structure and a key glycine residue known to directly engage the pthalimide moiety of IMiD®s.

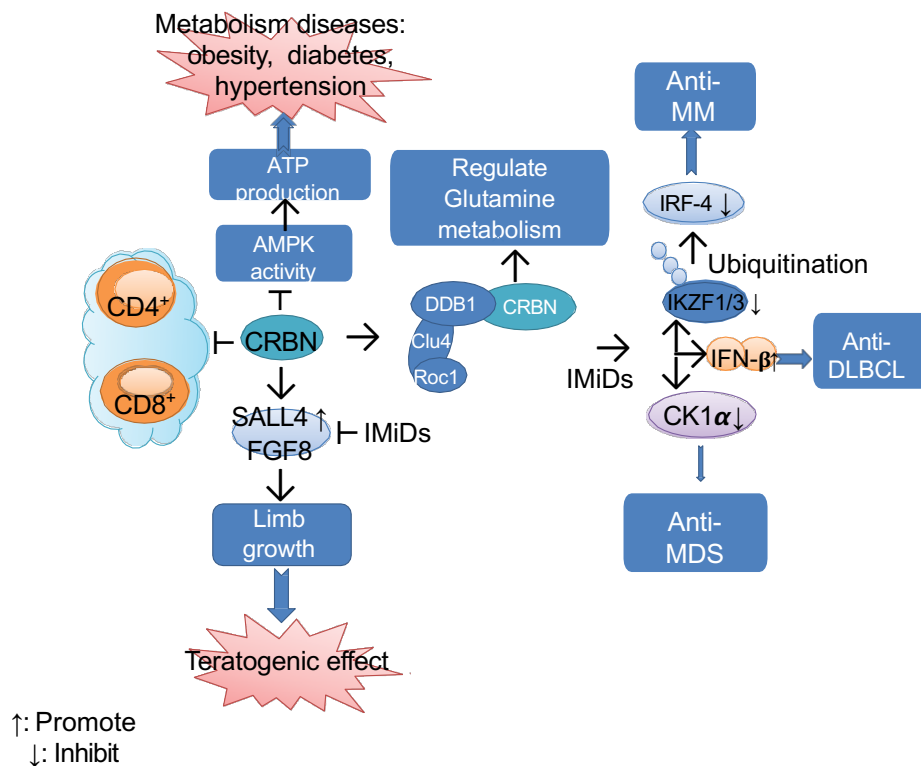


**Figure 5. Summary of IMiD®-dependent and independent functions of CRBN.** Adapted from Shi et al. [1]

Collectively the IMiD®-independent and dependent targets of CRBN are centered on processes such as cell metabolism, proliferation and embryonic development and appear to be cell-type specific[1](See Figure 5 for summary). Since IMiD®s have shown successful clinical responses in hematological malignancies, investigation into CRBN's endogenous function in hematopoietic cell lineages could improve our understanding of the therapeutic vulnerability of CRBN.

### **Introduction to Hematopoiesis**

Hematopoiesis is the continuous production of mature blood cells from a rare pool of self-renewing hematopoietic stem cells (HSC). HSCs sit at the top of a complex hierarchical system and are faced with the decision to remain quiescent, self-renew, differentiate, migrate/mobilize, or die [62]. Early studies by Weissman and colleagues identified a combination of cell surface markers that robustly classifies the pool of mouse (Lin<sup>-</sup>, CD34<sup>low/-</sup>-Sca-1<sup>+</sup>, Thy-1.1<sup>+/low</sup>, c-Kit<sup>+</sup>, CD38<sup>+</sup>) [63] and human (Lin<sup>-</sup>, c-Kit<sup>/low</sup>, CD38<sup>low/-</sup>, Thy-1.1<sup>+</sup>, CD59<sup>+</sup>, CD34<sup>+</sup>)[64, 65] hematopoietic stem and progenitor cells (HSPCs) capable of restoring a functional blood network when transplanted into lethally irradiated mice. Genetic and proteomic profiling in recent years have further fractionated HPSCs based on their cell surface markers and propensity to give rise to specific lineages in transplantation and in vitro colony formation assays[66].

In the classical hierarchal classification (Figure 6A), HSCs can be divided into two main subsets: long-term hematopoietic stem cells (LT-HSC) that are

capable of perpetual self-renewal, and short-term hematopoietic stem cells (ST-HSC) that self-renew for a defined interval[62]. ST-HSCs give rise to non-self-renewing multipotent progenitors (MPP), which in turn give rise to two progeny that are more restricted in their differentiating potential, the common myeloid progenitor (CMP) (with myeloid, megakaryocyte and erythroid potential) and the common lymphoid progenitor (CLP) (with only lymphoid potential). CMP further differentiate into bipotent granulocyte-macrophage (GMP) and megakaryocyte-erythroid (MEP) that eventually give rise to terminally differentiated neutrophils, basophils, eosinophils, macrophages, monocyte-derived dendritic cells, and megakaryocytes, platelets and erythrocytes, respectively (Figure 6). CLP give rise to T cells, B cells, natural killer (NK) cells and dendritic cells (DC) (Figure 6A).

Although this hierarchical system of differentiation was initially thought to be a one-directional stepwise process, recent studies challenge this models and suggest that stem cells are in a continuum of change[67-69]. Yamamoto et al and Sanjuan-Pla et al through single-cell sequencing and transplantation, identified myeloid-restricted progenitors with long-term repopulating activity and self-renewing platelet-primed HSCs the preferentially differentiate into platelets but have a long-term myeloid lineage bias, and can give rise to lymphoid-biased HSCs [70, 71]. These studies, among others, suggests a continuous differentiation model in which HSCs acquire lineage biases along multiple directions without passing through discrete hierarchically organized progenitor populations[67, 69, 72] (Figure 6B).

**Table 3.** Characterization of hematopoietic lineages

Population	Surface Markers	Self-renewal high (H), moderate(M), low (L) or no (N)?	Cell Cycle at steady-state
LT-HSC	Lin-, Sca-1+, c-Kit+, CD34-, CD135-, CD48- CD150+	H	G0: ~70% G1: ~20% S-G2/M: ≤10%
ST-HSC	Lin-, Sca-1+, c-Kit+, CD34+, CD135-, CD48- CD150-	M	G0: ~ 60% G1: ~20% S-G2/M: ≤ 20%
MPP	Lin-, Sca-1+, c-Kit+, CD34+,CD135+,CD48+, CD150-	M	G0: ~ 50% G1: ~40% S-G2/M: ≤ 20%
LSK	Lin- , Sca-1+, c-Kit+	L	G0: ~ 10% G1: ~ 60% S-G2/M: ≤ 20%
LK	Lin-, c-Kit+	N	G0: ~ 10% G1: ~ 60% S-G2/M: ≤ 20%
Lin-	Gr1- CD3- CD4- CD8- B220- CD11b- Ter119- CD19- CD127-	N	G0: ~ 10% G1: ~ 60% S-G2/M: ≤ 20%

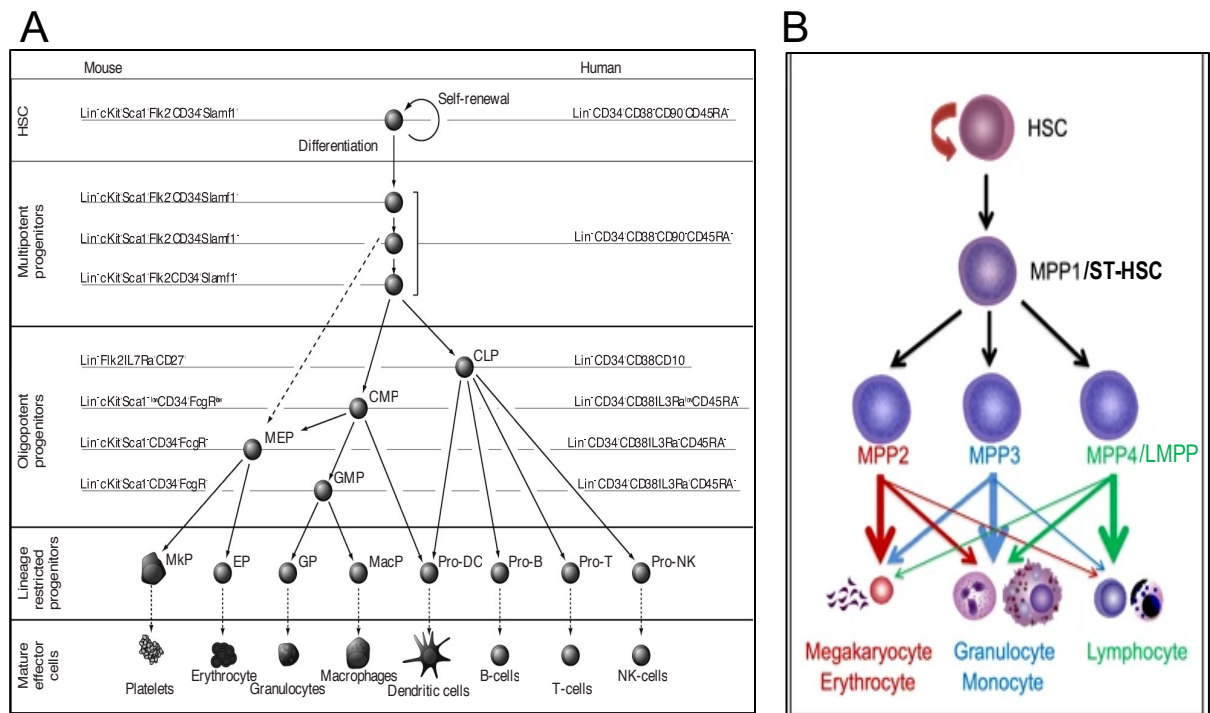


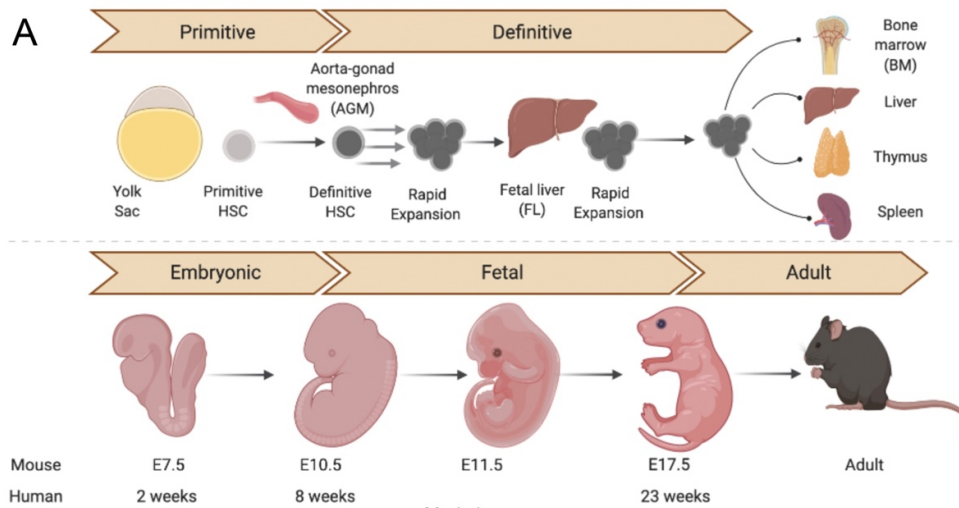
**Figure 6. Classical versus revised mouse and human hematopoietic cell hierarchy.** (A) The hematopoietic system is orchestrated by self-renewing hematopoietic stem cells (HSCs), which can be subdivided based on their temporal ability to sustain the whole spectrum of mature blood cell lineages. HSCs with self-renewal capabilities give rise to multiple types of multipotent progenitor cells (MPP), oligopotent progenitors: common lymphoid progenitors (CLPs), common myeloid progenitors (CMPs), granulocyte–macrophage progenitors (GMPs), and megakaryocyte–erythrocyte progenitors (MEPs), lineage restricted progenitors (megakaryocyte progenitor (MkP), erythrocyte progenitor (EP), granulocyte progenitor (GP), macrophage progenitor (MacP), pro-dendritic cell (ProDC), pro-B cell (Pro-B), pro-T cell (Pro-T), pro-natural killer cell (Pro-NK)) and finally mature blood cells of different lineages that, with some exceptions (certain B cell and T cell subsets, and tissue-resident macrophages), do not self-renew. (B) The revised hierarchy that describes HSC irreversibly differentiating into multipotent progenitors with lineage biased that give rise to a primary specific lineage (thicker arrows) but infrequently give rise to other lineages (thinner arrows).

### Hematopoietic stem cell origin.

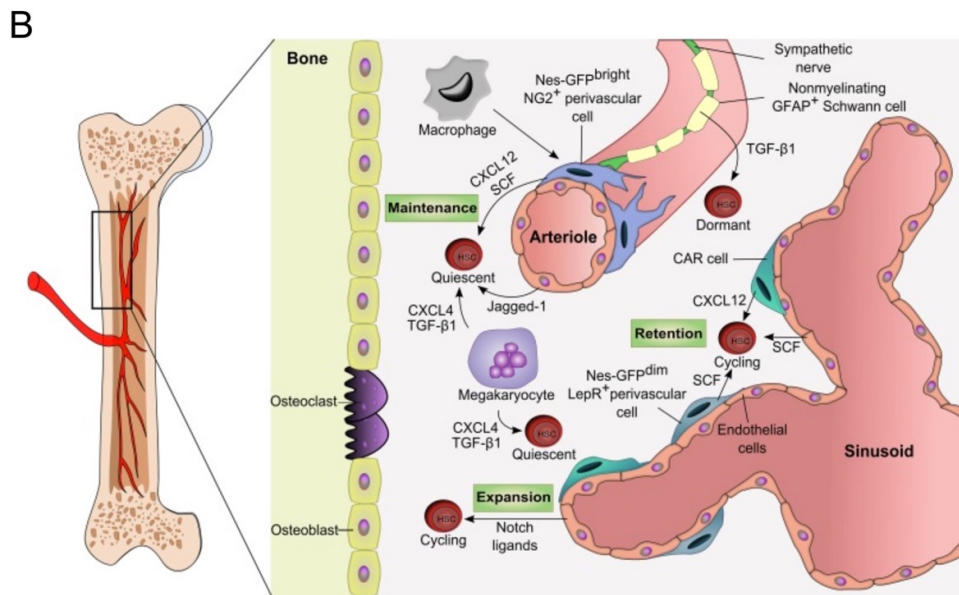
To understand the cell fate of HSCs and the factors leading to their heterogeneity much research has focused on their developmental origins. The early stages of mammalian hematopoiesis begin in the blood islands of the yolk

sac, during embryonic development and has been classified into two stages: primitive and definitive hematopoiesis[73-75]. Primitive (embryonic) hematopoiesis begins approximately at embryonic stage 7.5 (E 7.5) in mouse and 2 weeks in humans and is shortly followed by definitive (fetal) hematopoiesis which begins between E10 to E11 in mice and as early as 8 weeks in the aorta–gonad–mesonephros (AGM) region (Figure 7A). While primitive HSCs give rise to mainly nucleated pro-erythrocytes, definitive HSCs are able to give rise to all the blood lineages. HSCs undergo rapid activation and expansion in the AGM and thereafter migrate to the fetal liver where they undergo further expansion. Subsequently definitive HSCs localize to the bone marrow, thymus and spleen. After birth, the bone marrow becomes the main site of blood cells production and hematopoietic stem cells maintenance for the organism's lifetime.

In adult BM at homeostatic conditions, HSCs primarily become quiescent only dividing intermittently. Though broadly investigated, our understanding of the factors that determine HSC cell fate is limited. Thus far, studies have demonstrated that HSC pool itself is functionally and molecularly heterogeneous and that a combination of cell autonomous drivers and extrinsic molecular cues from non-hematopoietic and HSC-derived niche cells control HSC heterogeneity.



Made in  
biorender. Adapted from  
Kawahara, xPharm: The Comprehensive Pharmacology Reference, (2007) Pages 1-5,



Boulais PE, Frenette PS. Blood. 2015;125(17):2621–2629.

**Figure 7. Hematopoietic niches during development. (A)** Primitive (embryonic) hematopoiesis occurs in the yolk sac while definitive hematopoiesis occurs in the AGM region. At specified times HSCs migrate from AGM to the fetal liver and finally to the bone marrow, spleen, and thymus. **(B)** Illustration of adult bone marrow niche. Quiescent HSCs are located in the arteriole niches whereas activated HSCs are sinusoidal niche. NG2+ pericytes, Leptin receptor expressing (LepR+) perivascular cells, sinusoid, Mesenchymal stromal cells (MSC), CXCL12-abundant reticular (CAR) cells, megakaryocytes, macrophages, and sympathetic neurons are components of the HSC niche that work together to regulate HSC maintenance. A combination of HSC receptors (TIE2, MPL, CXCR4, c-KIT) and

niche adhesion molecules and secreted factors, CXCL12, ANG, TPO, TGF $\beta$ , CXCL4, JAGGED, work collaboratively to regulate HSCs maintenance, retention, dormancy and expansion.

### **Cellular components of the bone marrow niche**

The microenvironment in which HSC reside, referred to as the HSC niche, is an important determinant of the equilibrium between quiescence, self-renewal, migration and differentiation of HSCs at steady-state and in response to injuries and emergencies. A growing body of evidence indicates that HSCs in different activation states and differentiation stages are maintained in distinct BM niches [76, 77]. These niches are comprised of a complex integrated system of non-hematopoietic and hematopoietic cells that secrete factors and express receptors that regulate maintenance, proliferation, retention and quiescence summarized below in Figure 8[78].

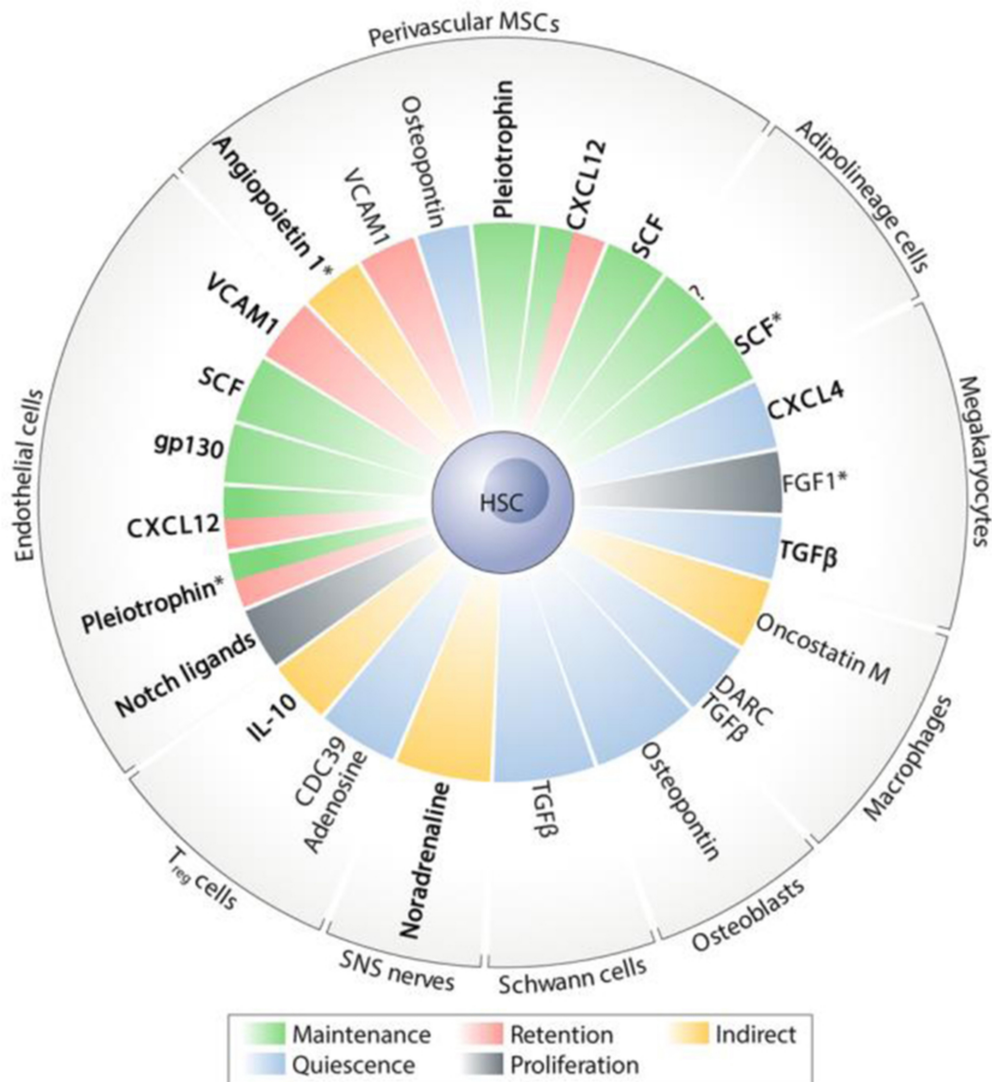
Earlier studies revealed the primary location of HSC niche to be the “endosteal niche” closest to the surface of the bone[79-81], however studies have since then identified multiple niches including the “sinusoidal/vascular niche” and more recently the “arteriole niche.” It is now currently accepted that distinct HSCs niches are located throughout the bone marrow[82]. Homed long-term repopulating HSCs preferentially localize to the endosteal niche proximal to trabecular bone surface [83] while the most quiescent HSC localize to the oxygen-low arteriolar niches in the endosteum [84] and the activated HSC migrate to sinusoidal niches located closer to the central artery and vein (Figure 7B)[85].

The various cell types implicated in regulating HSC activity, include perivascular mesenchymal stem cells (MSCs), endothelial cells, osteoblastic



lineages, adipolineage cells, sympathetic nervous system (SNS) nerves, non-myelinating Schwann cells, macrophages, megakaryocytes and regulatory T (Treg) cells. Osteoblasts were the first to be identified as a BM niches cell. Elegant confocal and other modern imaging techniques now show that osteoblast do not directly interact with HSCs but are often found proximal to HSC and the ablation of osteoblast significantly reduces HSC maintenance. This is thought to be mediated by osteopontin.

BM endothelial cells line the interior of all blood vessels and produce various factors, such as Notch ligands, CXCL12, SCF and pleiotrophin, that regulate the activity of HSCs. There are two main types of endothelial populations in the BM, the arteriolar endothelial cells (AECs) and sinusoid endothelial cells (SECs). AECs line the arterioles and secrete nearly all detectable endothelial-derived SCF in the BM. Arterioles are less permeable and therefore more hypoxic whereas sinusoid capillaries are leakier and have more oxygen. HSC isolated from areas rich in AECs are quiescent and contain low levels of ROS whereas those isolated from areas rich in SECs have increased ROS levels, leading to their activation and augmenting their differentiation and migration. Other niche components and their regulator function are summarized in **Figure 8** below.



Pinho S, Frenette PS. *Nat Rev Mol Cell Biol.* 2019;20(5):303-320

**Figure 8. Summary of niche cells and their contribution to HSC maintenance.** Perivascular mesenchymal stem cells (MSCs), endothelial cells, osteoblasts, adipolineage cells, sympathetic nervous system (SNS) nerves, non-myelinating Schwann cells, macrophages, megakaryocytes and regulatory T (Treg) cells collaboratively work together to release factors osteopontin, CXCL4, TGF-β, Adenosine that stimulate HSC quiescence, SCF, CXCL12, pleiotrophin that maintain HSCs, express membrane-bound CXCL12, VCAM1 that retain HSC, Notch ligands and FGF1 that promote HSC proliferation and other factors that are involved in HSC regulation.

## Signaling pathways involved in HSC regulation

Extrinsic modulators (including many cytokines, growth factors, and metabolites) and intrinsic regulators (such as certain transcription factors, cell cycle regulators, metabolites and molecular modulators) control HSC fate through numerous signaling pathways.

The chemokine receptor CXCR4 and its ligand the chemokine stromal cell-derived factor-1 (SDF-1, also known as CXCL12) are vital for HSC quiescence, BM retention and protection against oxidative stress [86-89]. Deletion of CXCR4 or CXCL12 resulted in perinatal lethality; however, the analysis of conditionally deficient CXCR4 or CXCL12 mice led to a reduction in HSC numbers, expansion in multipotent progenitors (only in CXCL12 deficient mice) and altered localization of HSC (absent along the endosteal surface, but predominantly in the perisinusoidal space) [86-89].

Tie2 is a receptor tyrosine kinase robustly expressed on a portion of HSC and endothelial cells. While Tie2 has been shown to be expressed on LT-HSC, Tie2 ablation studies show that it is dispensable for fetal liver HSC maintenance but plays a crucial role in adult HSC maintenance along with its ligand angiopoietin-1 (Ang-1) [90, 91]. The Tie2/Ang-1 axis promotes adhesion of Tie2<sup>+</sup> HSCs to fibronectin (FN) and collagen (COL) anchoring HSCs to their quiescent niche and protecting the HSC compartment from myelosuppressive stress [90, 91].

Notch signaling is vital for generating hematopoietic stem cells from endothelial cells during definitive hematopoiesis [92], however its role in adult HSC maintenance is controversial due to various conflicting results obtained in several

studies[93]. There are four Notch receptors (Notch1, 2, 3, and 4) expressed on HSCs and five membrane Notch ligands (Delta-like1, 3, and 4 and Jagged1 and 2) expressed on endothelial cells in the BM. Notch signaling is highly active in HSCs and reduced in differentiated cells. Pan-inhibition of all canonical Notch signaling approach mediated by the overexpression of a dominant negative form of Mastermind-like 1 (dnMAML1) resulted in a severe reduction of mouse LT-HSC through accelerated differentiation[94] Demonstrating the importance of notch signaling in LT-HSC maintenance.

Fetal stem cells are actively cycling and expanding and highly metabolically active to meet their energy requirements[62, 73-75]: whereas, adult stem cells typically maintain a metabolic inactive state to preserve long-term self-renewal capacity for tissue maintenance and prevent HSC exhaustion[95-99]. Quiescent HSCs primarily rely on anaerobic glycolysis to minimize mitochondrial oxidative phosphorylation (OXPHOS) and ROS production[95-99]. During hematopoietic recovery, HSCs shift their metabolic activity from glycolysis to OXPHOS, which provides energy and increases the production of ROS and other metabolites that stimulate signaling pathways leading to differentiation into different lineage-biased multipotent progenitors (MPP). Metabolic activity increases during differentiation and drastically decreases as terminally-differentiated mature populations are achieved[96]. Hypoxia and master transcription regulator, *Myc*, plays an important role in regulation HSC metabolism and therefore HSC cell fate[99].

## Abnormal hematopoiesis and hematological disorders

The balance between differentiation and self-renewal is tightly regulated to ensure hematopoietic homeostasis throughout life. Excessive differentiation with insufficient self-renewal depletes the HSC pool and causes HSC exhaustion (Figure 9). Restricted differentiation with unrestrained self-renewal can lead to myeloproliferative diseases or leukemia (Figure 9). Extreme stress or injury can lead to diminished HSC and mature cell populations that will result in bone marrow failure.

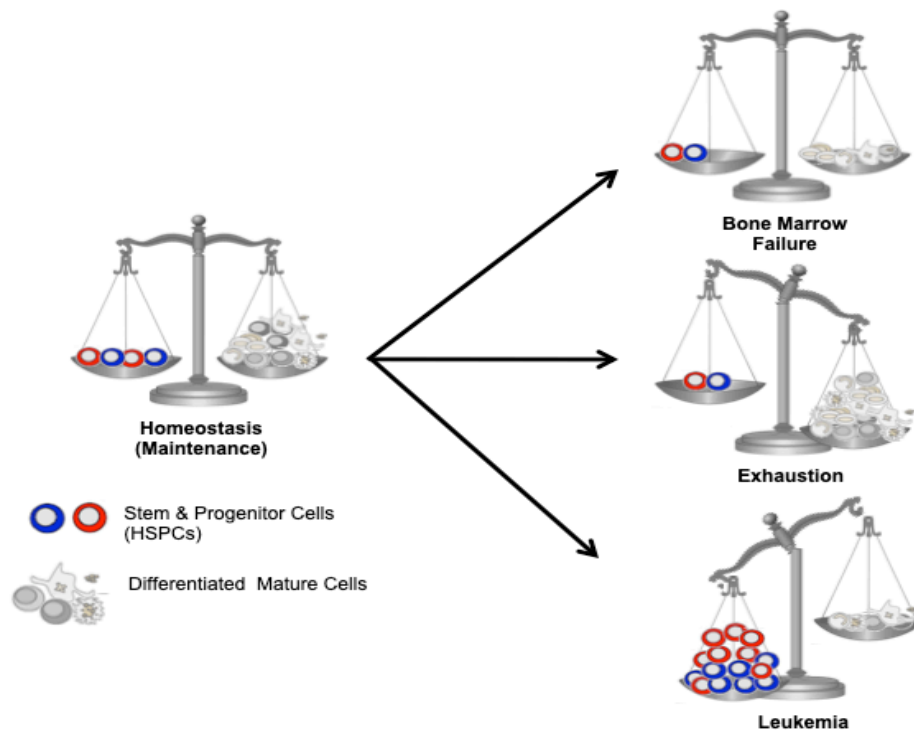


Figure 9. Consequences of abnormal hematopoiesis.

## CHAPTER TWO:

### LIGAND-MEDIATED PROTEIN DEGRADATION REVEALS FUNCTIONAL CONSERVATION AMONG SEQUENCE VARIANTS OF THE CUL4-TYPE E3 LIGASE SUBSTRATE RECEPTOR CEREBLON

**A note to the reader:** this chapter has been previously published in a research article in *Journal of Biological Chemistry*, Akuffo et. al 2018<sup>[100]</sup>

#### Introduction

CRBN binds to thalidomide, and other immunomodulatory drugs, including lenalidomide (Len) and pomalidomide (Pom), and is one of many DDB1 and CUL4-associated factors (DCAFs) that target specific protein substrates for ubiquitylation and proteasome-mediated degradation by the DDB1-CUL4A-Roc1-RBX1 E3 ubiquitin ligase complex [14, 28, 101]. Despite their teratogenic properties [6], immunomodulatory compounds have antineoplastic activity in multiple myeloma [10], myelodysplastic syndrome (MDS) associated with a somatically acquired deletion in chromosome 5 (del(5q) MDS) [18] and B cell malignancies [12, 102, 103] based on the substrates that are selected for proteosomal destruction by the bridging actions of these small molecules [14, 35, 101, 104-106]. Len, Pom and a newer derivative CC-122 (avadomide) [107] also potentiate the activation of T-cells. Though this function has been studied less thoroughly, it is thought that the drug-induced proteosomal-mediated degradation of transcriptional repressors of T-cells, Ikaros and Aiolos, may be necessary for this response in addition to their defined role in antineoplastic activity [33, 34, 108]. Unlike human cells, mouse cells are resistant to these compounds including antiproliferative multiple myeloma [109]

and thalidomide-associated teratogenicity[110]. While the overall amino acid sequence of mouse CRBN is highly conserved (Figure 10), and it forms the DDB1 interaction [28], minor species-related sequence variations in the thalidomide binding domain (TBD) of CRBN are thought to lead to non-conserved drug binding or altered E3-ligase recruitment functions. A single amino acid substitution, Val388 which is changed to isoleucine in mouse (Ile391), has been reported to render mouse CRBN unable to degrade Ikaros, Aiolos, and CK1 $\alpha$  binding through a  $\beta$ -hairpin-loop motif that is recognized only when CRBN is complexed with the immunomodulatory drugs [31]. Therefore, dysfunctional drug-induced substrate requirement possibly mediates drug resistance [31]. Thus far, conservation of mouse CRBN's E3-ubiquitin ligating function has not been definitely shown due to this loss of function as the native ligands that are regulated through this pathway are poorly defined. Moreover, drug binding affinity due to the V388I variant has not been studied in detail. A better understanding of this defect is important for future drug discovery efforts aimed at controlling intracellular protein degradation and understanding CRBN's endogenous role as an E3-ubiquitin ligase substrate receptor.

Here, we focused our analysis on non-primate CRBN. Using drug binding assays to several CRBN sequence variants, we investigate if these structural changes are likely to result in functional inactivation. We focused on CRBN's substrate recruiting function in mouse and human T-cells, as this is poorly studied and important for defining applications in immune therapy. Both the Bradner and Crews laboratories conjugated established chemical inhibitors of bromodomain and extraterminal domain (BET) family members, to a thalidomide analog to promote the CRBN-dependent degradation of BRD4[51, 52] Linkage of the BET-binding ligand (JQ1 or OTX-015) to an IMiD® redirects CRBN-E3

ligase activity toward BRD4 allowing for analysis of different substrates through a similar TBD-dependent mechanism (Figure 4B). Moreover, the E3-ubiquitin protein targeting approach, coined Proteolysis Targeting Chimera (PROTAC)[46, 50, 111], may be broadly applied clinically and experimentally to study the function of proteins that are difficult to target and in cells that are insensitive to genome editing techniques. Here, we use a PROTAC probe to investigate cellular engagement of an immunomodulatory drug to mouse CRBN. Collectively, our findings are important to understand sequence variants of CRBN and provide the first investigation of the E3-ubiquitin ligase substrate conjugating function of CRBN in a non-primate vertebrate model.

## Results

### **Thalidomide binding domain of CRBN has a conserved immunomodulatory compound binding motif**

First, we studied the sequence variants of CRBN in more detail. Based on crystal structures, immunomodulatory compounds bind to a conserved pocket within the C-terminal TBD of CRBN (Figure 10A)[13, 112]. These interactions are governed by hydrogen bonding, aromatic quadrupole, and Van der Waals (VDW) interactions. Analysis of the X-ray crystal structures of CRBN (human (hCRBN), mouse (mCRBN) and chicken (gCRBN)) in complex with thalidomide, Len, and Pom, respectively (Figure 10A) shows negligible variations of root mean square deviation (RMSD) between the inhibitor poses. Thus, an in-depth theoretical investigation of the molecular binding mechanics of immunomodulatory compounds in complex with CRBN was conducted to explore



possible differences in drug interactions between mouse and human CRBN caused by induced fit or protein flexibility.

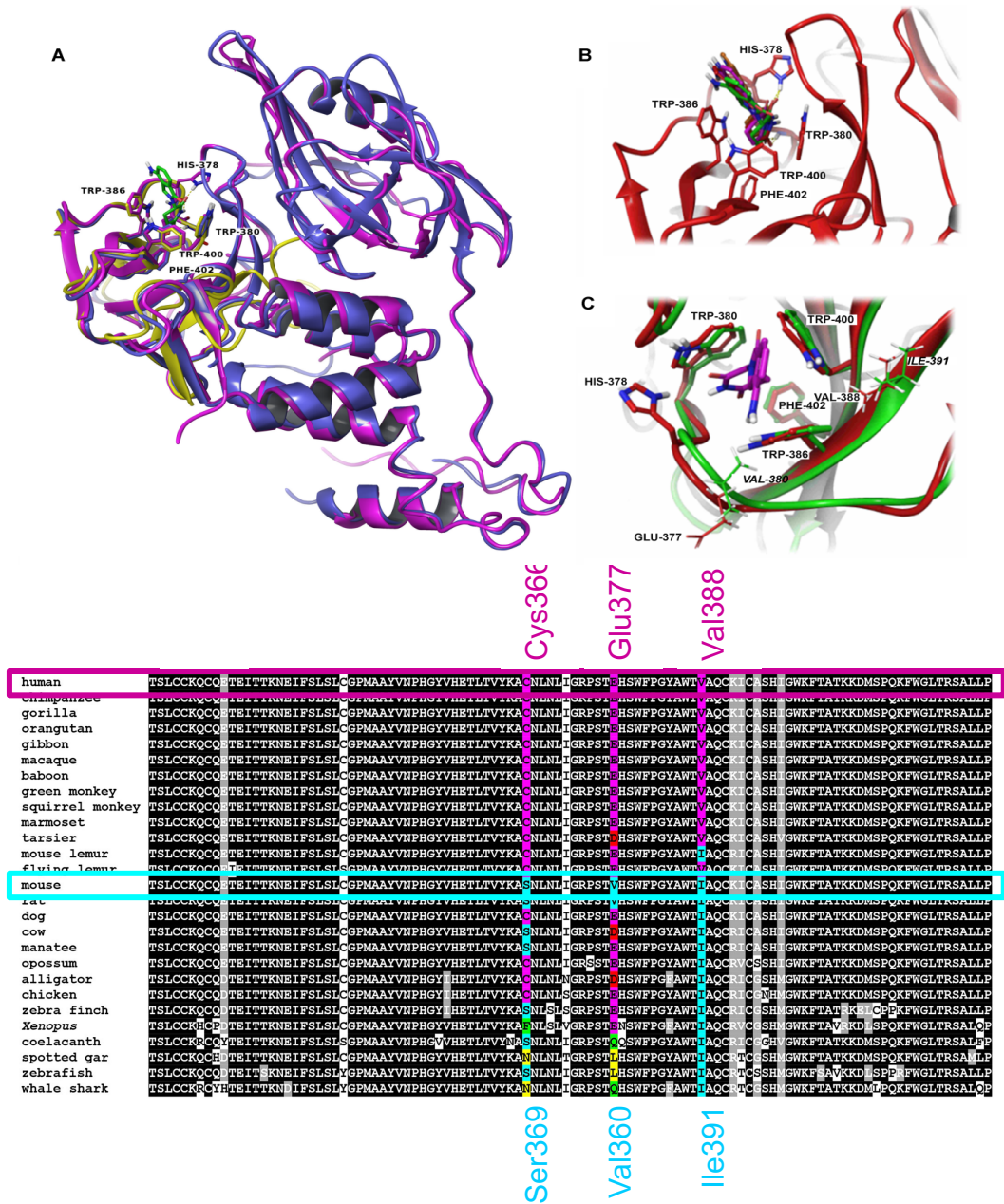


**Figure 10. Structure of cereblon is conserved across different species. (A)** Ribbon overlays of human (purple, PDB 4TZ4), chicken (blue, PDB 4CI2) X-ray crystal structures and post-MD structure of mouse (yellow, PDB 4TZ4) cereblon. Human immunomodulatory drug binding site residues His378, Trp380, Trp386, Phe402 and ligands thalidomide (yellow), lenalidomide (green) and pomalidomide (blue) shown for reference. **(B)** Superposition of ligand poses of lenalidomide (green) for the post-MD

equilibrated systems of the CRBN thalidomide binding site after induced fit docking (IFD) for hCRBN (red), hmCRBN (green), gCRBN (orange), shown with the post-MD equilibrated protein structure of hCRBN (red) shown for reference. **(C)** Overlays of human and mouse cereblon shows non-conserved residues Ile391 for mCRBN (human Val-388); Val-380 for mCRBN (human Glu-377) (mouse shown in *italic* font). **(D)** The CRBN protein sequences from diverse vertebrate species that correspond to the human thalidomide binding site were aligned using Clustal Omega [2]. Positions that are at least 90% identical are shaded in black and similar residues are shaded in gray. Shading in other colors highlight sequence diversity at three positions: Cys366, Glu377 and Val388 in human (above) and Ser369, Val380 and Ile391 in mouse (below). Arrows indicate cysteines involved in forming disulfide bridges. Sequences include: thirteen primates (human, NP\_001166953.1, common chimpanzee, XP\_001140433.1; western lowland gorilla, XP\_004033566.1; Sumatran orangutan, NP\_001127555.1; northern white-cheeked gibbon, XP\_012357648.1; rhesus macaque, NP\_001182576.1; olive baboon, XP\_003894216.1; green monkey, XP\_007983240.1; squirrel monkey, XP\_010336170.1; common marmoset, XP\_008980298.1; Philippine tarsier, XP\_021562663.1; gray mouse lemur, XP\_020139859.1; Sunda flying lemur, XP\_008581608.1), five non-primate mammals (mouse, NP\_067424.2; rat, NP\_001015003.1; domestic dog, XP\_005632293.1; cow, NP\_001068995.1; Florida manatee, XP\_012409572.1), one marsupial (gray short-tailed opossum, XP\_001374178.2), one reptile (American alligator, XP\_006263115.1), two birds (chicken, XP\_004944767.1; zebra finch, XP\_012429169.1), one amphibian (*Xenopus*, NP\_001008192.1), one lobe-finned fish (West Indian Ocean coelacanth, XP\_006001868.1), two ray-finned fish (Spotted gar, XP\_006630756.1; zebrafish, NP\_001003996.1) and one cartilaginous fish (whale shark, XP\_020385559.1).

For molecular dynamics (MD), simulations of the crystal structures of hCRBN (PDB 4TZ4)[112] and gCRBN (PDB 4CI1, 4CI2, and 4CI3)[112] in complex with DNA damage-binding protein 1 (DDB1) were used. The crystal structure of mCRBN (PDB 4TZC and 4TZU)[13] is monomeric and truncated to contain only the TBD (108 defined residues compared to 380 defined residues for hCRBN and gCRBN) and is not suitable for computational modeling. The amino acid differences in mouse CRBN (when compared to human) include C366S, E377V (which may be specific to rodents) and V388I (Figure 10D). Therefore, to further increase sampling and determine any structural dependence on these residues, the original hCRBN sequence of the equilibrated representative structure was mutated to the mouse sequence. The mCRBN analog and hmCRBN hybrid

developed from the hCRBN system is capable of reproducing the crystal ligand poses of mCRBN (PDB 4TZC and 4TZU) with minimal conformational deviation (Figure 10C) and was used for modeling purposes. Binding modes do not appear to differ between models and compounds as there are no significant differences in RMSD calculations between X-ray crystal binding poses (Table 4) and post-MD equilibrated models (Figures 10B and C). Induced fit docking (IFD) also predicts no observable difference in binding affinity between models and compounds (Table 4). All poses are within 1.8 Å RMSD, which is the expected threshold for the IFD protocol [113].

Although Val388 of hCRBN recruits Ikaros, Aiolos, and CK1 $\alpha$  upon immunomodulatory compound binding [31], the side chain is > 6 Å away from the immunomodulatory drug, and it is thus unlikely to alter binding affinity to the drugs. The second distinct amino acid is Glu377, which in the mouse is Val380, and could establish a weak hydrogen bond with Len's amino group. However, hydrogen bond analysis (Figure 11) of MD simulations suggests minimal interaction occurs between this residue and bound immunomodulatory drugs, mainly due to backbone dihedral strain tending to force the charged carboxyl moiety away from the binding site.

**Table 4.** RMSD Calculations.

		hmCRBN	hCRBN	hCRBN	gCRBN	gCRBN	mCRBN	mCRBN
		Post MD	Post MD	Crystal	Post MD	Crystal	Post MD	Crystal
<b>Thal</b>	Glide Score	-11.040	-11.049	-10.789	-11.408	-10.724	-10.082	-9.344
	Emodel	-81.796	-83.437	-78.630	-77.239	-79.853	-63.197	-63.881
	Pose RMSD	-	-	-	1.6615 <sup>a</sup>	1.1036 <sup>a</sup>	7.1958 <sup>b</sup>	7.0379 <sup>b</sup>
<b>Len</b>	Glide Score	-11.279	-11.574	-10.965	-10.976	-10.494	-8.0373	-9.544
	Emodel	-85.454	-87.014	-79.857	-78.197	-77.976	-52.240	-57.118
	Pose RMSD	0.5944 <sup>c</sup>	0.7384 <sup>c</sup>	1.7233 <sup>c</sup>	1.5859 <sup>d</sup>	1.0053 <sup>d</sup>	-	-
<b>Pom</b>	Glide Score	-11.200	-10.996	-10.800	-10.256	-11.634	-7.760	-8.339
	Emodel	-89.915	-86.330	-81.008	-80.357	-84.483	-51.789	-58.872
	Pose RMSD	-	-	-	1.7592 <sup>e</sup>	0.9482 <sup>e</sup>	4.6167 <sup>f</sup>	2.8715 <sup>f</sup>

<sup>a</sup> Pose RMSD calculated using PDB 4CI1 for comparison.

<sup>b</sup> Pose RMSD calculated using PDB 4TZC for comparison.

<sup>c</sup> Pose RMSD calculated using PDB 4TZ4 for comparison.

<sup>d</sup> Pose RMSD calculated using PDB 4CI2 for comparison.

<sup>e</sup> Pose RMSD calculated using PDB 4CI3 for comparison.

<sup>f</sup> Pose RMSD calculated using PDB 4TZU for comparison.

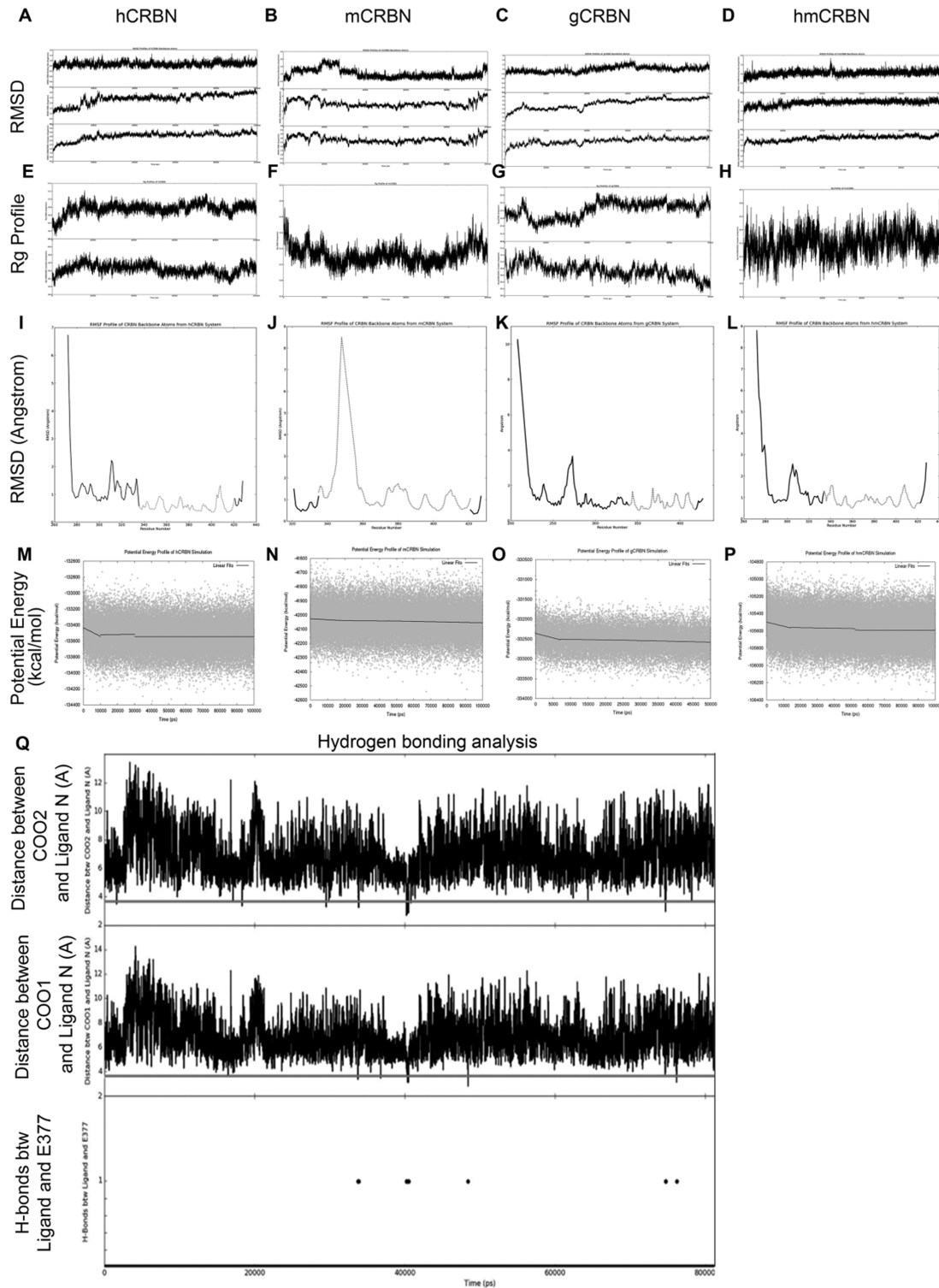


**Figure 11. RMSD profiles of hCRBN, mCRBN, gCRBN & hmCRBN.** (A) RMSD profiles of hCRBN. Profiles were created using backbone atoms and were calculated with hCRBN-DDB1 complex (Bottom Graph), hCRBN alone (Middle Graph), and binding site residues N335 to A421 (Top Graph). All measurement units are in Angstroms. (B) RMSD profiles of mCRBN. Profiles were created using backbone atoms and were calculated



with all hCRBN residues (Bottom Graph), binding site residues N335 to A421 (Middle Graph), and residues (357, 377, 379-383, 388-390, 401, 402, 404) located 6 Å away from the ligand (Top Graph). All measurement units are in Angstroms. **(C)** RMSD profiles of gCRBN. Profiles were created using backbone atoms and were calculated with hCRBN-DDB1 complex (Bottom Graph), gCRBN alone (Middle Graph), and binding site residues N337 to A423 (Top Graph). All measurement units are in Angstroms. **(D)** RMSD profiles of hmCRBN. Profiles were created using backbone atoms and were calculated with hmCRBN-DDB1 complex (Bottom Graph), hmCRBN alone (Middle Graph), and binding site residues N335 to A421 (Top Graph). All measurement units are in Angstroms. **(E)** Rg Profiles of hCRBN. Profiles were created from all atoms and were calculated with hCRBN-DDB1 complex (Bottom Graph) and hCRBN alone (Top Graph). All measurement units are in Angstroms. **(F)** Rg Profiles of mCRBN. Profiles were created from all atoms. All measurement units are in Angstroms. **(G)** Rg Profiles of gCRBN. Profiles were created from all atoms and were calculated with gCRBN-DDB1 complex (Bottom Graph) and hCRBN alone (Top Graph). All measurement units are in Angstroms. **(H)** Rg Profiles of hmCRBN. Profiles were created from all atoms and were calculated with hmCRBN-DDB1 complex (Bottom Graph) and hmCRBN alone (Top Graph). All measurement units are in Angstroms. **(I)** RMSF Profile of hCRBN. Profiles were created using backbone atoms and were calculated with hCRBN alone (DDB1 RMSF available upon request). Binding site residues N335 to A421 displayed as dashed line. All measurement units are in Angstroms. **(J)** RMSF Profile of mCRBN. Profiles were created using backbone atoms of mCRBN. Binding site residues N335 to A421 displayed as dashed line. All measurement units are in Angstroms. **(K)** RMSF Profile of gCRBN. Profiles were created using backbone atoms and were calculated with gCRBN alone (DDB1 RMSF available upon request). Binding site residues N337 to A423 displayed as dashed line. All measurement units are in Angstroms. **(L)** RMSF Profile of hmCRBN. Profiles were created using backbone atoms and were calculated with hmCRBN alone (DDB1 RMSF available upon request). Binding site residues N335 to A421 displayed as dashed line. All measurement units are in Angstroms. **(M)** Potential energy profile of hCRBN simulation. Multiple linear fits were characterized to determine asymptotic behavior by minimizing slope. **(N)** Potential energy profile of mCRBN simulation. Multiple linear fits were characterized to determine asymptotic behavior by minimizing slope. **(O)** Potential energy profile of gCRBN simulation. Multiple linear fits were characterized to determine asymptotic behavior by minimizing slope. **(P)** Potential energy profile of hmCRBN simulation. Multiple linear fits were characterized to determine asymptotic behavior by minimizing slope.

### **Immunomodulatory compound binding is conserved in CRBN sequence variants.**

Amino acids in mouse CRBN-TBD at Val380 (equivalent to human Glu377) and Ile391 (equivalent to human Val388) (Figure 12A-C) appear to have no relevance in the structure or corresponding immunomodulatory drug binding interaction based on theoretical modeling. To test the effects of these two non-conserved amino acids on

binding affinity, the recombinant human TBD motif (residues 319-425) was expressed in *E. coli* and mutated to the mouse variants (Figure 12A-C). Immunomodulatory drug binding was then analyzed using two distinct assays, intrinsic tryptophan fluorescence assay (IF) (Figure 12D-G) and isothermal titration calorimetry (ITC) (Figure 12H-K). The C366S amino acid mutation was not studied in binding assays as it is more than 20 Å away from the immunomodulatory drug binding pocket. The TBD is structurally stabilized by four cysteine residues (Cys323, Cys326, Cys391 and Cys394) that coordinate a single zinc ion [13, 112], located ~18 Å from the drug interacting site. To gain insights on the role of zinc, mutations in the CXXC domain of the TBD were also generated. Mutating any of the cysteine residues resulted in insoluble protein that aggregated in inclusion bodies (data not shown). This is indicative of misfolding due to loss of Zn<sup>2+</sup> ion coordination. To rule out improper folding or destabilization, a zincon assay [114] was performed on purified protein of all expressed recombinant CRBN-TBD proteins. These analyses revealed a 1:1 stoichiometric ratio of Zn<sup>2+</sup> bound to the TBD recombinant protein (data not shown).

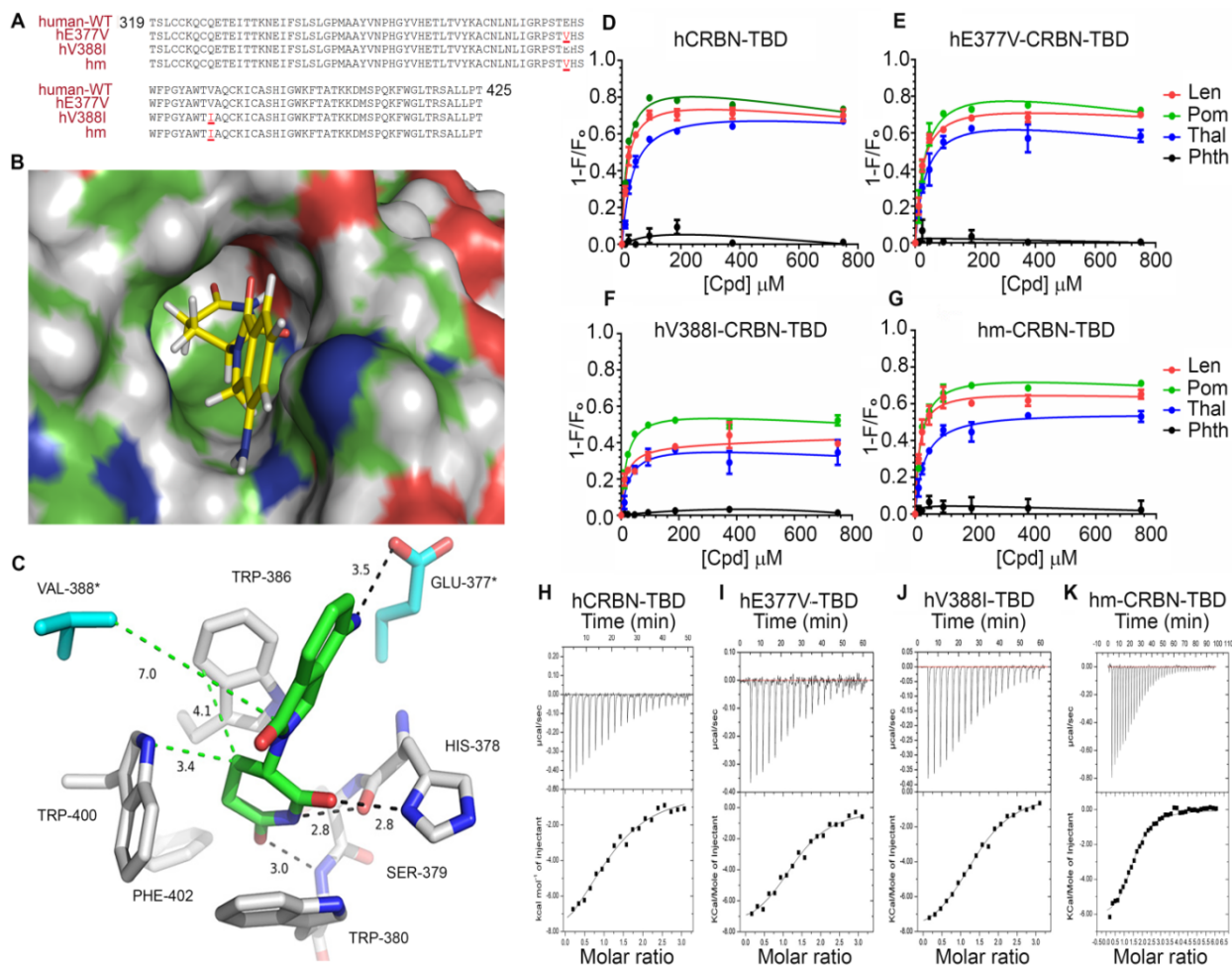


**Figure 12. Human and mouse CRBN binds IMiD@ with similar affinities. (A)** Sequence alignment of human CRBN and human to mouse mutations. Mutations introduced to convert human to mouse are highlighted in red. **(B)** IMiD@ interaction in the hydrophobic binding pocket. **(C)** Lenalidomide (green) interacts with the TBD site (gray) through hydrogen bonds (dashed black lines) with backbone residues His378, Ser379 and Trp380 VDW interactions (dashed green lines) occur with the side chains of Trp380, Trp386, Trp400, and Tyr402 (mouse: Trp383, Trp389, Trp403, and Phe405). The two residues differing between the human and the mouse proteins are highlighted in cyan. Titration of human TBD (D) wild-type, (E) E377V, (F) V388I, and (G) E377V/V388I (hm-CRBN-TBD) to lenalidomide (red), pomalidomide (green), thalidomide (blue) and pthalimide (black) by intrinsic tryptophan fluorescence assay.  $K_D$  values were calculated based on the magnitude of fluorescence differences ( $1-F/F_0$ ). **(H-K)** Isothermal titration calorimetry saturation curve using lenalidomide (LEN) for human TBD and mutants

Moreover, protein secondary structure consistent with proper folding was also evident using circular dichroism (data not shown). Both IF (Figure 12D-G) and ITC (Figure



12H-K) analyses demonstrated similar  $K_D$  values at equilibrium for thalidomide and the immunomodulatory compounds tested in binding to wild-type, E377V, V388I, and E377V/V388I (hm)-CRBN-TBD (Table 5) with no binding observed by phthalimide (Figure 13I-L) used as a negative control.

**Table 5.** Binding affinity ( $K_D$ , ( $\mu$ M)) of immunomodulatory compounds to WT and mutant human CRBN-TBD determined using ITC and Fluorescence intensity (FI) assay.

TBD	Assay	Lenalidomide	Pomalidomide	Thalidomide	Phthalimide	dBET1
hCRBN	ITC	11 $\pm$ 3	16 $\pm$ 4	65 $\pm$ 40	nb	np
	FI	13 $\pm$ 2	16 $\pm$ 3	38 $\pm$ 12	nb	16 $\pm$ 2
hCRBN- H378A	ITC	22 $\pm$ 3	35 $\pm$ 8	37.4 $\pm$ 10	nb	np
	FI	27 $\pm$ 4	22 $\pm$ 6	74 $\pm$ 20	nb	np
hCRBN- W380A	ITC	nb	nb	nb	nb	np
	FI	nb	nb	nb	nb	np
hCRBN- E377V	ITC	9.6 $\pm$ 2	35 $\pm$ 9	97 $\pm$ 100	nb	np
	FI	22 $\pm$ 2	30 $\pm$ 7	36 $\pm$ 8	nb	np
hCRBN- V388I	ITC	10 $\pm$ 1	28 $\pm$ 7	43 $\pm$ 20	nb	np
	FI	14 $\pm$ 4	16 $\pm$ 4	39 $\pm$ 1	nb	13 $\pm$ 2
hmCRBN- E377V/V3 88I	ITC	14 $\pm$ 2	8 $\pm$ 2	34 $\pm$ 2	nb	np
	FI	13 $\pm$ 3	19 $\pm$ 4	30 $\pm$ 8	nb	np

Data represents mean  $\pm$  standard deviation. TBD=thalidomide binding domain of CRBN, ITC=isothermal titration calorimetry, FI=fluorescence intensity, nb=non-binding, np=not performed

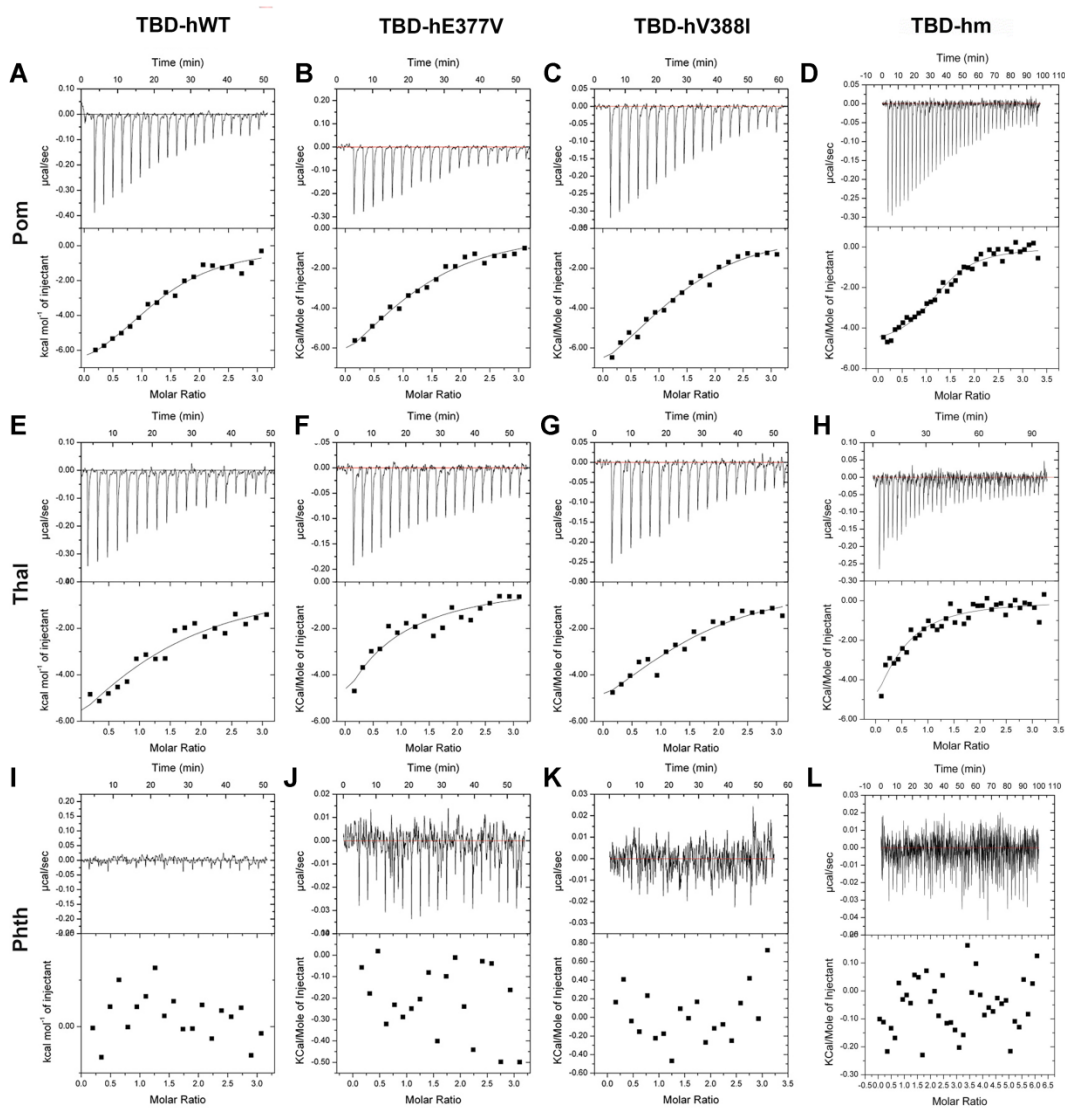


**Figure 13. Binding affinity of IMiD®s to TBD variants by ITC.** ITC binding curves of pomalidomide (A-D), thalidomide (E-H), pthalimide (I-L) with wild-type and mutant CRBN TBD protein

To assess the impact of binding pocket residues, Ala mutations of two residues were generated (Table 5) (7, 26, 27) to test the impact of H-bond formation and hydrophobic interaction with Trp380. Trp380A mutation completely abolished ligand

interactions. Although His378 forms two H-bonds with the glutarimide ring (Figure 12C), mutating this residue to Ala did not impact binding. This suggests that the backbone carbonyl of H378A retains the H-bond interaction with the NH group of the glutarimide ring. To further probe the role of His378 side chain in immunomodulatory drug binding, we conducted a pH-dependence study to measure the binding affinity of Len to CRBN-TBD by ITC. The  $K_D$  values measured at pH 4.5, 5.5, 6.5 and 7.5 are  $21.4 \pm 3$ ,  $23.7 \pm 8$ ,  $23.8 \pm 7$  and  $11.3 \pm 2 \mu\text{M}$ , respectively. Thus, protonation and deprotonation of the His378 imidazole group has no impact on immunomodulatory drug binding to the TBD.

#### **N-terminal stabilization of CRBN-immunomodulatory compound interactions.**

Finally, we compared binding affinities of Len to CRBN-TBD and full-length CRBN-DDB1 protein complex using ITC to assess the impact of residues outside of the TBD. The full-length CRBN-DDB1 complex displayed a  $K_D$  value of  $0.64 \mu\text{M} \pm 0.24 \mu\text{M}$  (pH 7.0) (Figure 14A). This affinity is similar to published data using a fluorescence polarization (FP)-based assay (32). Moreover, these results are consistent with a single binding site within the protein complex. To gain more insight on immunomodulatory compound binding to CRBN-TBD, we synthesized *N*-methyl-Len as a negative control, where the *N*-methyl group of the glutarimide ring is predicted to cause steric hindrance in the binding pocket and lacks the key H-bond donor to His378. As expected, *N*-methyl-Len did not bind to either the CRBN-TBD or CRBN-DDB1 complex (Figure 14B), as measured by ITC, indicating that the complex-drug interaction is mediated predominantly by the glutarimide binding pocket of the TBD. Interestingly, the binding affinity of Len to the CRBN-TBD is about 30-fold lower than the full-length CRBN-DDB1 complex. Moreover,

full-length CRBN and CRBN-TBD have endothermic and exothermic reactions, respectively. Therefore, residues in the full-length protein appear to augment protein-ligand interactions in the binding pocket.

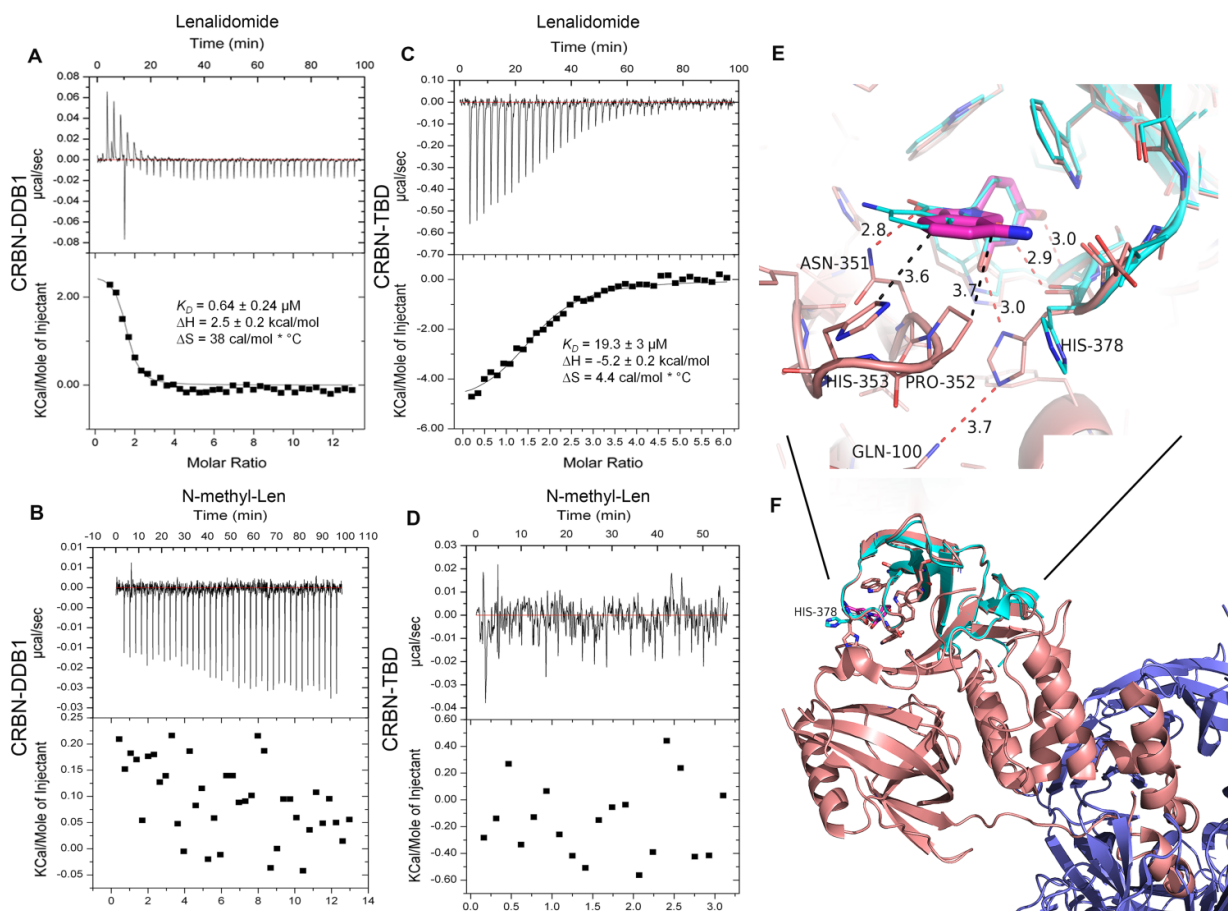


**Figure 14. Lenalidomide binds to the TBD and CRBN-DDB1 protein complex.** ITC binding curves of lenalidomide (A, C) and N-methyl-lenalidomide (B, D) titrated with (A, B) CRBN-DDB1 complex and (C, D) CRBN-TBD. (E and F) Schematic view of lenalidomide interaction in the binding pocket of full-length human cereblon; human full-length CRBN (salmon) and DDB1 (blue) with bound lenalidomide (magenta) (PDB 5FQD), superimposed with mouse TBD-CRBN (cyan) (PDB 4TZU). Hydrogen bonds and hydrophobic interactions are shown in red and black dashed lines, respectively.

## Resistance of mouse cells to immunomodulatory compounds.

Comparative analyses of CRBN sequences from representative vertebrate species revealed that Ile391 is conserved among many non-primate mammals (mouse, rat, dog, manatee and opossum), birds (chicken and zebra finch), reptiles (alligator), amphibians (*Xenopus*), bony fish (zebrafish and spotted gar) and cartilaginous fish (whale shark) (Figure 10D)[2]. Interestingly, both chicken and zebrafish are susceptible to thalidomide-induced teratogenicity despite expressing the Ile391 variant [28]. In contrast, Val388 is present in all examined primate sequences (human, chimpanzee, gorilla, orangutan, gibbon, macaque, baboon, green monkey, squirrel monkey, marmoset, tarsier and Sunda flying lemur) with the exception of gray mouse lemur, which encodes Ile in this position (Figure 10D). Therefore, Val388 is a recently derived feature present in most primates.

Immunomodulatory drug-induced ubiquitin-mediated degradation of Ikaros and Aiolos (encoded by *IKZF1* and *IKZF3*, respectively)[14, 115] appears sufficient to augment IL-2 production by T-cells[116] in the absence and presence of anti-CD28 co-stimulation [108, 117, 118]. In Len-treated human T-cells stimulated with anti-CD3 $\epsilon$  antibody to cross-link the T-cell receptor (TCR), levels of *IL2* mRNA (Figure 15A) and protein (Figure 15B) were significantly increased relative to DMSO-(vehicle) treated cells. Comparing purified human (Figure 16A) and mouse T-cells (Figure 16B) pretreated with vehicle or 10  $\mu$ M Len, only human T-cells displayed the expected Len-induced increase in IL-2 when stimulated in the absence (Figure 16A,B) or presence (Figure 15C-D) of anti-CD28 antibody using doses of anti-CD3 $\epsilon$  that ranged from 0.01 – 10  $\mu$ M.

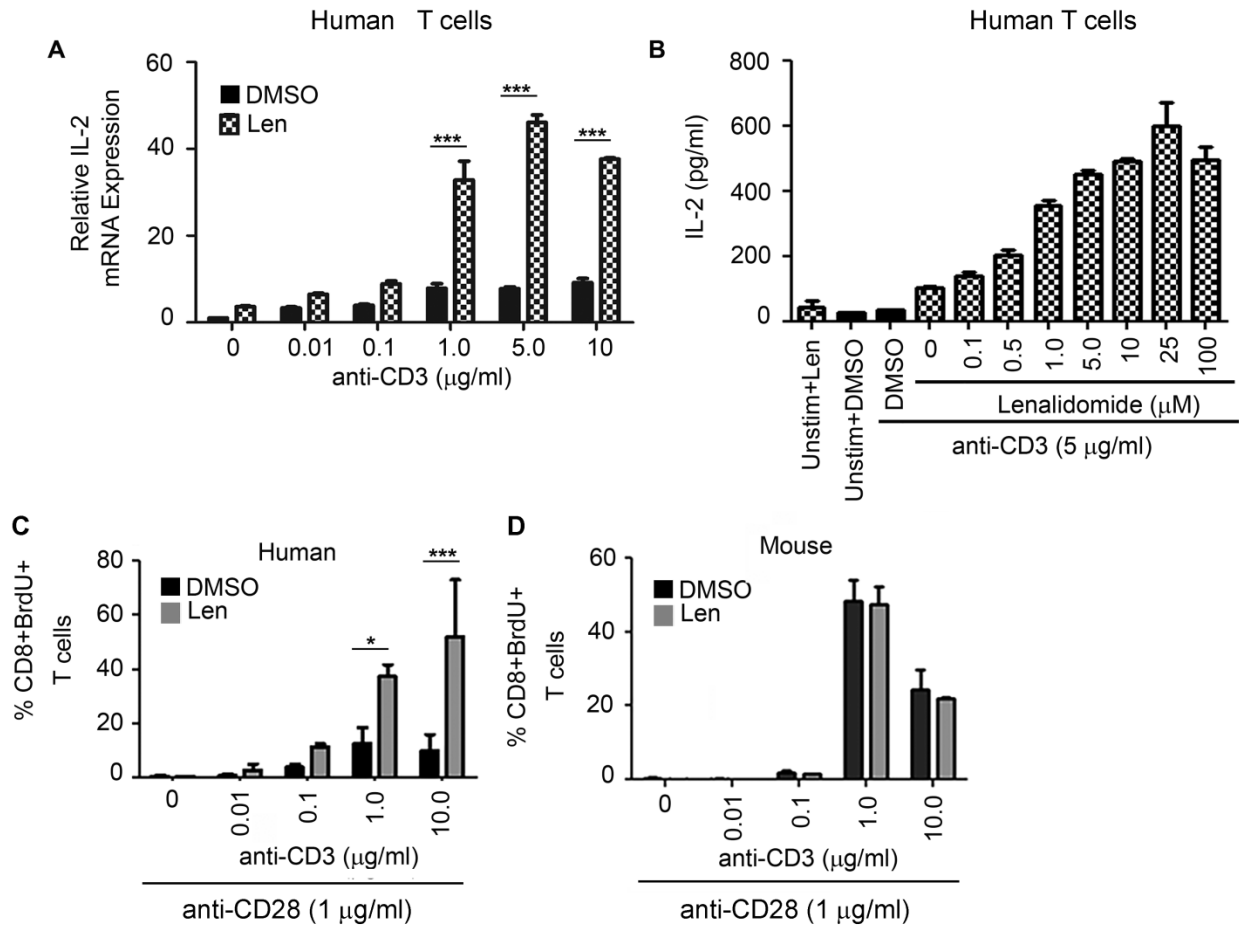


**Figure 15. Lenalidomide treatment induces IL-2 production and proliferation in T cells. (A)** Relative IL-2 mRNA production with increasing concentrations anti-CD3 (0.01 – 10 µg/mL) stimulation. **(B)** IL-2 secretion by ELISA in unstimulated cells and after treatment with anti-CD3 (5µg/mL) and anti-CD28 (1 µg/ml) with increasing concentrations of lenalidomide. **(C)** Proliferation in human T cells and **(D)** mouse T cells treated with DMSO (vehicle) or lenalidomide (10 µM) measured by S-phase transition as indicated by incorporation of bromodeoxyuridine (BrdU) with detection by flow-cytometry in cells stained for CD8+ surface expression,

Thalidomide, Len and Pom's antiproliferative effects in multiple myeloma cell lines also reportedly differ based on the presence of mouse CRBN[31, 32, 109]. In U266 (Table 6), H929 (Table 6), and MM1.S multiple myeloma cell lines (Figure 16C, Table 6), the antiproliferative effects (IC<sub>50</sub>s) of Pom ranged from 0.05 to 0.51 μM and for Len from 1.5 to 10 μM. In contrast, the mouse multiple myeloma cell line 5TGM1 was resistant to immunomodulatory drugs (Figure 16D, Table 6). Further, Ikaros protein expression was unaffected in primary mouse T-cells compared to almost completely depleted in human cells (Figure 16E) as predicted from previous structural and functional studies in multiple myeloma cell lines and in the Ba/F3 mouse lymphoma cell line [31, 35].

**Table 6.** IC<sub>50</sub> (μM) of Multiple Myeloma Cell Lines.

Drug	H929	U266	MM1.S	5TGM1
<b>Lenalidomide</b> (Len)	5.13	10.0	1.48	>>100
<b>Pomalidomide</b> (Pom)	0.046	0.51	0.099	>>100

H929, U266 and MM1.S are human multiple myeloma cell lines while 5TGM1 is a mouse multiple myeloma cell line. IC<sub>50</sub> (μM) calculated as follows: log(inhibitor) vs response based on variable slope (four parameters),  $Y = \text{bottom (best fit value)} + (100 - \text{Bottom}) / (1 + 10^{(\text{LogEC50} - X) \cdot n})$ .

$$IC_{50} = \frac{(100 - \text{Bottom})}{50 - \text{Bottom}} \times EC_{50}^{1/n}$$

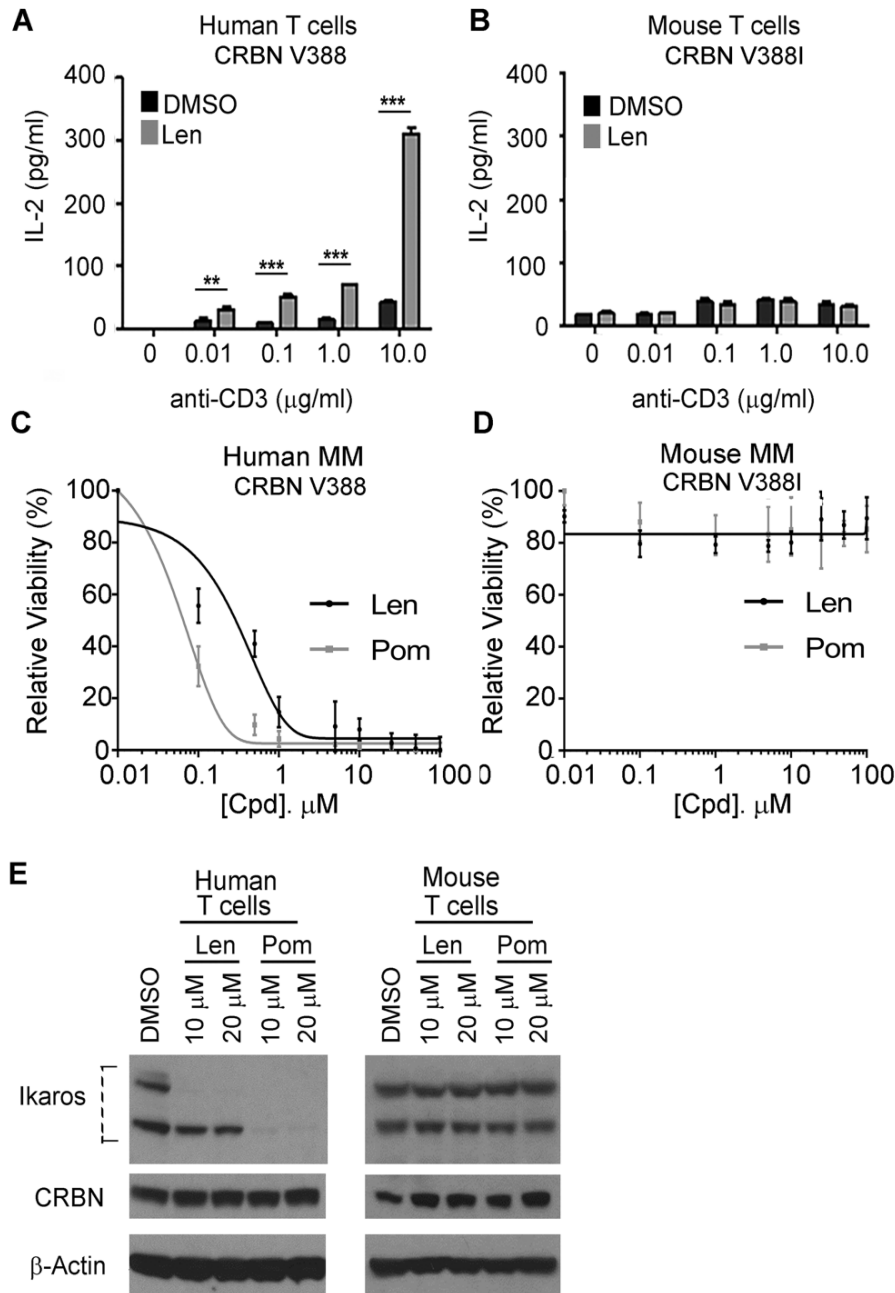


**Figure 16. Mouse cells are resistant to immunomodulatory drugs.** (A) T cells purified from healthy donor peripheral blood mononuclear cells (PBMCs) or (B) from mouse spleens of C57BL6 mice and stimulated in the presence of increasing concentrations of anti-CD3 $\epsilon$  antibody in the presence of 10  $\mu\text{M}$  lenalidomide (Len) or vehicle control (DMSO) without anti-CD28. IL-2 production was determined from the culture supernatant by ELISA. (C) The human MM1.S or (D) mouse 5TGM1 multiple myeloma cells were cultured for 7 days with increasing concentrations of lenalidomide (Len), pomalidomide (Pom) and vehicle (DMSO). Percentage relative cell viability is shown. (E) Western blot analysis of Ikaros, CRBN and  $\beta$ -actin (loading control) in human and mouse T cells stimulated with anti-CD3 $\epsilon$  5  $\mu\text{g/ml}$  + 1  $\mu\text{g/ml}$  anti-CD28 antibody for 24 h with DMSO, 10



and 20  $\mu\text{M}$  lenalidomide and pomalidomide. Results are representative of three independent experiments. Statistical analysis was conducted using ANOVA, followed by Dunnett's multiple comparison test.  $*=p<0.05$ ,  $***=p<0.001$

### **Acquired ubiquitin-proximity ligation in mouse cells establishes conserved ligase functions of mouse and human CRBN variants.**

The substrate recruiting function of CRBN was then investigated using dBET1, which maintains the CRBN-TBD targeting domain, but switches the substrate-recruitment domain to recognize BRD4 and other JQ1-associated targets [51]. Using IF (Figure 17A), the saturation binding curves for dBET1 is similar to that of Len, whereas, as expected, JQ1 alone does not bind to the CRBN-TBD. The structures of dBET1 and *N*-methyl-dBET1 (used as a negative control based on the results of *N*-methyl-Len) are provided in Figure 17B to show the CRBN and BET targeting groups. Moreover, *N*-methyl-dBET1 confirms that this analog is interacting with similar residues in the TBD. Next, the function of dBET1 in activated human T-cells was assessed and results are shown in Figure 17C-F, statistical analysis provided in Table 7. Unlike Len and Pom which activate T-cells, BRD4 and c-Myc inhibition is expected to induce cell death or functionally repress these cells as they are critical mediators of T-cell proliferation and survival [119, 120]. Relative viability of activated T-cells is reduced by dBET1 treatment compared to DMSO and is more active relative to treatment with increasing doses of JQ1 (Figure 17C) suggesting that growth suppression by the heterobifunctional conjugate is superior to JQ1, as shown previously in leukemia cells [51].

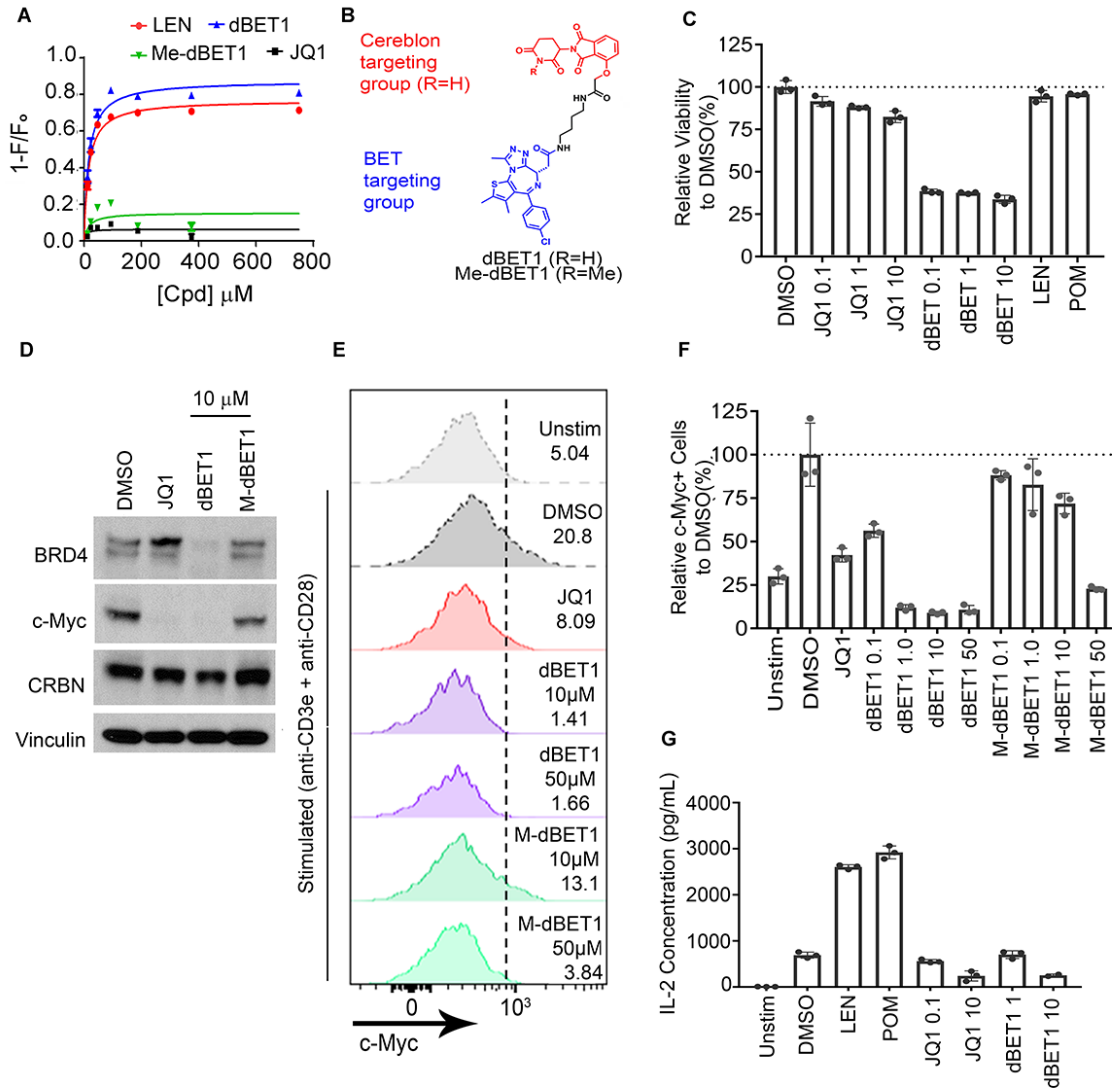


**Figure 17. Functional activity of lenalidomide, JQ1 and dBET1 in human T cells and binding affinities of JQ1, dBET1 and Len to human CRBN. (A)** Saturation binding curves of human TBD wild-type titrated with lenalidomide (Lenalidomide,  $K_D=15.6\pm 2.2$ ), JQ1 (no binding), dBET1 ( $K_D=26.0\pm 2.1$ ), *N*-methyl-dBET1 (no binding) by fluorescence assay (see also Table 1 for a summary of all  $K_D$  values). **(B)** Structure of dBET1 and *N*-methyl-dBET1. **(C)** Human T-cells purified from peripheral blood mononuclear cells (PBMCs) from healthy donors and stimulated with anti-CD3 $\epsilon$  /CD28. At the time of TCR stimulation, DMSO (vehicle control), indicated concentrations of JQ1 and dBET1, 10  $\mu$ M lenalidomide (Len) and 10  $\mu$ M pomalidomide (Pom) were added to the cell cultures. Cell viability was determined after 72 h by flow cytometry using Zombie NIR™ staining. **(D)** Western blot analysis for expression of BRD4, CRBN, c-Myc and vinculin in human T cells stimulated with anti-CD3 $\epsilon$  /CD28 and treated simultaneously with vehicle (DMSO, 0.1%), JQ1, dBET1 (10 $\mu$ M) and *N*-methyl-dBET1 (10  $\mu$ M) for 48 h. Unstimulated cells are not shown in D. **(E)** c-Myc expression by flow cytometry (histogram data) is shown following 48 hrs stimulation with anti-CD3 $\epsilon$  /CD28. Drug treatments and doses are

indicated. Expression of c-Myc requires stimulation based on comparison with unstimulated cells (unstim). Values represent % positive relative to unstimulated cells based on gate (dotted line). **(F)** Quantification of flow data shown in **(E)** represented as % of DMSO. Bar height is the mean of individual values shown representative of three independent experiments. Error bars represent standard deviation from an exemplary experiment. **(G)** Unstimulated (unstim) or anti-CD3 $\epsilon$  /CD28 stimulated T-cells were treated with 10  $\mu$ M Len, 10  $\mu$ M Pom, and indicated doses of JQ1 or dBET1. Enzyme-linked immunosorbent assays (ELISA) were used to quantify IL-2 concentrations (pg/mL) from supernatants harvested at 48 hrs. Results shown are representative of three independent experiments. Bar height represents mean of individual values and error bars represent standard deviation from an exemplary experiment. Results of statistical analysis provided in Table 7.

Importantly, decreased BRD4 protein expression is only evident with dBET1 treatment, while both dBET1 and JQ1 suppress the activation of c-Myc protein expression by Western blot analysis (Figure 17D) and flow cytometry (Figure 17E, summary of data Figure 17F), as expected, through BRD4 functional repression. Notably, the effect on BRD4 is reversed by incubation with *N*-methyl-dBET1 at doses of 0.1 – 10  $\mu$ M. Repression of c-Myc at very high doses of *N*-methyl-dBET1 is consistent with activity of the JQ1 targeting molecule (Figure 17D and F). From these results, we conclude that human T-cells respond to dBET1 through interactions that are mediated by the hydrophobic pocket of the CRBN-TBD. Finally, the suppressive effects observed with dBET1 treatment shows that the CRBN targeting molecule in this compound is no longer activating IL-2 as shown in Len and Pom (Figure 17G).

**Table 7.** Statistical analysis of Human T cells treated with IMiD@s, JQ1 and dBET1

	Comparisons	P value	Summary
Relative Viability to DMSO (%)	DMSO vs. JQ1 0.1	0.0035	**
	DMSO vs. JQ1 1	0.0001	***
	DMSO vs. JQ1 10	0.0001	****
	DMSO vs. dBET 0.1	0.0001	****
	DMSO vs. dBET 1	0.0001	****
	DMSO vs. dBET 10	0.0001	****
	DMSO vs. LEN	0.0794	ns
	DMSO vs. POM	0.2305	ns
	JQ1 0.1 vs. dBET 0.1	0.0001	****
	JQ1 1 vs. dBET 1	0.0001	****
	JQ1 10 vs. dBET 10	0.0001	****
Relative c-Myc+ cells to DMSO (%)	DMSO vs. Naïve	0.0001	****
	DMSO vs. JQ1	0.0001	****
	DMSO vs. dBET 0.1	0.0001	****
	DMSO vs. dBET 1	0.0001	****
	DMSO vs. dBET 10	0.0001	****
	DMSO vs. dBET 50	0.0001	****
	DMSO vs. M-dBET 0.1	0.3672	ns
	DMSO vs. M-dBET 1	0.0777	ns
	DMSO vs. M-dBET 10	0.0016	**
	DMSO vs. M-dBET 50	0.0001	****
IL-2 Concentration (pg/mL)	DMSO vs. Unstimulated	0.0001	****
	DMSO vs. Len 10	0.0001	****
	DMSO vs. Pom 10	0.0001	****
	DMSO vs. JQ1 0.1	0.2527	ns
	DMSO vs. JQ1 10	0.0001	****
	DMSO vs. dBET 0.1	0.9997	ns
	DMSO vs. dBET 10	0.0002	***
	<i>P value: * &lt; 0.05, ** &lt; 0.01, *** &lt; 0.001, **** &lt; 0.0001</i>		
	<i>Note: One-way ANOVA test and unpaired two tailed t-tests were performed</i>		

Next, saturation-binding curves of V388I-TBD mutant titrated with Len ( $K_D=15.6\pm 2.2 \mu\text{M}$ ), dBET1 ( $K_D=26.0\pm 2.1 \mu\text{M}$ ), and *N*-methyl-dBET1 (non-binding control) shows that the mode and binding affinity of dBET1 is similar to the human-TBD protein (Table 5, Figure 18A). Mouse T-cells were purified from *Crbn*<sup>+/+</sup> and *Crbn*<sup>-/-</sup> mice and used to evaluate the role of mouse CRBN in BRD4 degradation (Figure 18B, C), activation-induced proliferation, viability, c-Myc and CD98 (Myc target gene) (Figure 18D-G) expression in response to dBET1 treatment (Figure 17B). TCR stimulation with anti-CD3 $\epsilon$  + anti-CD28 is required for the induction of *c-myc* in primary mouse T-cells (data not shown). Both JQ1 and dBET1 suppressed c-Myc in activated T-cells, but the reduction in protein expression of BRD4 was only observed after dBET1 treatment in *Crbn*<sup>+/+</sup> mouse T-cells consistent with proteasome engagement (Figure 18B) through a CRBN-dependent mechanism. Pomalidomide treatment failed to impact BRD4 expression and further supports redirection of CRBN's ubiquitin-conjugating function through JQ1. To assess whether dBET1 is interacting directly with the TBD of mouse CRBN *in vivo*, an assay was performed using mouse *Crbn*<sup>+/+</sup> T-cells treated with Pom in the presence and absence of dBET1. Results shown in Figure 6C show that at high concentrations of Pom (10-fold excess), the impact of dBET1 on c-Myc and BRD4 expression was reversed suggesting that dBET1 is directly engaging the TBD of mouse CRBN. We next examined proliferation (i.e., division index) measured by dilution of cell trace violet (CTV) using methods described previously[121], expression of a c-Myc target gene (CD98), and viability using flow cytometry (Figure 18D). Histograms (Figure 18D) and summarized results (Figures 18E-G) show that the division index (based on CTV data) and CD98 expression (median fluorescence intensity, MFI) is induced through activation (unstimulated

vs DMSO) and that there is a differential response to dBET1 treatment in *Crbn*<sup>+/+</sup> and *Crbn*<sup>-/-</sup> T-cells at 0.1 and 1 μM. The suppression of T-cells at 10 μM is likely related to be mediated by JQ1 targeting molecule since proliferation, c-Myc-regulated CD98 expression, and viability were suppressed independent of CRBN expression. Moreover, BRD4 degradation by dBET1 is similar in MM1.S human and 5TGM1 mouse multiple myeloma cells confirming the conserved ubiquitin conjugating functions of CRBN (Figure 19).

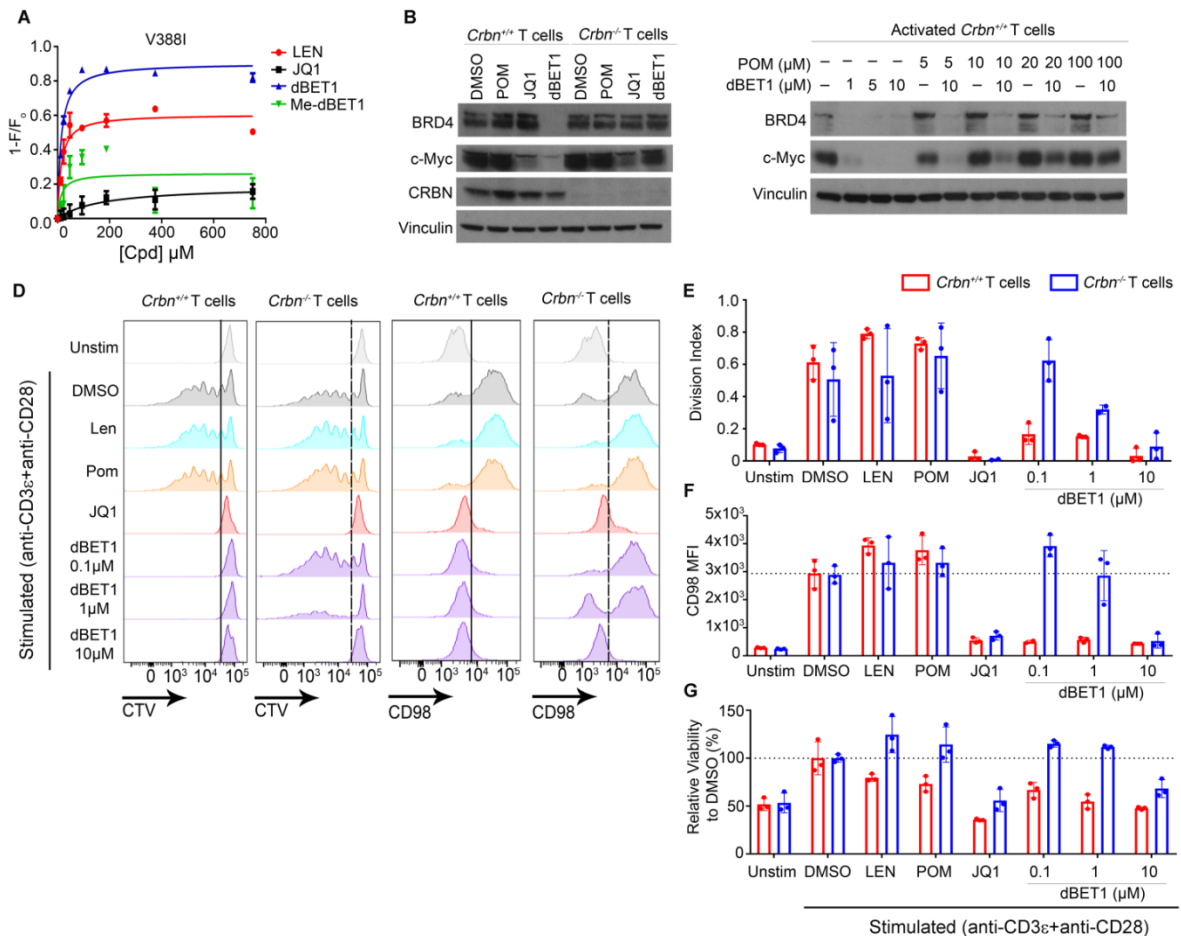


**Figure 18 Functional activity of lenalidomide, pomalidomide, JQ1 and dBET1 in mouse T cells. (A)** Saturation binding curves of human V388I mutant TBD titrated with lenalidomide (Lenalidomide, KD=18±4), JQ1 (no binding), dBET1 (KD=18±3), N-methyl-dBET1 (no binding) by fluorescence assay (see also Table 1) **(B)** Mouse T cells purified from spleens of C57BL/6j mice with homozygous deletion of *Crbn* and wild-type littermates were stimulated with anti-CD3ε /CD28 in the presence of 0.1% DMSO

(vehicle control), 10  $\mu$ M pomalidomide (Pom), 10  $\mu$ M JQ1 or 10  $\mu$ M dBET1. Western blots for BRD4, c-Myc, CRBN and vinculin (loading control) expression are shown. **(C)** Western blot analysis showing expression of BRD4, c-Myc and vinculin from *Crbn*<sup>+/+</sup> T cells stimulated with anti-CD3 $\epsilon$  /CD28 for 12 hrs with indicated doses of dBET1, pomalidomide (Pom) or combined treatment. **(D)** Purified *Crbn*<sup>+/+</sup> and *Crbn*<sup>-/-</sup> mouse T cells stimulated with anti-CD3 $\epsilon$  /CD28 and treated with 0.1% DMSO (vehicle control), 10  $\mu$ M lenalidomide (Len), 10  $\mu$ M pomalidomide (Pom), 10  $\mu$ M JQ1 or increasing doses of dBET1, for 72 hrs. Histogram plots from one experiment showing proliferation (determined by dilution of CellTrace™ Violet, CTV) and CD98 expression of T cells. **(E)** Proliferation index based on CTV data was used to calculate the amount of proliferation using an algorithm available with Flowjo analysis software (Tree Star). **(F)** Expression of CD98 was calculated relative to unstimulated cells using gates shown based on mean fluorescence intensities (MFI) of T cells as shown in Figure 6(D). **(G)** Cell viability was determined after 72 h by flow cytometry using Zombie NIR™ staining. Results shown are representative of three independent experiments. Bar height represents mean of individual values and error bars represent standard deviation from an exemplary experiment. Results of statistical analysis provided in Table 8.

**Table 8.** Statistical analysis of *Crbn*<sup>+/+</sup> and *Crbn*<sup>-/-</sup> mouse T cells treated with IMiD@s, JQ1 and dBET1

	Comparisons	<i>Crbn</i> <sup>+/+</sup> T cells		<i>Crbn</i> <sup>-/-</sup> T cells		
		P value	Summary	P value	Summary	
Division Index	DMSO vs. Unstimulated	0.0001	****	0.0414	*	
	DMSO vs. Len 10	0.0033	**	0.9997	ns	
	DMSO vs. Pom 10	0.0606	ns	0.8222	ns	
	DMSO vs. JQ1 10	0.0001	****	0.0332	*	
	DMSO vs. dBET1 0.1	0.0001	****	0.9258	ns	
	DMSO vs. dBET1 1	0.0001	****	0.7327	ns	
	DMSO vs. dBET1 10	0.0001	****	0.0486	*	
CD98 MFI	DMSO vs. Unstimulated	0.0001	****	0.0001	***	
	DMSO vs. Len 10	0.0042	**	0.8548	ns	
	DMSO vs. Pom 10	0.0166	*	0.8545	ns	
	DMSO vs. JQ1 10	0.0001	****	0.0007	***	
	DMSO vs. dBET1 0.1	0.0001	****	0.1391	ns	
	DMSO vs. dBET1 1	0.0001	****	0.9999	ns	
	DMSO vs. dBET1 10	0.0001	****	0.0003	***	
Relative Viability to DMSO (%)	DMSO vs. Unstimulated	0.0001	****	0.0008	***	
	DMSO vs. Len 10	0.0403	*	0.0888	ns	
	DMSO vs. Pom 10	0.0058	**	0.5164	ns	
	DMSO vs. JQ1 10	0.0001	****	0.0014	**	
	DMSO vs. dBET1 0.1	0.0009	***	0.4613	ns	
	DMSO vs. dBET1 1	0.0001	****	0.6999	ns	
	DMSO vs. dBET1 10	0.0001	****	0.0201	*	
<i>P</i> value: * < 0.05, ** < 0.01, *** < 0.001, **** < 0.0001						
Note: One-way ANOVA test was performed						
Treatment	Division Index		CD98 MFI		Relative Viability to DMSO (%)	
	P value	Summary	P value	Summary	P value	Summary
Unstimulated	0.155588597		0.05084322		0.83166901	
DMSO	0.504634139		0.892919422		>0.999999999	
Len 10	0.199850179		0.330034149		0.015520559	*
Pom 10	0.556480278		0.340153344		0.024144854	*
JQ1 10	0.38380327		0.175397332		0.041173393	*
dBET1 0.1	0.005508063	**	0.0013032	**	0.000683123	***
dBET1 1	0.001725291	**	0.011696605	*	0.000215894	***
dBET1 10	0.355268196		0.567427617		0.019352985	*
<i>P</i> value: * < 0.05, ** < 0.01, *** < 0.001, **** < 0.0001						
Note: Holm-Sidak multiple comparison <i>t</i> -test was performed comparing <i>Crbn</i> <sup>+/+</sup> to <i>Crbn</i> <sup>-/-</sup> T cells						



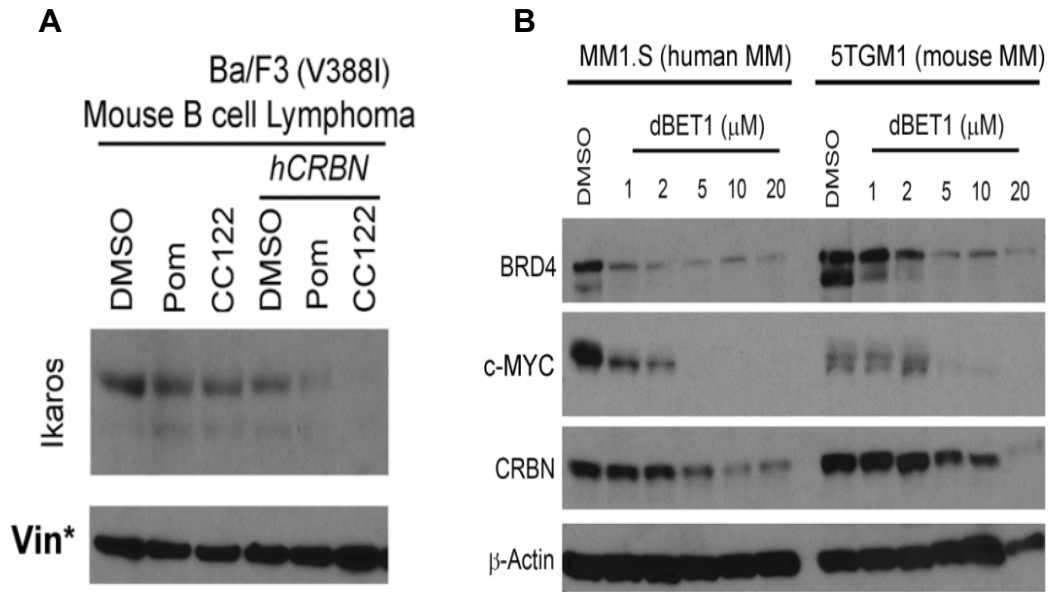


**Figure 19. Drug Treatment of human and mouse multiple myeloma cell lines. (A)** BaF/3, mouse B cell lymphoma, and BaF/3 with full length human CRBN (hCRBN) overexpression were treated with Pom, CC-122 (Ava) or vehicle control DMSO. Ikaros and vinculin (loading control) expression levels were assessed via western blot analysis. **(B)** MM1.S and 5TGM1 cells were treated with increasing concentrations of dBET1 for 24 hours. Protein expression levels of BRD4, c-Myc, CRBN,  $\beta$ -actin were determined by western blot.

## Discussion

CRBN was first identified in mild autosomal recessive non-syndromic intellectual disability (ID) [122], but has poorly defined physiological functions. Interactions have been reported with the AMP-activated protein kinase (AMPK)  $\alpha$ 1 subunit [58], TAK1/TRAF6 [123], and CD147/MCT1 complex [61] where CRBN plays ubiquitin-independent roles in pathway regulation. The mechanistic underpinnings for induced limb deformities in chickens and zebrafish, but not in mice, appears dependent on sequence differences in mouse CRBN [31], which brings into question whether these differences in CRBN render it functionally inactive. Although reference CRBN sequences for nearly all examined

primates possess Val388, according to the Exome Aggregation Consortium (ExAC), the Ile391 variant occurs in humans at a frequency of 0.005% (rs756414303). Our data shows that mutating Val388 to Ile (V388I) does not alter binding affinity to the immunomodulatory compounds suggesting that the contact between the immunomodulatory drug and the CRBN-TBD is maintained and potentially functionally active. When bound to immunomodulatory drugs (Len, Pom, and CC-122), CRBN induces the destruction of three substrates Ikaros, Aiolos, and CK1 $\alpha$  [35] via a V388 interaction [14]. In T cells, the IKZF-family transcription factors repress *IL2* so that ubiquitin-mediated destruction may be responsible for promoting T cell activation [33, 35]. Our data solidifies the mechanistic involvement of CRBN Ile391 in drug resistance in mouse cell lines, as suggested previously by overexpression of *hCRBN* with V388, but not I391 in Ba/F3 cells was sufficient to restore Ikaros protein destruction [31, 35].

As expected, using dBET1, there was no Ikaros degradation in mouse T-cells or mouse myeloma cell lines. However, we found that dBET1, impressively reduced the expression of BRD4 in both human and mouse cells. Therefore, proximity-associated ubiquitin conjugating functions of mouse and human CRBN are confirmed using dBET1. *Crbn*<sup>-/-</sup> T-cells demonstrated that dBET1 functions through a CRBN-TBD dependent process. Competition with Pom further suggests that the TBD of human and mouse CRBN have similar binding modes for immunomodulatory compounds suggesting that there is both structural and functional conservation. Thus, the endogenous E3-ubiquitin ligase activity and assembly of the CRBN-DDB1-CUL4A containing complex is fundamentally conserved across the vertebrate lineage, including the mouse, and likely other species, expressing Ile391. Moreover, other sequence variants present in mouse

CRBN, including difference in the N-terminus, fail to impact its substrate recruiting functions when targeting BRD4. This observation along with the high degree of CRBN conservation indicates that selective pressure has maintained the overall structure and function in CRBN for over 400 million years.

Using ITC and fluorescence-based binding assays, we establish that the dissociation constants of thalidomide and other immunomodulatory compounds to mouse CRBN are similar to human CRBN, which is consistent with analysis of the crystal structure of human CRBN-DDB1 in complex with Len [13, 112]. As suggested previously [112], the W380A mutant completely abolished binding and confirms that this is one of the key residues of the binding pocket. Trp380 also appears to work synergistically with other binding pocket residues (Trp386, Trp400 and Phe402) for ligand interaction. The  $K_D$  values of immunomodulatory compounds in complex with the human TBD (aa 319-425) are in the  $\mu\text{M}$  range similar to those of *C. elegans* and *Magnetospirillum gryphiswaldense* [124]. Based on the conserved CRBN structure, we synthesized *N*-methyl derivatives of Len and dBET1 which proved useful in assessing the functional contribution of this ligand interaction *in vivo* in mouse and human cells.

Here, we show an interesting reliance of the rigid TBD binding pocket on N-terminal sequences and plays a previously unappreciated role in optimal ligand binding. A conformational change in full-length CRBN-DDB1 may occur upon ligand binding as shown by the difference in their  $\Delta H$  and  $\Delta S$  values (Figure 13). Notably, the CRBN-DDB1 complex and CRBN-TBD show marked difference in Len binding affinity by ITC. In fact, a closer inspection of the crystal structure of full-length CRBN in complex with Len illustrates that a disordered loop in the TBD consisting of residues Asn351, Pro352, and

His353 stabilizes the interaction of Len. Asn351 forms a hydrogen bond to carbonyl oxygen of Len's isoindolinone ring and both Pro352 and His353 form hydrophobic interactions with the aromatic system of the immunomodulatory drug (Figure 13E). Importantly, the mouse TBD crystal structure shows poor electron density in this loop structure suggesting it is a highly unstructured and dynamic region. Alternatively, other residues outside the TBD could have stabilized this loop. The side chain of Gln100, which is located in the LON domain of CRBN, forms a weak hydrogen bond interaction to the  $\epsilon^2\text{NH}$  group of His378. This in turn positions the  $\delta^1\text{NH}$  of His378 as a hydrogen donor to the immunomodulatory drugs. These important structural domains should be further investigated in immunomodulatory drug discovery.

Collectively, our results suggest that PROTAC molecules and possibly other CRBN-bound compounds may adopt an active conformation that is susceptible to CRBN-directed, cullin-RING E3 ligase-mediated polyubiquitination in mouse cells. PROTAC molecules are designed to harness the CRBN-binding properties of IMiD®s and initiate the degradation of oncogenic targets. Several IMiD®-based BET targeting PROTACs such as dBET-1, ARV-825 and BETd-260 have been developed to potentially degrade BRD4 [52, 125, 126]. Intracellular protein degradation of FK506 binding protein (FKBP12) was also achieved by a conjugate of thalidomide [51, 127], but originally, methionine aminopeptidase-2 (MetAP-2) [46], estradiol (E2) and dihydrotestosterone (DHT) were degraded by engaging the Skp1-Cullin-F-box (SCF) ubiquitin ligase through a 10 amino acid phosphopeptide derived from I $\kappa$ B $\alpha$  [50, 128]. PROTAC with specificity for the von Hippel-Lindau (VHL) ubiquitin ligase E3 have also been developed [129, 130]. Recently, BRD4 and ERK1/2 degradation was induced by the interaction of two smaller precursors

molecules that undergo intracellular self-assembly which improves solubility and cellular permeability of thalidomide-containing PROTAC inhibitors [131]. Importantly, our studies establish that mouse platforms can indeed be used for preclinical development of dBET1, and possibly other PROTAC-based chemical degraders that are designed to re-direct CRBN's substrate binding function toward specified endogenous proteins [46, 50, 51, 125, 131, 132]. Toxicology and functional testing of such agents in rodents and mouse tumor models may yield important preclinical information. CRBN interacts intracellularly with calcium-activated potassium channels and the metabolic sensor adenosine monophosphate-activated protein kinase (AMPK), which in the latter, suppresses its activation and its downstream target mammalian target of rapamycin (mTOR) [58, 133, 134]. Collectively, this data suggests that there may be multiple endogenous substrates of CRBN and that the immunomodulatory drugs may influence its physiological function. One study in particular proposes a ubiquitin-independent physiological role CRBN as a chaperon stabilizing the CD147-MCT1 complex [135]. In this study, researchers show the CD147-MCT1 complex is vital for the regulation of cellular metabolism and expression of fibroblast growth factor 8, which is the transcription factor reported to mediate thalidomide-associated teratogenicity in zebrafish and chickens [28]. Furthermore, through elegantly designed experiments, researchers show that thalidomide treatment destabilizes the CD147-MCT1 complex and that morpholino-induced loss of CD147 suppress limb development similar to drug treatment [135].

Collectively, these studies provide insight into aspects of CRBN biology relevant for the preclinical development of PROTAC compounds in humans. Moreover, we highlight the potential disadvantages of using CRBN-targeting PROTAC compounds as

they all may harbor teratogenic potential. Using new agents, it may be possible to understand fundamental roles for CRBN and avoid its proteasome or non-proteasome-related protein targets that are associated with fetal development.

## **Experimental Procedures**

### **Animals and cell lines**

Germline *Crbn* deficient mice (*Crbn*<sup>-/-</sup>) were described previously [122] and gene deletion was confirmed using wild-type and *Crbn*-KO-specific primers. C57BL/6 (*Crbn*<sup>+/+</sup>) mice were purchased from Jackson Laboratory (Farmington, CT) and were then bred to *Crbn*<sup>-/-</sup> mice. *Crbn*<sup>+/+</sup> and *Crbn*<sup>-/-</sup> littermates from *Crbn*<sup>+/-</sup> intercrosses were used for our studies. Mice were maintained and bred at the H. Lee Moffitt Cancer Center and Research Institute under a protocol approved by the Institutional Animal Care and Use Committee (IACUC). The human multiple myeloma cells including U266, H929, MM1.S, and the mouse multiple myeloma cell line 5TGM1, were generous gifts of Drs. Ken Shain and Connor Lynch (Moffitt Cancer Center, Tampa, FL). All cell lines were mycoplasma free and sequence verified.

### **T-cell isolation, activation and drug treatments**

Human polyclonal CD3<sup>+</sup> T cells or CD8<sup>+</sup> T cells were isolated from peripheral blood donations to the Southwest Florida Blood Services. Since personal identifying information is unavailable, the research was deemed non-human research. Human and mouse T cells were isolated from *Crbn*<sup>+/+</sup> and *Crbn*<sup>-/-</sup> splenocytes by immunomagnetic negative selection (Miltenyi Biotec, San Diego, CA) and >95% purity was confirmed by

flow cytometry. For drug treatment experiments, 12-well flat bottom plates were coated with 5 µg/mL anti-CD3ε (clone# HIT3a, eBioscience or clone# 145-2C11) in 1x PBS at 37°C for 60 min. Cells were plated at 2-4x10<sup>6</sup> cells per well with anti-CD28 (clone# CD28.2, eBioscience or clone# 37.51, eBioscience). Following 12 h of activation, the cells were treated with DMSO (0.1%, Sigma-Aldrich, MO), Len (10 µM) (Celgene, NJ), Pom (Sigma-Aldrich), and JQ1 (doses indicated) (Cat# SML0974, Sigma-Aldrich). *N*-methyl-Len, dBET1, and *N*-methyl-dBET1 were all synthesized at Moffitt Cancer Center (described in supplementary material) and used at the doses indicated. After 12 hrs of drug treatment, cells were harvested, and protein levels were examined by western blot analysis. For proliferation experiments using mouse T cells, 0.1-10 µg/mL anti-CD3ε (clone# 145-2C11, eBioscience) was used with cells plated with and without anti-CD28 for 72 h. Cytokine expression was determined using supernatants that were harvested at 24 or 48 h and quantified from standard curves by enzyme-linked immunosorbent assay (ELISA) according to the manufacturer's protocol. Kits were purchased from eBioscience (IL-2) and R&D Systems for other cytokines. For functional analysis of T cells treated with JQ1, murine CD3<sup>+</sup> T cells from *Crbn*<sup>+/+</sup> and *Crbn*<sup>-/-</sup> splenocytes and human T cells were labeled with 5-10 µM CellTrace Violet (C34557, ThermoFisher) and activated with 5 µg/mL anti-CD3ε and 1µg/mL anti-CD28 for 72 h in round-bottom 96-well plates. Cells were stained with CD98-PE (clone# RL388, Biolegend), 7-AAD (BD Pharmingen) and Zombie NIR™ Fixable Viability Kit (Cat # 423105, Biolegend) and analyzed on a BD LSRII.

## qRT-PCR

Isolated T cells from *Crbn*<sup>+/+</sup> and *Crbn*<sup>-/-</sup> mice were lysed, homogenized (Qiashredder, Qiagen), and total RNA extracted (RNeasy, Qiagen) according to manufacturer protocol. Complementary DNA was generated from isolated RNA (iScript cDNA synthesis Kit, Bio-Rad). RNA expression was analyzed by quantitative real time-polymerase chain reaction (qRT-PCR) using Taqman Universal PCR Master Mix for Taqman probes (Thermo Fischer Scientific) against (cDNA) *c-Myc* (Mm00487804\_m1) and (cDNA)  $\beta$ 2M (Mm00437762\_m1). Samples were run on an Applied Biosystems 7900 HT and Sequence Detection Systems software.

## Treatment of multiple myeloma cells

Mouse and human multiple myeloma cell lines were plated at  $2-4 \times 10^6$  cells per well in a 12-well plate with various concentrations of Len and Pom. To confirm target degradation, the cells were treated with varying concentrations of dBET1 (0, 0.01, 0.1, 1, and 10  $\mu$ M) for 12-24 h. Following drug treatment, protein levels were examined by western blot analysis relative to vinculin or  $\beta$ -actin to normalize for protein expression. For proliferation studies,  $1-2 \times 10^4$  cells per well were seeded in a 96-well plate and were treated with using cell-counting-8 kit (CCK8) (Dojindo, Rockville, MD) according to manufacturer's protocol.

## General chemistry information

All reagents were purchased from commercial suppliers and used without further purification (except where mentioned otherwise). <sup>1</sup>H NMR spectra were recorded on an



Agilent-Varian Mercury 400 MHz spectrometer with DMSO-d<sub>6</sub> as the solvent. All coupling constants are measured in Hertz, and the chemical shifts ( $\delta$ H) are quoted in parts per million relative to TMS ( $\delta$  0), which was used as the internal standard. High-resolution mass spectroscopy was carried out on an Agilent 6210 LC-MS (ESI-TOF) system. HPLC analysis was performed using a JASCO HPLC system equipped with a PU-2089 Plus quaternary gradient pump and a UV-2075 Plus UV-Vis detector, using an Alltech Kromasil C-18 column (150 × 4.6 mm, 5  $\mu$ m) and an Agilent Eclipse XDB-C18 column (150 × 4.6 mm, 5  $\mu$ m). The purities of the final compounds used for the biochemical and functional studies were >95% as measured by HPLC. Melting points were recorded on an Optimelt automated melting point system (Stanford Research Systems). Thin-layer chromatography was performed using silica gel 60 F254 plates (Fisher Scientific), with observation under UV when necessary. Anhydrous dimethylformamide was used as purchased from Sigma Aldrich. Burdick and Jackson HPLC-grade solvents were purchased from VWR for HPLC, HPLC-MS and high-resolution mass analysis. dBET1 (HPLC purity 98%) was prepared from JQ1 as described [51]. Detailed information about the synthesis of *N*-methyl-Len, and *N*-methyl-dBET1 synthesis are provided in the supplementary material.

### **Cloning, protein expression and purification**

The full-length hCRBN protein (isoform 1) in complex with the DNA-damage binding protein (DDB1) was a generous gift from Celgene Corporation (San Diego, CA). The gene coding for the human TBD (aa 319-425) was synthesized and subcloned into the BamHI-NotI restriction sites of the pGEX-6P-1 vector by GeneArt® Gene Synthesis. The gene was engineered with silent mutations that utilize the favored *E. coli* codons.

TBD E377V, V388I, H378A and W380A mutations were performed using polymerase chain reaction. Details of primer sequences are provided in supplemental material. Mutations were confirmed by sequencing. The recombinant DNA plasmids were transformed into *E. coli* Rosetta™ 2(DE3)pLysS competent cells (EMD Millipore, Billerica, MA) for subsequent protein expression. The GST-tagged TBD proteins linked with PreScission protease proteolytic site were expressed and purified as follows: A single colony of freshly transformed cells was cultured at 37 °C for 16 h in 5 mL of Luria-Bertani (LB; Thermo Fisher Scientific) medium containing 100 µg/mL of ampicillin (Sigma-Aldrich) and 34 µg/mL of chloramphenicol (Sigma-Aldrich). 1 mL of the culture was then used to inoculate 25 mL of Terrific Broth-phosphate medium (TB; Thermo Fisher Scientific) with 100 µg/mL ampicillin at 37 °C for 16 h. The culture was then transferred to 1.5 L of TB medium supplemented with 50 µM ZnCl<sub>2</sub> (Sigma-Aldrich). The resultant culture was incubated with continuous shaking at 250 rpm to an OD<sub>600</sub> of 0.70 and then induced with isopropyl-β-D-1-thiogalactopyranoside (IPTG; 0.5 mM final concentration; Thermo Fisher Scientific) at 16 °C for 20 h prior to harvesting by centrifugation at 6000 rpm for 30 min. The cells were lysed by homogenization in 50 mM Tris (pH 8.0; Sigma-Aldrich), 500 mM NaCl (Thermo Fisher Scientific), 1 mM TCEP (Sigma-Aldrich), 0.1% Triton X-100 (Sigma-Aldrich), 10 µM ZnCl<sub>2</sub> (Acros Organics, Thermo Fisher Scientific) and protease inhibitor cocktail (Roche). The protein was then purified by affinity chromatography on an AKTA Explorer or AKTA Purifier (GE Healthcare Life Sciences) using a glutathione-Sepharose matrix (GE Healthcare Life Sciences, Pittsburgh, PA) pre-equilibrated with 50 mM Tris (pH 8.0), 500 mM NaCl, 1 mM TCEP, and 10 µM ZnCl<sub>2</sub>, and eluted with the same buffer with the addition of 10 mM reduced glutathione (Sigma-Aldrich). Purity of the protein in

the different fractions was determined by SDS-PAGE and the best fractions were pooled. GST was cleaved from the pooled GST-TBD fractions by digestion with PreScission protease at 4 °C for 4 h. GST was removed from the resultant digest by a second round of GST affinity chromatography. Proteins were further purified by size-exclusion chromatography in a Superdex 75 column (GE Healthcare Life Sciences). Fractions with >90% purity were pooled, concentrated by ultrafiltration (10K Amicon tubes, EMD Millipore) and stored at -80 °C.

### **Isothermal titration calorimetry (ITC)**

The binding of CRBN-DDB1 complex and CRBN-TBD wild-type and mutant variants to immunomodulatory compounds was analyzed with MicroCal iTC200 titration calorimeter (Malvern, Westborough, MA). The compound phthalimide was used as the negative control. The proteins were re-buffered into binding buffer (50 mM HEPES (pH 7.5, Sigma-Aldrich), 200 mM NaCl, 0.1 mM TCEP and 0.6% DMSO). For the titrations of the protein constructs, a total of 19 aliquots (2.05  $\mu$ l each) of the respective compounds (~600  $\mu$ M) were injected into 200  $\mu$ l of the protein solutions (40  $\mu$ M) at 25°C. The ITC cell mixture was constantly stirred at 1000 rpm and recorded for 160 s between injections at low feedback. The corrected heat values were fitted using a nonlinear least square curve-fitting algorithm (Microcal Origin 7.0, OriginLab, Northampton, MA) to obtain binding constants ( $K_D$ ) and values for n (number of binding sites),  $\Delta H$  (enthalpy) and  $\Delta S$  (entropy).

## **Intrinsic tryptophan fluorescence assay**

Binding of compounds to wild-type and mutant TBD was monitored by fluorescence spectroscopy, using an adapted previously published method [107, 124]. All chemicals used in this assay were purchased from Sigma-Aldrich unless otherwise stated. In this assay, changes in emission spectra are induced by interactions of these compounds with the three Trp residues (Trp380, Trp386 and Trp400) in the binding site [13, 112]. TBD proteins (final concentration, 10  $\mu\text{M}$ ) were incubated with varying final concentrations (0-750  $\mu\text{M}$ ) of compounds in assay buffer (50 mM Tris, pH 7.5, 200 mM NaCl, 0.1% Pluronic-F127, and 1 mM TCEP) to a final volume of 40  $\mu\text{L}$  in a black 96-well half area plate (Corning, Corning, NY). A 0.5% final DMSO concentration was used in each well. Samples were excited at 280 nm and fluorescence emission intensities were measured at 340 nm using Wallac Envision 2102 multilabel plate reader (Perkin Elmer, Waltham, MA). All measurements were done in triplicate and corrected for inner filter effect to subtract for ligand-associated fluorescence, as described [136]. The magnitude of fluorescence difference ( $1-F/F_0$ ) was measured where F is the fluorescence emission at a given concentration of ligand;  $F_0$  is the intrinsic fluorescence intensity of 10  $\mu\text{M}$  of TBD protein alone. Graph plotting and curve fitting to obtain apparent dissociation constant ( $K_D$ ) values were calculated by fitting the relative change in intrinsic fluorescence at 340 nm ( $1-F/F_0$ ) versus ligand concentration to a nonlinear regression with one-site binding hyperbola with GraphPad Prism Software (GraphPad Software, La Jolla, CA).

## **Theoretical Calculations**

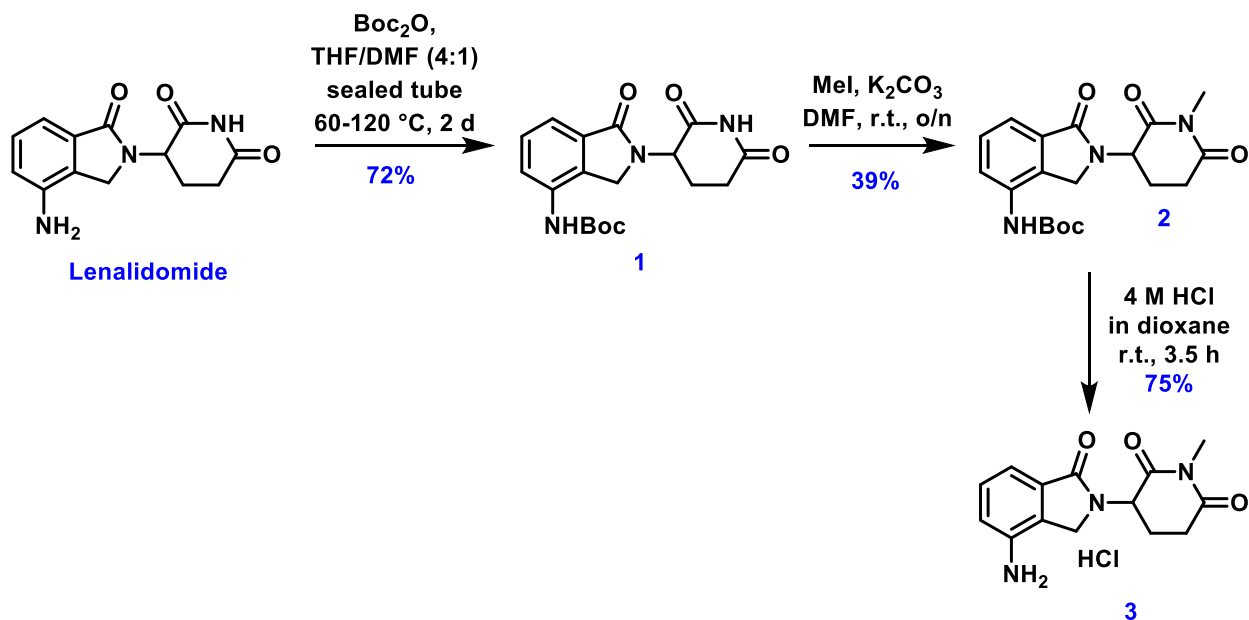
The preparation of the protein systems for human cereblon (hCRBN, PDB

4TZ4[112], murine cereblon (mCRBN, PDB 4TZC and 4TZU)[112] and galline cereblon (gCRBN, PDB 4CI1, 4CI2, and 4CI3)[13] were done using the Schrodinger software suite (Maestro, version 9.7, Schrödinger, LLC, New York, NY, 2014). Protein structure coordinates were downloaded from the Protein Data Bank (PDB) [137, 138] and prepared with the Protein Preparation Wizard (PrepWizard) in Maestro (Schrödinger Suite 2014-1 Protein Preparation Wizard; Epik version 2.7, Schrödinger, LLC, New York, NY, 2013; Impact version 6.2, Schrödinger, LLC, New York, NY, 2014; Prime version 3.5, Schrödinger, LLC, New York, NY, 2014)[139]. Final system equilibration was determined by the observation of asymptotic behavior of the potential energy, RMSD, and Rg profiles and visual inspection of trajectories guided by RMSF profiles (supplementary material provides additional detailed settings). MD simulations were performed with the Desmond MD program with additional details provided in Supplementary Materials and Methods (Desmond Molecular Dynamics System, version 3). After equilibration was determined, a hierarchical average linkage clustering method based on RMSD was utilized to determine an average representative structure for each equilibrated system. The program PROPKA was then implemented again on the equilibrated structures to test consistency of side chain protonation states at 7.4 pH.

### **Detailed chemical methods**

#### **Synthesis of *tert*-Butyl (2-(2,6-dioxopiperidin-3-yl)-1-oxoisindolin-4-yl)carbamate**

**(1):**



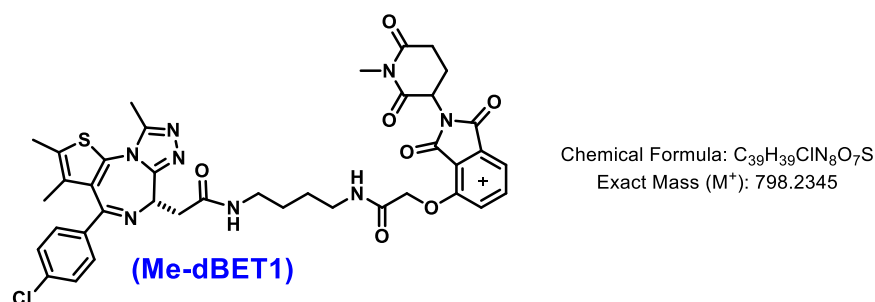
Lenalidomide (259 mg, 1 mmol) and  $\text{Boc}_2\text{O}$  (218 mg, 1.1 mmol) were mixed in THF (1 mL) in a sealed tube and stirred at 60 °C overnight. The next day,  $\text{Boc}_2\text{O}$  (110 mg, 0.5 equiv.), THF (1 mL), and DMF (0.5 mL) were added and the solution was further stirred at 120 °C overnight. Water (20 mL) was added and the mixture was sonicated. The precipitate was filtered, washed with water (10 mL), and dried. The resulting solid was triturated using EtOH/EtOAc/hexanes and filtered to give the desired product as an off-white solid (258 mg, 72%). Mp: 196–198 °C. HPLC–MS (ESI+):  $m/z$  741.3 ((100%,  $2\text{M}+\text{Na}^+$ ), 719.4 ((40%,  $2\text{M}+\text{H}^+$ ), 360.2 ((90%,  $\text{M}+\text{H}^+$ )).  $^1\text{H}$  NMR (400 MHz,  $\text{DMSO-}d_6$ ):  $\delta$  11.00 (s, 1H), 9.21 (s, 1H), 7.74 (dd,  $J = 6.8, 1.7$  Hz, 1H), 7.49–7.39 (m, 2H), 5.10 (dd,  $J = 13.3, 4.7$  Hz, 1H), 4.41 (d,  $J = 17.6$  Hz, 1H), 4.32 (d,  $J = 17.6$  Hz, 1H), 2.95–2.83 (m, 1H), 2.64–2.54 (m, 1H), 2.40–2.26 (m, 1H), 2.05–1.95 (m, 1H), 1.46 (s, 9H). Compound 1 was reported previously [51].

***tert*-Butyl (2-(1-methyl-2,6-dioxopiperidin-3-yl)-1-oxoisoindolin-4-yl)carbamate (2):**

To a mixture of **1** (100 mg, 0.278 mmol) and  $K_2CO_3$  (38 mg, 0.278 mmol) in DMF (0.8 mL) was added methyl iodide (0.017 mL, 0.278 mmol) dropwise at room temperature under Argon. The mixture was stirred overnight. Water (10 mL) was added and extracted with EtOAc (2 × 20 mL). The combined organic layers were dried ( $Na_2SO_4$ ), filtered, and concentrated under reduced pressure. The resulting yellow oil was purified by flash chromatography ( $SiO_2$ ) eluting with hexanes in EtOAc (80% to 100%) to provide the title compound as a white solid (40.37 mg, 39%). Mp: 192 °C (dec). HPLC–MS (ESI+):  $m/z$  741.3 ((100%,  $2M+Na$ )<sup>+</sup>), 719.4 ((40%,  $2M+H$ )<sup>+</sup>), 360.2 ((90%,  $M+H$ )<sup>+</sup>). <sup>1</sup>H NMR (400 MHz,  $DMSO-d_6$ ):  $\delta$  9.20 (s, 1H), 7.73 (dd,  $J = 6.5, 2.3$  Hz, 1H), 7.49–7.41 (m, 2H), 5.16 (dd,  $J = 13.4, 5.1$  Hz, 1H), 4.42 (d,  $J = 17.6$  Hz, 1H), 4.30 (d,  $J = 17.6$  Hz, 1H), 3.02–2.90 (m, 1H), 2.99 (s, 3H), 2.80–2.71 (m, 1H), 2.40–2.27 (m, 1H), 2.07–1.97 (m, 1H), 1.46 (s, 9H).

**3-(4-Amino-1-oxoisoindolin-2-yl)-1-methylpiperidine-2,6-dione (3 or *N*<sup>1</sup>-methyl-lenalidomide):** **2** (35 mg, 0.093 mmol) was stirred in 4 M HCl in dioxane (0.5 mL) for 3.5 h at room temperature. The white suspension was concentrated under reduced pressure and the resulting solid was triturated in DCM/hexanes, washed with EtOAc and hexanes (10 mL each), and dried to provide the title compound as light yellow flakes (21.81 mg, 75%). Mp: 207 °C (dec). HPLC: 99% ( $t_R = 11.6$  min, 10% MeOH, 90% water (with 0.1% TFA), 20 min). <sup>1</sup>H NMR (400 MHz,  $DMSO-d_6$ ):  $\delta$  7.29 (t,  $J = 7.5$  Hz, 1H), 7.11 (d,  $J = 7.5$  Hz, 1H), 6.99 (d,  $J = 7.5$  Hz, 1H), 5.17 (dd,  $J = 13.4, 4.7$  Hz, 1H), 5.20–4.80 (br s, 2H, disappeared on  $D_2O$  shake), 4.28 (d,  $J = 17.0$  Hz, 1H), 4.17 (d,  $J = 17.0$  Hz, 1H), 3.05–2.91 (m, 1H), 2.99 (s, 3H), 2.80–2.70 (m, 1H), 2.39–2.25 (m, 1H), 2.08–1.97 (m, 1H). HPLC–MS (ESI+):  $m/z$  569.2 ((30%,  $2M+Na$ )<sup>+</sup>), 274.2 (

(100%, M+H)<sup>+</sup>). LC–MS (ESI<sup>+</sup>): 569.2 (40%, (2M+Na)<sup>+</sup>), 296.1 (100%, (M+Na)<sup>+</sup>). HRMS (ESI<sup>+</sup>): *m/z* calcd for C<sub>14</sub>H<sub>15</sub>N<sub>3</sub>O<sub>3</sub> (M+H)<sup>+</sup> 274.1186, found 274.1176.



**2-((S)-4-(4-Chlorophenyl)-2,3,9-trimethyl-6H-thieno(3,2-f)(1,2,4)triazolo(4,3-a)(1,4)diazepin-6-yl)-N-(4-(2-((2-(1-methyl-2,6-dioxopiperidin-3-yl)-1,3-**

**dioxoisindolin-4-yl)oxy)acetamido)-butyl)acetamide (Me-dBET1):** This was prepared from *N*-Boc amino glutarimide as a white solid. HPLC: 99% (*t<sub>R</sub>* = 24.7 min, gradient 5-95%, MeOH-water (with 0.1% TFA), 30 min). <sup>1</sup>H NMR (400 MHz, Methanol-*d*<sub>4</sub>) δ 7.82 (dd, *J* = 8.4, 7.4, Hz, 1H), 7.53 (dd, *J* = 7.2, 0.4 Hz, 1H), 7.47–7.38 (m, 5H), 5.14 (dt, *J* = 12.9, 5.1 Hz, 1H), 4.78 (s, 2H), 4.62 (ddd, *J* = 9.0, 5.2, 0.7 Hz, 1H), 3.44–3.34 (m, 3H), 3.30–3.22 (m, 3H), 3.11 (2 xs, 3H), 2.86–2.82 (m, 2H), 2.73–2.62 (m, 4H), 2.43 (2 x d *J* = 0.9 Hz, 3H), 2.12–2.03 (m, 1H), 1.72–1.69 (m, 3H), 1.67–1.59 (m, 4H); HPLC–MS (ESI<sup>+</sup>): *m/z* 821.2 ((100%, M+Na)<sup>+</sup>), 799.3 ((70%, M+H)<sup>+</sup>); HRMS (ESI<sup>+</sup>): *m/z* calcd for C<sub>39</sub>H<sub>39</sub>ClN<sub>8</sub>O<sub>7</sub>S (M)<sup>+</sup> 798.2345, found 798.2368.

**Detailed protein production of wild-type and mutant CRBN.**

The primers used are:

1. 5'-CCAGTCTGTGTTGTAAACAGAGCCAAGAAACC-3' and 5'-GGTTTCTTGGCTCTGTTTACAACACAGACTGG-3';
2. 5'-GGTTATGCATGGACCATCGCACAGTGTAATAATTTGTGC-3' and 5'-GCACAAATTTTACTGTGCGATGGTCCATGCATAAC-3';



3. 5'-CGTCCGAGCACCGAAGCAAGCTGGTTTCCGGGTTATGC-3' and  
5'- GCATAACCCGGA AACCAGCTTGCTTCGGTGCTCGGACG-3';
4. 5'-CGAGCACCGAACATAGCGCGTTTCCGGGTTATGCATGG-3' and  
5'-CCATGCATAACCCGGAAACGCGCTATGTTCCGGTGCTCG-3',

## CHAPTER THREE

### CEREBLON E3 UBIQUITIN LIGASE RECEPTOR CONTROL OF HEMATOPOIESIS

#### Introduction

The hematopoietic system consists of heterogeneous populations that undergo continuous processes leading to the hierarchical differentiation of immature multifunctional blood cell lineages that originate from a primordial hematopoietic stem cell population (HSC) with the capacity for multipotent differentiation. During embryonic development, HSCs emerge from the hemogenic endothelium in the dorsal aorta-gonad mesonephros (AGM) region [73] at gestational day 10 (E10) and subsequently colonize the fetal liver. Thereafter during adult hematopoiesis, HSCs primarily reside in complex bone marrow niches where both internal and external factors control the differentiation of multipotent and committed progenitors into defined mature blood cell populations including erythrocytes, megakaryocytes, platelets, lymphocytes, monocytes, and granulocytes. While mature blood cells are predominantly short lived, the most rare and primitive stem cells, long-term HSCs (LT-HSCs) ( $\text{Lin}^- \text{Sca-1}^+ \text{c-Kit}^+ \text{CD150}^+ \text{CD48}^- \text{CD34}^- \text{CD135}^-$ ) in particular, maintain extensive self-renewal capabilities throughout life.

Mature LT-HSCs reside in specified bone marrow niches, predominantly the endosteal and sinusoidal niches, where they maintain long-term quiescence with brief intervals of self-renew. Control of HSC cell fate consists of an intricate network of cell-intrinsic and extrinsic factors (listed in Table 9) [140]. Although studies in recent decades have expanded our knowledge of HSC maintenance in adult bone marrow and during fetal development, knowledge gaps represent critical barriers for the success of

hematopoietic stem cell transplantation, human germline gene editing, and therapy for benign and malignant hematopoietic diseases.

**Table 9.** Cell intrinsic and extrinsic regulators of HSC quiescence<sup>[71]</sup>

Cell Intrinsic			Cell Extrinsic		
Category	Gene	Control Of Quiescence	Ligand	Receptor	Effect on Quiescence
Cell cycle	p21 p27 p18 p57 Rb/p107/p130 CyclinD1/D2/D3 Cdk4/6	+ + + + + - -	Ang-1	Tie2	+
Transcription	JunB Pbx1 FoxO1/3/4 FoxO3a Nurr1 Sc1 P53 Necdin Egr1 ELF4 AML1/Runx1 Stat5	+ + + + + + + + + - - -	THPO	Mpl	+
Other	Fbw7 Lkb1 Tsc1-mTOR Cited2 Txnip Atm Mi-2β Paf Ott1 G0S2 Akt1/2 Lnk	+ + + + + + + + + + - -	Wnt	Frizzled	+
			TGFβ	TGFBR	+ only after cytoablation
			IFNγ	IFNGR	-
			CXCL12	CXCR4	+
			OPN		+
			Hh	Patched	-
			SCF	c-kit	+

IMiD@s are highly efficacious drugs in several malignancies of hematopoietic origin including multiple myeloma (a plasma cell disease), mature B cell malignancies such as chronic lymphocytic leukemia (CLL) and non-Hodgkin's leukemia (NHL) as well as myelodysplastic syndrome (MDS) harboring a chromosome 5q deletion (del5qMDS). All of these are largely incurable diseases that arise from self-renewing leukemia stem cell population. Cereblon, the sole molecular target of IMiD@s, may have an unidentified contribution to HSC regulation given their ability to target stem cells and promote differentiation. While CRBN has not been characterized in the hematopoietic stem cell compartment, it regulates the Slo alpha subunit of the BK(Ca<sup>2+</sup>) ion channel that is involved in neuronal excitation, and in other cell types CRBN appears to control metabolism, by directing degradation of glutamine synthetase (GS) via interactions with acetylated lysines of GS that are triggered by high intracellular glutamine concentrations, and by CRBN-directed regulation of AMP-activated protein kinase (AMPK), a regulator of energy homeostasis. Finally, CRBN binds to the CD147-SLC16A1 (MCT1) lactate transporter complex in multiple myeloma cells. When treated with IMiD@s, patients with a somatic mutation in del(5q) MDS, a therapeutic response is associated with CD34<sup>+</sup> stem and progenitor cell ablation with parallel expansion of circulating lymphocytes and early erythroid precursors[141]. Interestingly, hematopoietic stem and progenitor cell (HSPC) defects in drug-treated del(5q) MDS patient's bone marrow are quenched while erythropoiesis and HSPC differentiation improve [141].

To address more fully the role that CRBN plays in HSCs regulation, we combined both *in vitro* and *in vivo* assays to study murine CRBN-deficient HSCs. We show that germline depletion of CRBN results in a significant reduction in HSC numbers yet an

expansion of lymphoid and myeloid cells in the peripheral blood. Despite their reduced numbers, CRBN-depleted HSCs have extensive self-renewal capacity following serial bone marrow transplantation, however, do not possess a fitness advantage over wild-type CRBN-expressing (*Crbn*<sup>+/+</sup>) HSCs in competitive transplantation. Collectively, our results demonstrate that CRBN plays a previously undefined regulatory role in HSC maintenance by controlling adhesion during adult and fetal hematopoiesis.

## Results:

### CRBN expression in adult hematopoietic stem and progenitor cells

Because of the birth defects induced by thalidomide and its derivatives known collectively as “immunomodulatory drugs” in humans, chicken and zebrafish, we first characterized gross limb and organogenesis in CRBN germline deficient mice and found no detectable malformations at birth or through maturation (Figure 20A). Moreover, *Crbn*<sup>-/-</sup> mice had no obvious organ defects at necropsy although a significant reduction in body weight, in males and females, was observed at 3 months and in aged mice (Figure 20B). The reduction in body weight was pronounced at 13 months where the age-associated weight gain observed in *Crbn*<sup>+/+</sup> (37.925g ± 3.88g) mice was significantly reduced in *Crbn*<sup>-/-</sup> (33.65g ± 2.93g, p=0.02) littermates (Figure 20B), which is consistent with previous reports of a role for CRBN in controlling diet-induced obesity[142].

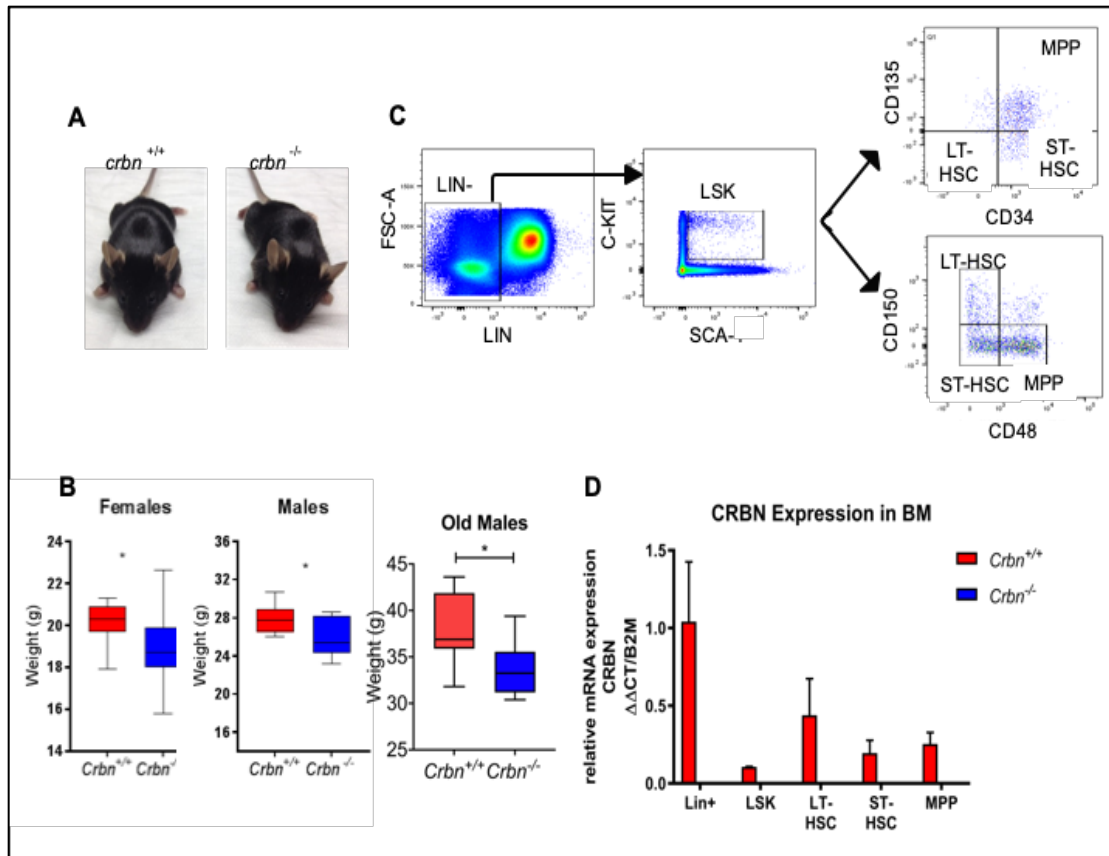


**Figure 20. CRBN deletion does not lead to gross abnormalities or birth defects.** Three-month old and eighteen-month old *Crbn*<sup>-/-</sup> and *Crbn*<sup>+/+</sup> littermates were assessed for normal limb formation, weight and *Crbn* mRNA expression in hematopoietic lineages. **(A)** *Crbn*<sup>-/-</sup> mice have normal limb development. **(B)** Twelve-week-old male and female *Crbn*<sup>-/-</sup> and their *Crbn*<sup>+/+</sup> littermates (n=22-25 per genotype) were weighed. Ten to thirteen-month old males *Crbn*<sup>-/-</sup> (n=8) and their *Crbn*<sup>+/+</sup> (n=8) littermates were weighed. **(C)** Gating strategy to identify the hematopoietic lineages, Lin-, LSK, LT-HSC, ST-HSC, SLAM HSC, MPP1, MPP2, MPP3, MPP4 populations using combination of cell surface markers (lineage cocktail, c-Kit, Sca-1, CD34, CD135, CD48 and CD150). **(D)** Purified Lin+, LSK, LT-HSC, ST-HSC & MPP were FACS sorted from bone marrow isolated from 2 tibias, 2 femurs and 2 iliac crest per mouse from *Crbn*<sup>+/+</sup> (n=7) and *Crbn*<sup>-/-</sup> (n=8). mRNA expression of *Crbn* normalized to Beta-2 microglobulin ( $\beta$ 2M) and relative to Lin+ *Crbn*<sup>+/+</sup> was confirmed in all lineages. Multiple Student's t-test per population was performed and significance achieved at \* $p < 0.05$ , \*\* $p < 0.01$ , \*\*\* $p < 0.001$ , \*\*\*\* $p < 0.0001$

Interestingly, *Crbn* mRNA levels in lineage positive (Lin<sup>+</sup>), LSK (Lin<sup>+</sup>Sca-1<sup>+</sup>c-Kit<sup>+</sup>), LT-HSC (Lin<sup>+</sup>Sca-1<sup>+</sup>c-Kit<sup>+</sup>CD48<sup>+</sup>CD150<sup>+</sup>), ST-HSC (Lin<sup>+</sup>Sca-1<sup>+</sup>c-Kit<sup>+</sup>CD48<sup>+</sup>CD150<sup>-</sup>), and MPP (Lin<sup>+</sup>Sca-1<sup>+</sup>c-Kit<sup>+</sup>CD48<sup>+</sup>CD150<sup>-</sup>), populations from femoral and tibial bone marrow of

*Crbn*<sup>-/-</sup> (n=8) and *Crbn*<sup>+/+</sup> (n=7) littermates (Figure 20C) showed that lineage positive cells (Lin<sup>+</sup>) have the highest expression of CRBN while the pluripotent LSK population has the lowest expression and, as expected, no *Crbn* mRNA detectable in *Crbn*<sup>-/-</sup> bone marrow cells. Compared to Lin<sup>+</sup> cells, CRBN expression levels was lower in LT-HSCs and this difference was even more pronounced in the ST-HSC and MPP populations (Figure 20D). Hence, CRBN's expression pattern may reflect a cell-specific dependency on its function.

### **CRBN regulates the frequency of adult hematopoietic stem and non-committed progenitor cells**

To further address the role of CRBN in HSCs under homeostatic conditions, we evaluated the frequency of HSPCs in the bone marrow of age- and sex-matched *Crbn*<sup>-/-</sup> mice and *Crbn*<sup>+/+</sup> littermates. Using flow cytometry and cell counts, the proportion and absolute number of all stem and non-committed progenitor cells was > 2-fold lower in *Crbn*<sup>-/-</sup> bone marrow (Figure 21B-E) with no notable changes in the precursor populations including CMP (Lin<sup>-</sup>Sca-1<sup>-</sup>c-kit<sup>+</sup>CD34<sup>+</sup>FcγR<sup>lo</sup>), GMP (Lin<sup>-</sup>Sca-1<sup>-</sup>c-kit<sup>+</sup>CD34<sup>+</sup>FcγR<sup>hi</sup>), and MEP (Lin<sup>-</sup>Sca-1<sup>-</sup>c-kit<sup>+</sup>CD34<sup>-</sup>FcγR<sup>lo</sup>) (Figure 21F) and a trending decrease in BM cellularity (Figure 21A). Interestingly, while the frequency of LSK cells in the BM of *Crbn*<sup>-/-</sup> and *Crbn*<sup>+/+</sup> mice were similar, (Figure 21G) their absolute numbers were reduced (Figure 21D). *Crbn*<sup>-/-</sup> LT-HSC had the highest decrease in absolute counts (Figure 21E, p= 0.00004) and frequency (Figure 21H) over control. Flow cytometric analysis of caspase 3/7 (activated proteases that mediate programmed cell death) showed no differences in total apoptosis in *Crbn*<sup>-/-</sup> compared to *Crbn*<sup>+/+</sup> WBM cells or apoptosis frequencies in distinct populations including Lin<sup>-</sup>, LSKs, MPP, ST-HSC and LT-

HSC (Figure 21I) suggesting that the reduction in HSCs is not coupled to enhanced caspase activation and associated apoptotic cell death.

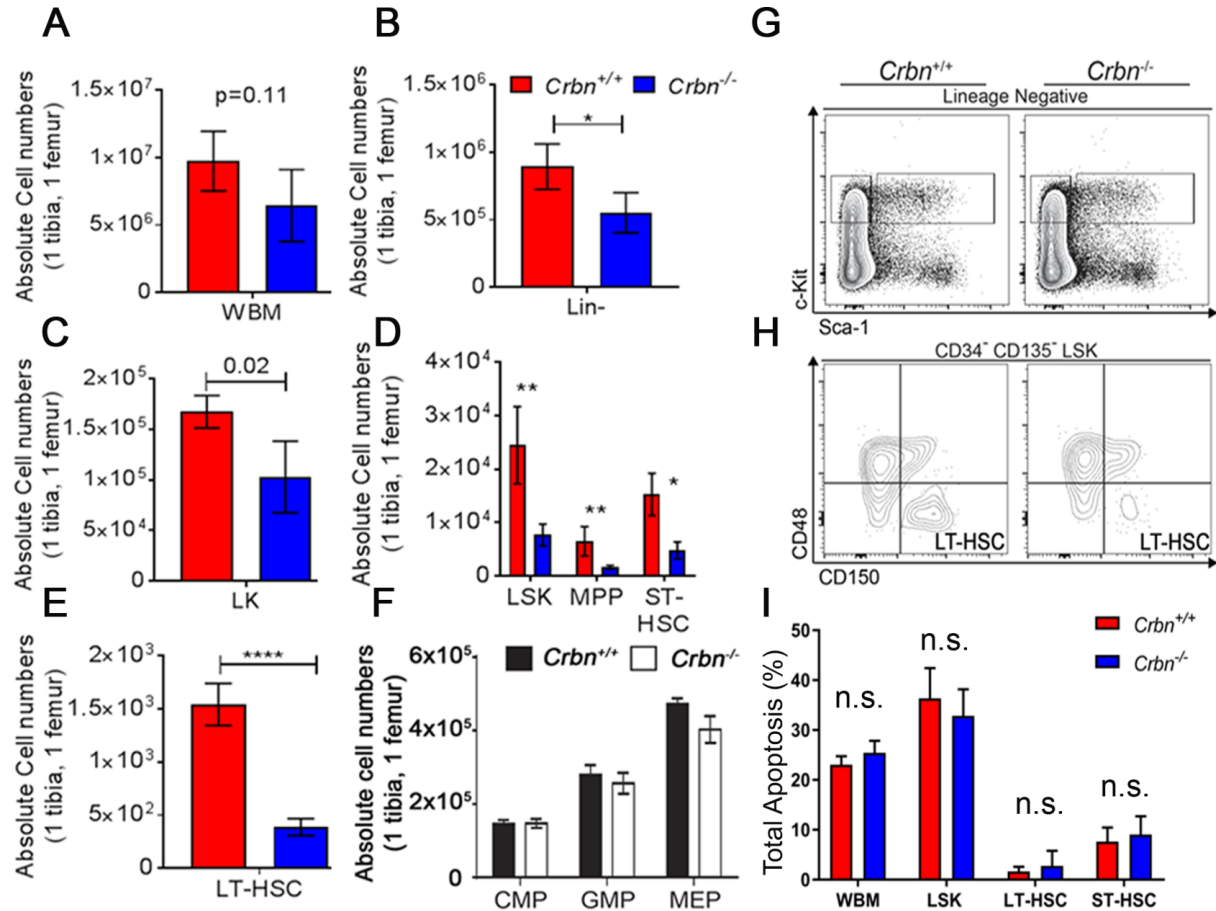


**Figure 21. CRBN deletion causes a loss in absolute hematopoietic stem and progenitor counts.** *Crbn*<sup>-/-</sup> and *Crbn*<sup>+/+</sup> bone marrow (1 tibia and 1 femur) were analyzed via flow cytometry for frequency and absolute counts (extrapolated from whole bone marrow counts (WBM)) at 2-3 months (n=4-5/genotype). Absolute counts of WBM (A), Lin-(B), Lin-c-Kit+(LK) (C), Lin-Sca-1+c-Kit+(LSK), multipotent progenitor (MPP) & short-term hematopoietic stem cell (ST-HSC) (D) and long-term HSC (LT-HSC) (E) from freshly isolated bone marrow of *Crbn*<sup>-/-</sup> (n=4) and *Crbn*<sup>+/+</sup> mice (n=4). (F) Absolute cell counts of more committed progenitors, CMP, GMP, MEP populations from mice in (A-E). Representative scatter plots comparing LSK (G) and LT-HSC (H) frequencies between *Crbn*<sup>-/-</sup> and *Crbn*<sup>+/+</sup>. (I) Total apoptosis measured by caspase 3/7 expression in hematopoietic cells from *Crbn*<sup>-/-</sup> (n=5) and *Crbn*<sup>+/+</sup> (n=4) littermates. Multiple Student's t-test per population was performed and significance achieved at \*p<0.05, \*\*p<0.01, \*\*\*p<0.001, \*\*\*\*p<0.0001



## Age-related hematopoiesis

Stem and progenitor cells drastically change in both frequency and function with age[143]. In *Crbn*<sup>+/+</sup> at 3 months LT-HSC, ST-HSC and MPP represent ~7%, 20% and ~70% of LSKs. These frequencies remain relatively consistent at 6 months. However, by 13 months LT-HSC expand at the expense of ST-HSC and MPP population with frequencies at ~40%, 16% and ~40% (Figure 22A) consistent with literature[143, 144]. Enumeration of primitive LT-HSC frequencies ( $39.7 \pm 10.0\%$ ) and absolute numbers showed an age-dependent accumulation in older *Crbn*<sup>+/+</sup> mice (18 months old, n=3); whereas, the LT-HSCs demonstrated lower frequencies ( $17.5 \pm 4.7\%$ , p=0.01) and numbers in *Crbn*<sup>-/-</sup> mice (n=4) (Figure 22C,F). LT-HSC decreased numbers in *Crbn*<sup>-/-</sup> mice were accompanied by trending increases in WBM, Lin- and MPP populations that failed to reach significance but suggest increased differentiation (Figure 22F).

Under homeostasis, HSCs are slow cycling therefore limit the need for metabolic activity and thus generate low levels of reactive oxygen species (ROS). However, with aging, ROS levels accumulate which contribute to increased proliferation, senescence, or apoptosis[145, 146]. ROS levels increased over time in *Crbn*<sup>+/+</sup> LT-HSC (Figure 22B) but there were no detectable changes in ROS levels between *Crbn*<sup>+/+</sup> and *Crbn*<sup>-/-</sup> mice at 18 months (Figure 22D). Interestingly, however *Crbn*<sup>-/-</sup> LT-HSC demonstrated a trending increase in total apoptosis as measured by caspase 3/7 expression (p=0.09) (Figure 22E). Suggesting that while ROS level are similar, sensitivity to ROS-induced cell death is heightened in *Crbn*<sup>-/-</sup> LT-HSC.

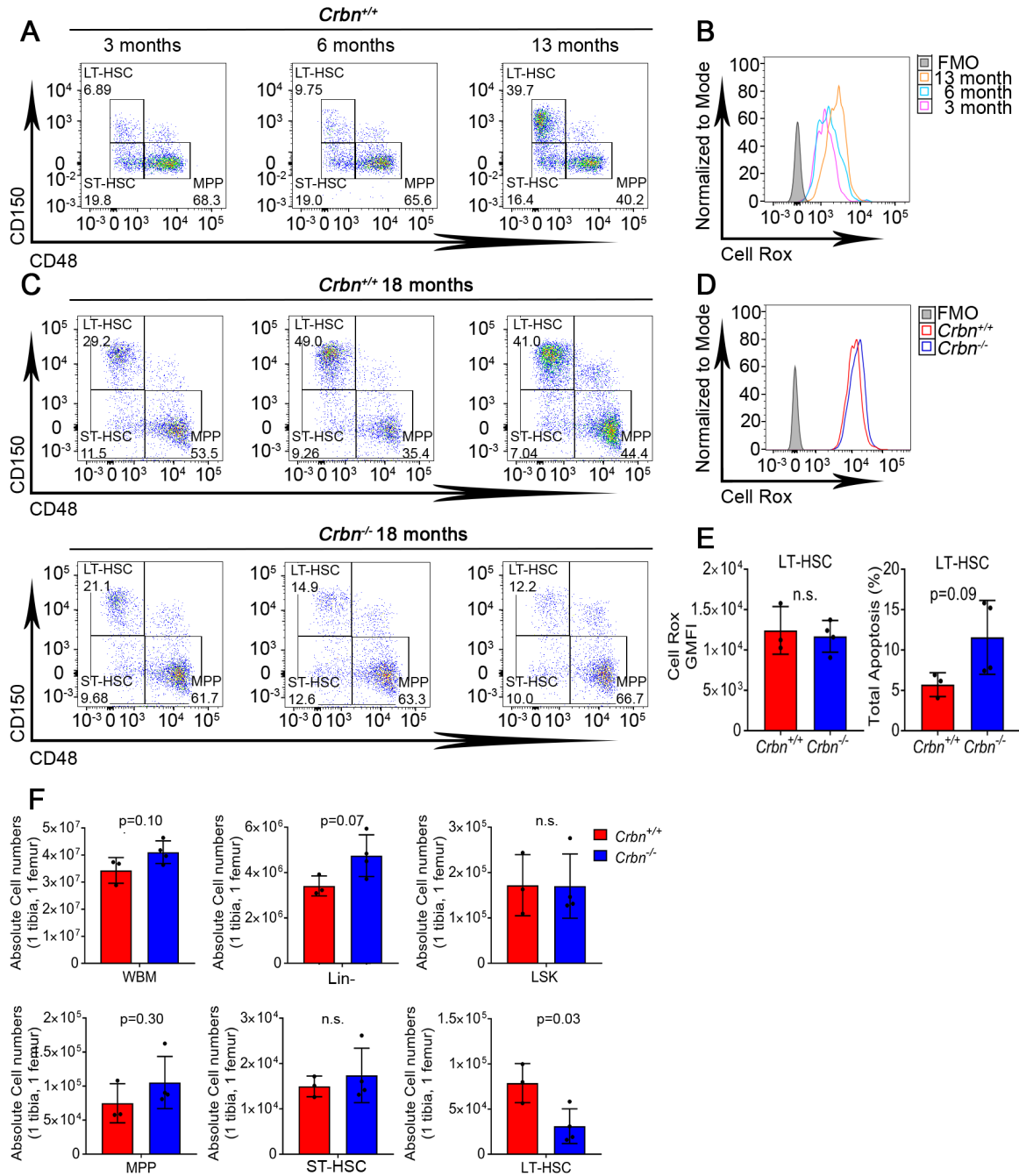


**Figure 22. Loss of HSC pool persists in aged *Crbn*<sup>-/-</sup>.** (A) Stem cell levels and intracellular reactive oxygen species (ROS) (B) levels were measured via flow cytometric analysis from *Crbn*<sup>+/+</sup> mice aged 3,6,13 months (n=1). Data represents one out of 3 experiments. (C) Stem cell frequencies from 18-month old *Crbn*<sup>+/+</sup> (n=3) and *Crbn*<sup>-/-</sup> (n=4, only 3 shown) were analyzed and intracellular ROS in LT-HSC was measured (D). (E) ROS levels in LT-HSC were quantified by geometric mean fluorescent intensities (left) and total apoptosis in LT-HSC via caspase 3/7 staining (right) from mice in (C). (F) Absolute cell counts from mice in (C). \*p<0.05, \*\*p<0.01, \*\*\*p<0.001, \*\*\*\*p<0.0001

## **CRBN expression is required for normal embryonic HSC development**

While all mature blood cells arise from the bone marrow, fetal hematopoiesis in vertebrates, including mice and humans, initiates from aorta-gonad mesonephros (AGM) regions and then colonize the fetal liver where colonization, survival and proliferation are defined by recruitment and localization in a fetal BM-like microenvironment. To determine if the reduction in HSPCs occurred in the developing fetus, fetal livers (FL) were harvested from embryonic stage 14.5 (E14.5) and the number of HSPC determined by flow cytometry. Gross inspection revealed that FLs from *Crbn*<sup>-/-</sup> mice (n=4) were visibly smaller than those from *Crbn*<sup>+/+</sup> mice (n=4) and the total number of cells significantly decreased (Figure 23A). Moreover, flow cytometry characterization of the distinct hematopoietic precursor cells showed that all primitive populations, including LT-HSCs (Figure 32A), were significantly reduced. Interestingly other non-hematopoietic cell populations were modestly reduced, in absolute cell numbers, these differences did not reach statistical significance. These data suggest that CRBN controls HSC development from primitive hematopoiesis.

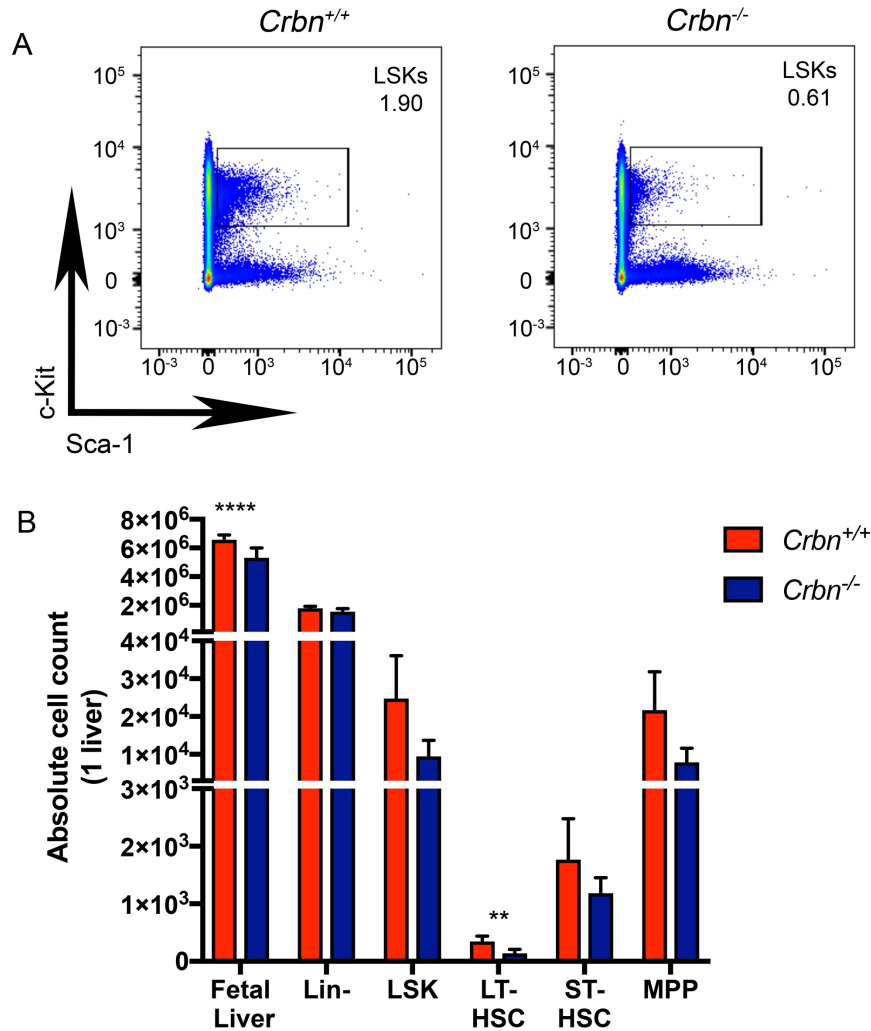


**Figure 23. CRBN deficiency provokes loss of HSC in fetal liver.** Fetal livers (FL) were harvested from *Crbn*<sup>-/-</sup> (n=4) and *Crbn*<sup>+/+</sup> (n=4) fetuses at E14.5. **(A)** Representative scatter plot showing LSK frequencies measured by flow cytometry. **(B)** Stem and progenitor absolute cell counts were extrapolated from frequencies measured via flow cytometry and whole FL counts. Multiple Student's t-test per population was performed and significance achieved at \**p*<0.05, \*\**p*<0.01, \*\*\**p*<0.001, \*\*\*\**p*<0.0001

### CRBN controls HSC stemness associated molecules and stimulates quiescence

Multipotent HSCs can differentiate into a limited range of cell types compared to the relative potency of embryonic stem cells, but express “stem-associated” genes that maintain homeostasis by controlling the balance of self-renewal and differentiation. A

“stemness” gene signature consisting of *Tek*(gene that encodes TIE2), *Mpl*, *Gata1*, and *Notch1* is characteristic of the multipotent HSC population at the top level. Indeed, TIE2 controls HSC quiescence within the stem cell niche, a function that is critical for maintenance of the stem cell compartment and make them resistant to drugs (such as 5-fluorouracil, 5-FU) that induces apoptosis in actively cycling cells [91]. Using FACS-purified LSKs from adult bone marrow, RNA-seq analyses and qPCR validation from purified LT-HSC was performed to examine a documented “stemness”-related gene signature[147].

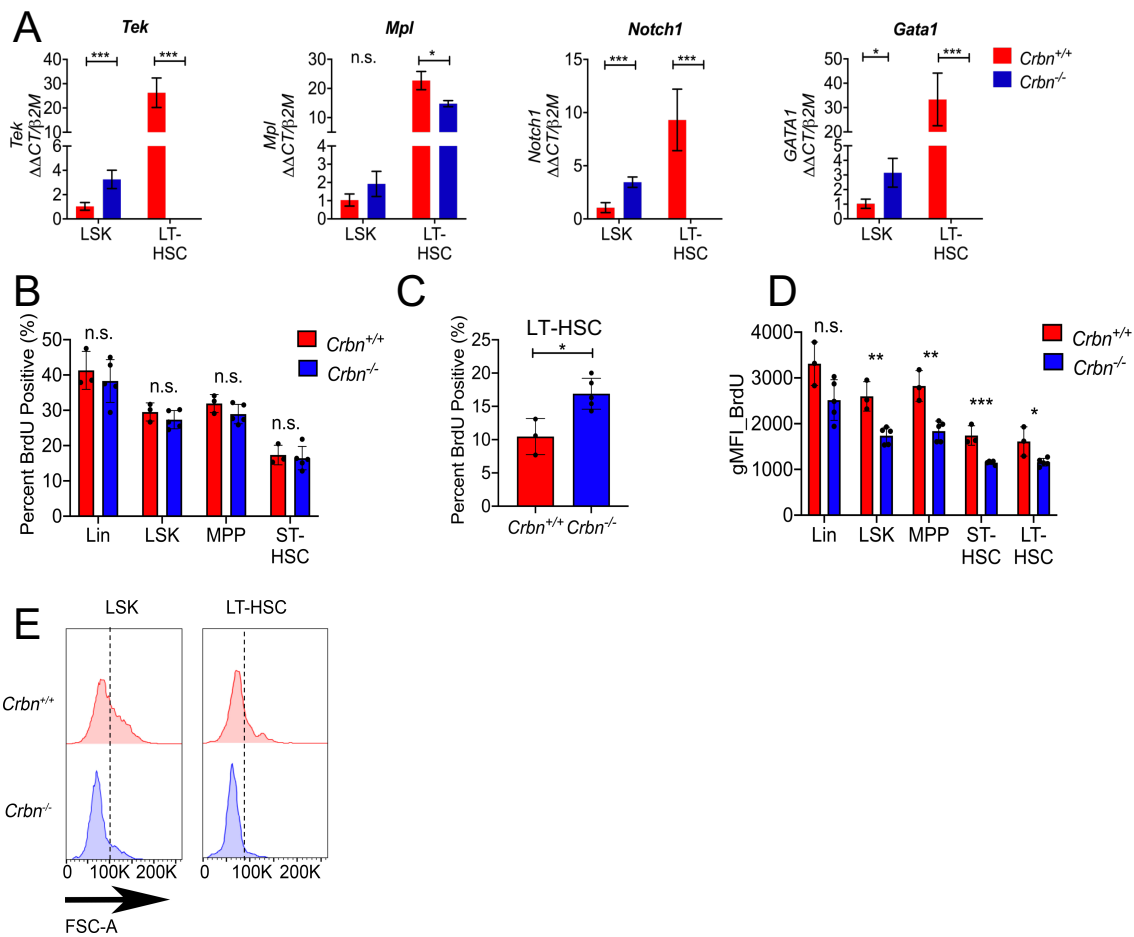


**Figure 24. CRBN deficiency leads increased HSC proliferation. (A)** Femurs and tibias were harvested from *Crbn*<sup>-/-</sup> (n=7) and *Crbn*<sup>+/+</sup> (n=7) mice. Following lineage depletion cells were stained with flow panel (Table13) and FACS-sorted into Lin<sup>+</sup>, Lin<sup>-</sup>, LSK, MPP, ST-HSC & LT-HSC. RNA was isolated and cDNA synthesized, and qRT-PCR performed to assess mRNA expression of stemness-related genes *Tek*, *Mpl*, *Notch1*, *Gata1*. Gene expression was normalized to  $\Delta\Delta CT$  values obtained from control gene,  $\beta 2M$  and then

normalized to  $Crbn^{+/+}$  LSK cells. **(B)** Lin<sup>-</sup>, LSK, MPP, ST-HSC & T-HSC **(C)** proliferation levels from  $Crbn^{-/-}$  (n=5) and  $Crbn^{+/+}$  (n=3) mice were measured via in vivo BrdU labelling. Percent BrdU<sup>+</sup> **(B-C)** and geometric mean fluorescence intensities (gMFI) **(D)** are graphed. **(E)** Histograms of forward scatter area from  $Crbn^{-/-}$  and  $Crbn^{+/+}$  LSK and LT-HSC. Multiple Student's t-test per population was performed and significance achieved at \* $p < 0.05$ , \*\* $p < 0.01$ , \*\*\* $p < 0.001$ , \*\*\*\* $p < 0.0001$

Interestingly,  $Crbn^{-/-}$  HSCs showed a markedly lower level of “stemness” gene expression consisting of *Tek*, *Gata1*, *Mpl*, and *Notch1* (Figure 24 A) suggesting that CRBN is required to maintain cells in the quiescent, undifferentiated state.

Given the reduction in TIE2 and other stem-related genes that control quiescence, steady state proliferation of adult bone marrow stem and progenitor cells was examined using *in vivo* labeling with 5-bromo-2'-deoxyuridine (BrdU), a thymidine analog that is incorporated into cycling cells.  $Crbn^{-/-}$  (n=5) and  $Crbn^{+/+}$  (n=3) mice were injected intraperitoneally with (IP) BrdU and then femoral and tibial bone marrow cells harvested and analyzed after 18 hours to detect actively dividing cells. The percentage of each cell population labeled with BrdU was then assessed via multiparameter flow cytometric analysis. Interestingly, no appreciable differences of the percent of BrdU positive cells was detected among Lin<sup>-</sup>, LSK, MPP and ST-HSC populations (Figure 24B), but a significant increase in proliferating BrdU positive LT-HSC ( $p=0.01$ ) was detected in  $Crbn^{-/-}$  (16.9%  $\pm$  2.08) compared to  $Crbn^{+/+}$  LT-HSC (10.5%  $\pm$  2.21)(Figure 24C). Interestingly, all CRBN-deficient stem and progenitor cells had decreased DNA-content as demonstrated by a significant reduction in the geometric mean fluorescence intensity of BrdU in each population (Figure 24D) and smaller cell size as shown by forward scatter plots of bone marrow cells from  $Crbn^{+/+}$  versus  $Crbn^{-/-}$  mice(Figure 24E). Since cellular quiescence is essential for maintenance of stem-like properties in hematopoietic stem

cells, an increased in LT-HSC proliferation may be responsible for lower detectable LT-HSC numbers in the bone marrow of CRBN-deficient mice through enforced differentiation.

### **CRBN's role in differentiation in homeostatic and transplant models**

CRBN regulates hematopoietic stem cell quiescence in adult bone marrow and is required for normal HSC development during embryogenesis. Next complete blood counts (CBCs) from *Crbn*<sup>-/-</sup> mice showed a significant increase ( $p=0.0027$ ) in total white blood cells (WBC) compared to *Crbn*<sup>-/-</sup> littermates (Figure 25A). Moreover, there was a statistically significant increase in lymphocytes ( $p= 0.0297$ ) (Figure 25B), and a modest increase in monocytes (Figure 25C) ( $p=0.29$ ) and neutrophils (Figure 25D) ( $p=0.11$ ) that did not reach statistical difference. In contrast, basophils (data not shown), eosinophils (data not shown) and platelets were similar in *Crbn*<sup>+/+</sup> and *Crbn*<sup>-/-</sup> mice. Striking decreases were noted in total red blood cells (RBCs) (Figure 25E) ( $p= 0.0002$ ) with a corresponding increase in reticulocytes (Figure 25F) ( $p= 0.0075$ ) indicating an induction in erythropoiesis. While there is a normocytic anemia present, hemoglobin and hematocrit were not impacted by genotype. Together these data suggest that CRBN increases mature cell output in the white blood cell lineages and has a substantial impact on erythropoiesis.

To further investigate the role of CRBN in mature cell output we examined splenocyte count from *Crbn*<sup>-/-</sup> and *Crbn*<sup>+/+</sup> mice at 8 to 14 weeks. *Crbn*<sup>-/-</sup> had a significant increase in absolute cell splenocytes numbers ( $89.25 \times 10^7 \pm 2.63 \times 10^7$ /spleen,  $p= 0.0216$ ) in comparison to their control littermates ( $67.56 \times 10^7 \pm 2.16 \times 10^7$ /spleen) (Figure 25G).



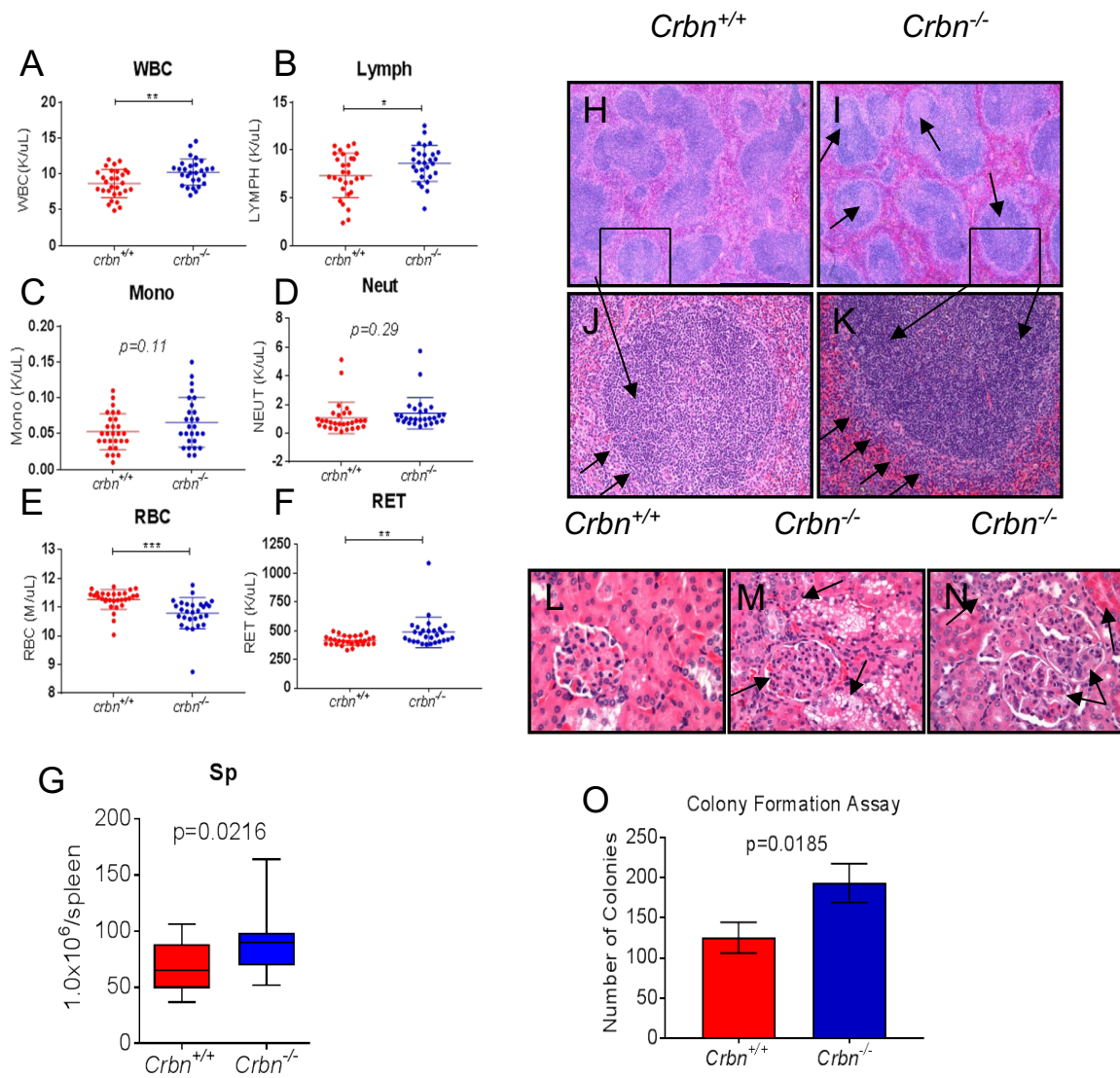


**Figure 25. CRBN-deficient HSC have increased differentiation capacity both *in vivo* & *in vitro*.** Complete blood counts (CBCs) from submandibular bleeds from *Crbn*<sup>-/-</sup> (n=29) and *Crbn*<sup>+/+</sup> (n=30) mice at 2 to 3 months. White blood cells (WBC) (A), lymphocyte (Lymph) (B), monocyte (Mono) (C), neutrophil (Neut) (D), red blood cell (RBC) (E) and reticulocyte (F) counts were measured. (G) Splenocyte counts from *Crbn*<sup>+/+</sup> (n=15) and *Crbn*<sup>+/+</sup> (n=13) mice. Histological appearance of the spleen of 6-month-old *Crbn*<sup>+/+</sup> mice (H, J) and age-matched *Crbn*<sup>-/-</sup> mice (I, K). Lymphoid follicles with germinal centers (H&I, arrows) and basophilic corona (J&K, upper arrows), surrounded by a cellular marginal zone (J&K, lower arrows) from *Crbn*<sup>-/-</sup> and *Crbn*<sup>+/+</sup> spleens. Histological appearance of the kidney of 9-month-old *Crbn*<sup>+/+</sup> mice (L) compared to that of age-matched *Crbn*<sup>-/-</sup> mice (M), and that of 24-month-old *Crbn*<sup>-/-</sup> mice (N). Tubular epithelium in *Crbn*<sup>-/-</sup> mice had foamy, vacuolated cytoplasm (M, lower right arrow), or were intensely eosinophilic (M, upper right arrow), or were cuboidal, basophilic with nuclear crowding (M, upper left arrow) (N, upper left arrow). Glomeruli of *Crbn*<sup>-/-</sup> mice had increased mesangial matrix, thickening of capillary basement membranes, and increased cellularity (M, lower left



arrow) (**N**, paired lower right arrows), compared to WT controls (**L**) (**L-N**, each 630X). (**O**) Whole bone marrow from *Crbn*<sup>-/-</sup> (n=3) and *Crbn*<sup>+/+</sup> (n=3) femurs and tibias were seeded into methylcellulose medium containing (SCF, IL6, IL3, EPO) and colonies counted 7 days later. Multiple Student's t-test per population was performed and significance achieved at \**p*<0.05, \*\**p*<0.01, \*\*\**p*<0.001, \*\*\*\**p*<0.0001

Next various tissues harvested from 3,6 ,9 and 24 month-old *Crbn*<sup>-/-</sup> and matched *Crbn*<sup>+/+</sup> littermates (n=3/genotype per age group(3,6,9); 3 *Crbn*<sup>-/-</sup> mice at 24 month-old) including lung, kidney, bone marrow, liver, spleen, lymph node, salivary glands, pancreas, thymus, large intestine, and adrenal gland were evaluated. Based on histological examination of hematoxylin & eosin (H&E) stained sections, CRBN was found to be dispensable for gross bone marrow and splenic architecture and bone marrow cellularity at 3 months (data not shown). However, at 6 months and older *Crbn*<sup>-/-</sup> spleens appeared more cellular and reactive with prominent lymphoid follicles with germinal centers (Figure 25I, arrows) and densely basophilic corona (Figure 25K, upper arrows), surrounded by a broadly cellular marginal zone (Figure 25K, lower arrows) compared to that of *Crbn*<sup>+/+</sup> mice (Figure 25H,J) with less basophilic corona (Figure 25J, upper arrow) and a narrow, indistinct marginal zone (Figure 23J, lower arrows) suggesting leukocyte infiltration (Figure 25H-K). *Crbn*<sup>-/-</sup> kidneys had evidence of glomerulonephritis with tubular injury and regeneration at 9 months (Figure 25M) which was heightened by 24 months. *Crbn*<sup>-/-</sup> mice (9 of 12) ages 3-24 months, but not *Crbn*<sup>+/+</sup> mice (0 of 9) ages 3-9 months old had rare, mild, focal mononuclear leukocyte infiltrates in the liver, salivary gland, lung and/or kidney.

To further evaluate the differentiation capacity of mature hematopoietic progenitors, cells that were present in roughly equal frequencies in bone marrow, a short-term colony-formation assay in methylcellulose was performed. Equal numbers of WBM

( $1 \times 10^5$ ) were seeded in methylcellulose media supplemented with a cocktail of recombinant cytokines (SCF, IL3, IL6, EPO). After 7 days in culture, we observed a significant increase in the total colony counts generated from *Crbn*<sup>-/-</sup> ( $193.3 \pm 24.01$ ,  $p=0.0185$ ) compared to *Crbn*<sup>+/+</sup> bone marrow (Figure 25O). Although this does not evaluate long-term colony forming units or stem cell fitness/function, the distribution capacity for differentiation *in vitro* and response to hematopoietic growth factors was superior in *Crbn*<sup>-/-</sup> bone marrow which suggests while there is no obvious bone marrow failure phenotype present in *Crbn*<sup>-/-</sup> mice, they have impaired stem cell quiescence, lower stem-related gene expression, and greater proliferation.

### **CRBN ablation does not impair fitness and reconstitution capabilities in adult mice**

A hallmark of HSC fitness and function is the ability to fully repopulate lethally irradiated recipients either in a competitive or non-competitive transplantation. First, we investigated whether bone marrow homing (BM seeding) of intravenously injected HSPCs is impaired using carboxyfluorescein diacetate succinimideylester (CFSE) labeling (Figure 26A). CD45.2<sup>+</sup> CFSE-labeled Lin<sup>-</sup> cells from *Crbn*<sup>-/-</sup> and *Crbn*<sup>+/+</sup> were transplanted into lethally irradiated WT (CD45.1) recipients. We found that *Crbn*<sup>+/+</sup> and *Crbn*<sup>-/-</sup> HSPCs showed equivalent homing capacities based on the recovery of equal frequencies of CFSE<sup>+</sup> cells after 18 hours (Figure 26B).

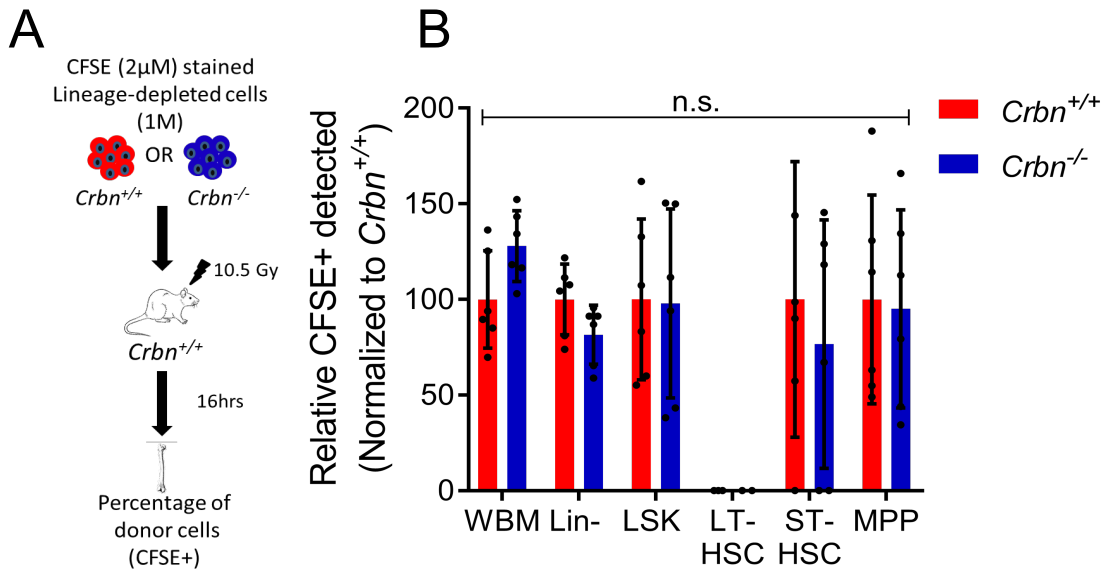


**Figure 26. CRBN ablation does not impair HSPC homing to bone marrow. (A)** Experimental design. **(B)** CFSE-labelled Lin<sup>-</sup> cells were transplanted into lethally irradiated mice. Relative percent of CFSE<sup>+</sup> *Crbn*<sup>-/-</sup> (n=7) HSPCs to *Crbn*<sup>+/+</sup> (n=6) HSPCs was graphed. Graph depicts combination of 2 experiments. Multiple Student's t-test per population was performed and significance achieved at \**p*<0.05, \*\**p*<0.01, \*\*\**p*<0.001, \*\*\*\**p*<0.0001

Based on these homing experiments, a serial competitive chimeric transplantation experiment (Figure 27A) was conducted using WBM ( $1 \times 10^6$  cells) from *Crbn*<sup>-/-</sup> or *Crbn*<sup>+/+</sup> mice (CD45.2) combined with WBM ( $1 \times 10^6$  cells) from *Crbn*<sup>+/+</sup> (CD45.1) in a 1:1 ratio transplanted into lethally irradiated WT (CD45.1) mice. We observed a significant decrease in donor engraftment (percent of CD45.2<sup>+</sup> donor cells) in the peripheral blood (PB), spleen (Sp) and bone marrow (BM) in recipients that received WBM from *Crbn*<sup>-/-</sup>

mice (Figure 27B-D, H). Multi-lineage donor chimerism in the spleen also declined in animals that received *Crbn*<sup>-/-</sup> WBM (Figure 27E-F).

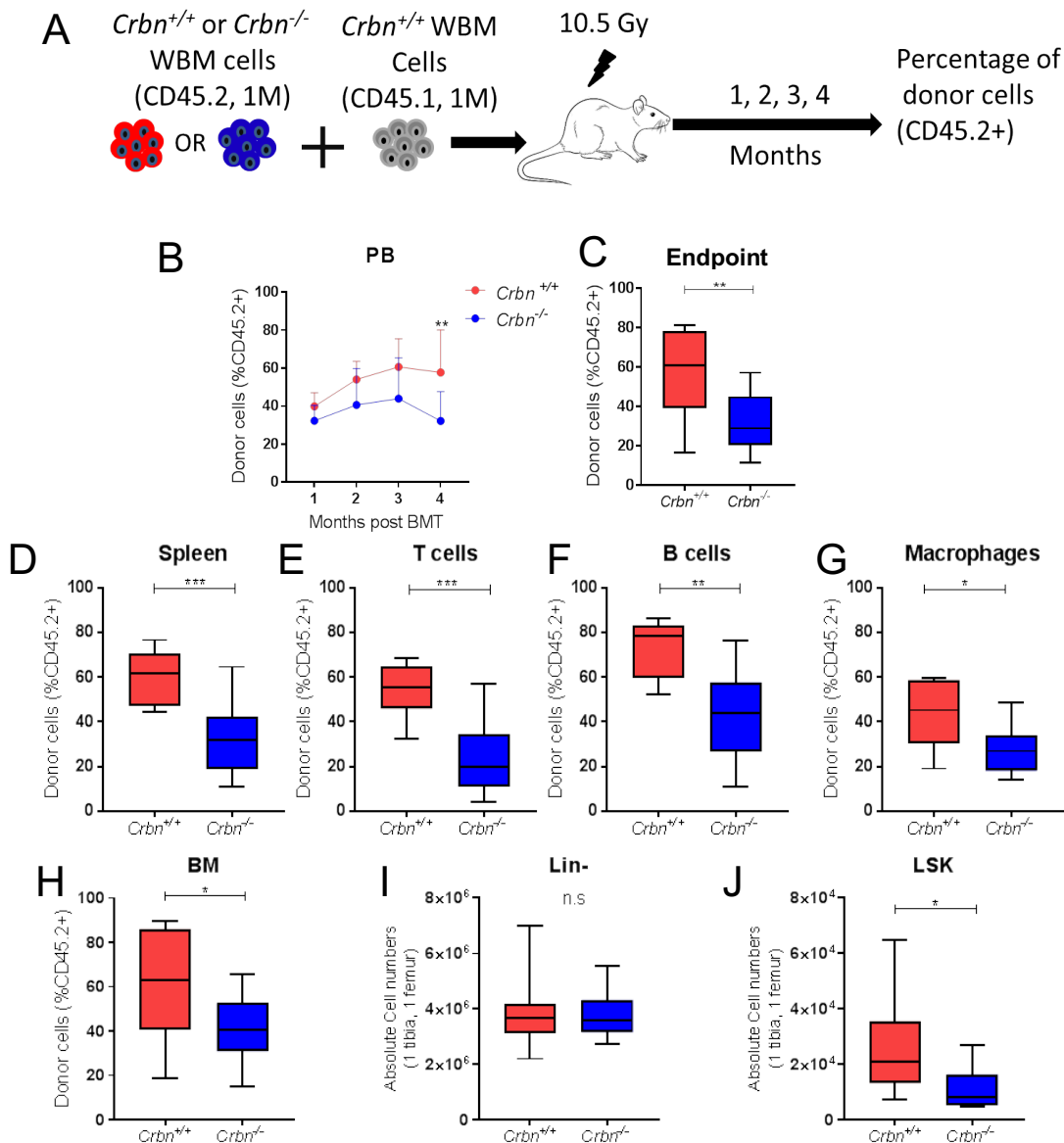


**Figure 27. CRBN-deficient HSCs do not outcompete control HSC in 3:1 ratio in competitive primary bone marrow transplant. (A)** Experimental design. One million WBM cells from *Crbn*<sup>-/-</sup> (n=3) or *Crbn*<sup>+/+</sup> (n=3) CD45.2 were mixed with 1X10<sup>6</sup> cells from control CD45.1 mouse and transplanted into lethally irradiated CD45.1 recipients (n=10 per genotype). **(B)** Peripheral Blood (PB) chimerism was monitored over time and endpoint (4 months post bone marrow transplant (BMT) **(C)**. **(D)** Total spleen, T cell **(E)**, B cell **(F)** and macrophage **(G)** chimerism at endpoint. **(H)** Total BM, Lin- **(I)** and LSK **(J)** chimerism was analyzed at endpoint. Multiple Student's t-test per population was performed and significance achieved at \*p<0.05, \*\*p<0.01, \*\*\*p<0.001, \*\*\*\*p<0.0001

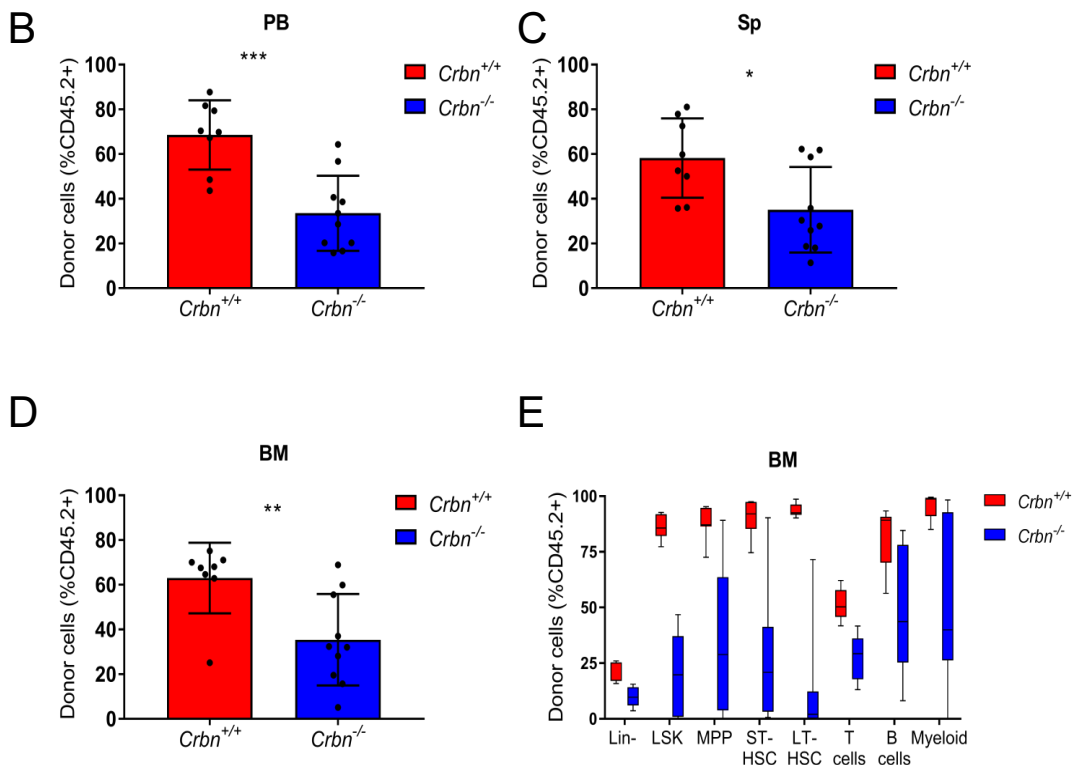
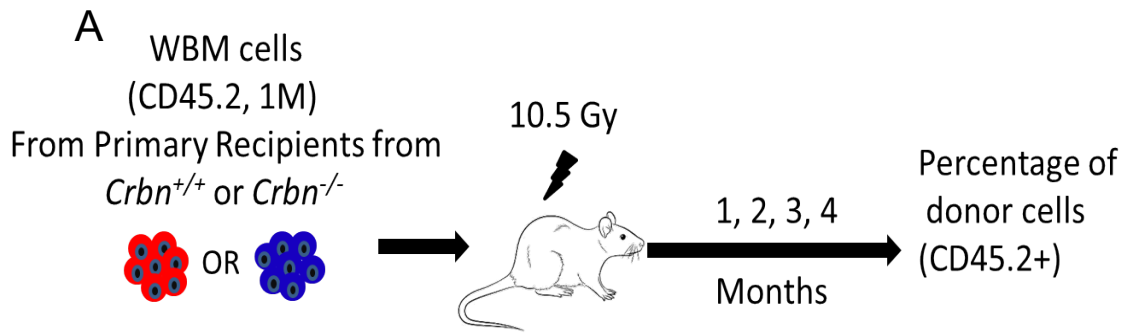


**Figure 28. CRBN-deficient HSCs do not outcompete control HSC in 3:1 ratio in competitive secondary bone marrow transplant.** (A) Experimental design. WBM ( $1 \times 10^6$ ) cells from primary *Crbn*<sup>-/-</sup> (n=10) and *Crbn*<sup>+/+</sup> (n=10) recipients were and transplanted into lethally irradiated CD45.1 recipients (n=10 per genotype). (B) Peripheral Blood (PB), Spleen (C) and BM (D) chimerism at endpoint (4 months post bone marrow transplant (BMT)). (E) Lin<sup>-</sup>, LSK, MPP, ST-HSC, LT-HSC, T cell B cell and myeloid chimerism at endpoint was determined. Multiple Student's t-test per population was performed and significance achieved at \* $p < 0.05$ , \*\* $p < 0.01$ , \*\*\* $p < 0.001$ , \*\*\*\* $p < 0.0001$

Notably, while the total number of donor-derived LSKs in the BM of recipients receiving *Crbn*<sup>-/-</sup> WBM was significantly reduced ( $p < 0.05$ ) (Figure 27J), the total number of donor-derived Lin<sup>-</sup> cells remained similar between recipients receiving *Crbn*<sup>+/+</sup> WBM (Figure 27I). These data suggest superior differentiation of mature populations by *Crbn*<sup>-/-</sup> bone marrow, but significantly fewer functional LT-HSCs with repopulation capacity.

As expected upon secondary transplantation (Figure 28A), animals that received WBM from primary *Crbn*<sup>-/-</sup> WBM recipients experienced further diminution in bone marrow chimerism (from levels seen in the primary recipients) in PB, Sp and BM (Figure 28B-D). Moreover, donor-derived HSPCs were virtually exhausted at 4 months post-transplant (Figure 28E) and donor-derived T, B and myeloid cells in the BM were drastically reduced (Figure 28E).

Overall despite their increased differentiation potential, *Crbn*<sup>-/-</sup> HSCs were unable to compete with *Crbn*<sup>+/+</sup> HSCs following competitive serial transplantation. It is important to note that the competitive transplant was performed using a 1:1 ratio of *Crbn*<sup>+/+</sup>:*Crbn*<sup>-/-</sup> WBM cells; whereas, the HSC ratio was approximately 3:1 (*Crbn*<sup>+/+</sup>:*Crbn*<sup>-/-</sup>).

### **Long-term reconstitution potential is enhanced by CRBN depletion in LT-HSC**

Next, the role of CRBN in LT-HSC reconstitution was expressly examined in non-competitive serial transplantation with a saturating dose of purified *Crbn*<sup>-/-</sup> LKs (Lin<sup>-</sup>c-Kit<sup>+</sup>) or *Crbn*<sup>+/+</sup> LKs. Following lethal irradiation, one million purified LKs were injected intravenously into congenic WT recipients (CD45.1) (Figure 29A).

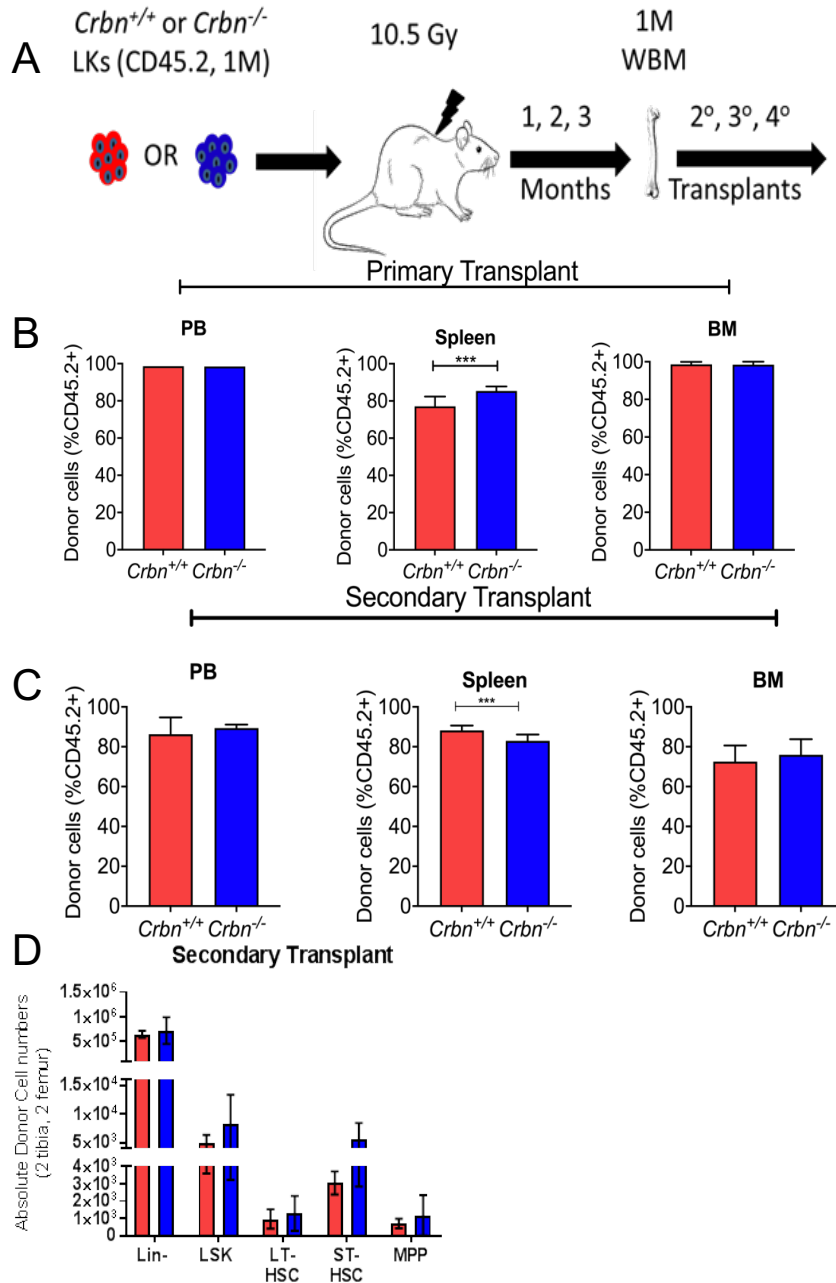


**Figure 29. CRBN deficiency does not impair HSC reconstitution potential in non-competitive serial transplants.** (A) Experimental design. Lin-c-Kit<sup>+</sup> (LK) ( $1 \times 10^6$ ) cells were harvested from *Crbn*<sup>-/-</sup> ( $n=7$ ) and *Crbn*<sup>+/+</sup> ( $n=6$ ) CD45.2 mice and transplanted into lethally irradiated CD45.1 recipients. (B) Perohepral blood (PB), spleen (Sp), and bone marrow (BM) chimerisms after 3 months was determined. *Crbn*<sup>-/-</sup> and *Crbn*<sup>+/+</sup> recipients were pooled per genotype and WBM ( $1 \times 10^6$ ) cells were transplanted into secondary recipients. (C) Perohepral blood (PB), spleen (Sp), and bone marrow (BM) chimerisms after 3 months was determined. (D) HSPC absolute cell counts extrapolated from flow cytometric analyses from secondary recipients from (C). Multiple Student's t-test per population was performed and significance achieved at \* $p < 0.05$ , \*\* $p < 0.01$ , \*\*\* $p < 0.001$ , \*\*\*\* $p < 0.0001$

Repopulation dynamics (donor engraftment and donor-derived HSPC numbers) were largely similar during the primary and secondary transplant suggesting that high LKs, and thus higher LT-HSC numbers (Figure 29B-D) showed limited impact on spleen and bone marrow engraftment.

However, in tertiary transplantations, recipient mice with control LKs exhibited lower PB, spleen and BM reconstitution compared to *Crbn*<sup>-/-</sup> LK recipients (Figure 30 A, C, E). *Crbn*<sup>+/+</sup> LKs undergo exhaustion due to proliferative stress and demand for continuous self-renewal potential resulting in a significant decrease in all donor-derived HSPC frequencies and total cell numbers in the BM (Figure 30G-H) of recipient mice. Intriguingly, recipient mice receiving *Crbn*<sup>-/-</sup> LKs maintained significantly higher numbers of long-term multi-lineage cells. Compared to the defects observed in the fetal liver and adult bone marrow (Figure 30 B, D, F), significant myeloid skewing in the peripheral blood, spleen and bone marrow suggests that CRBN may play a different role in embryonic development compared to mature hematopoiesis.



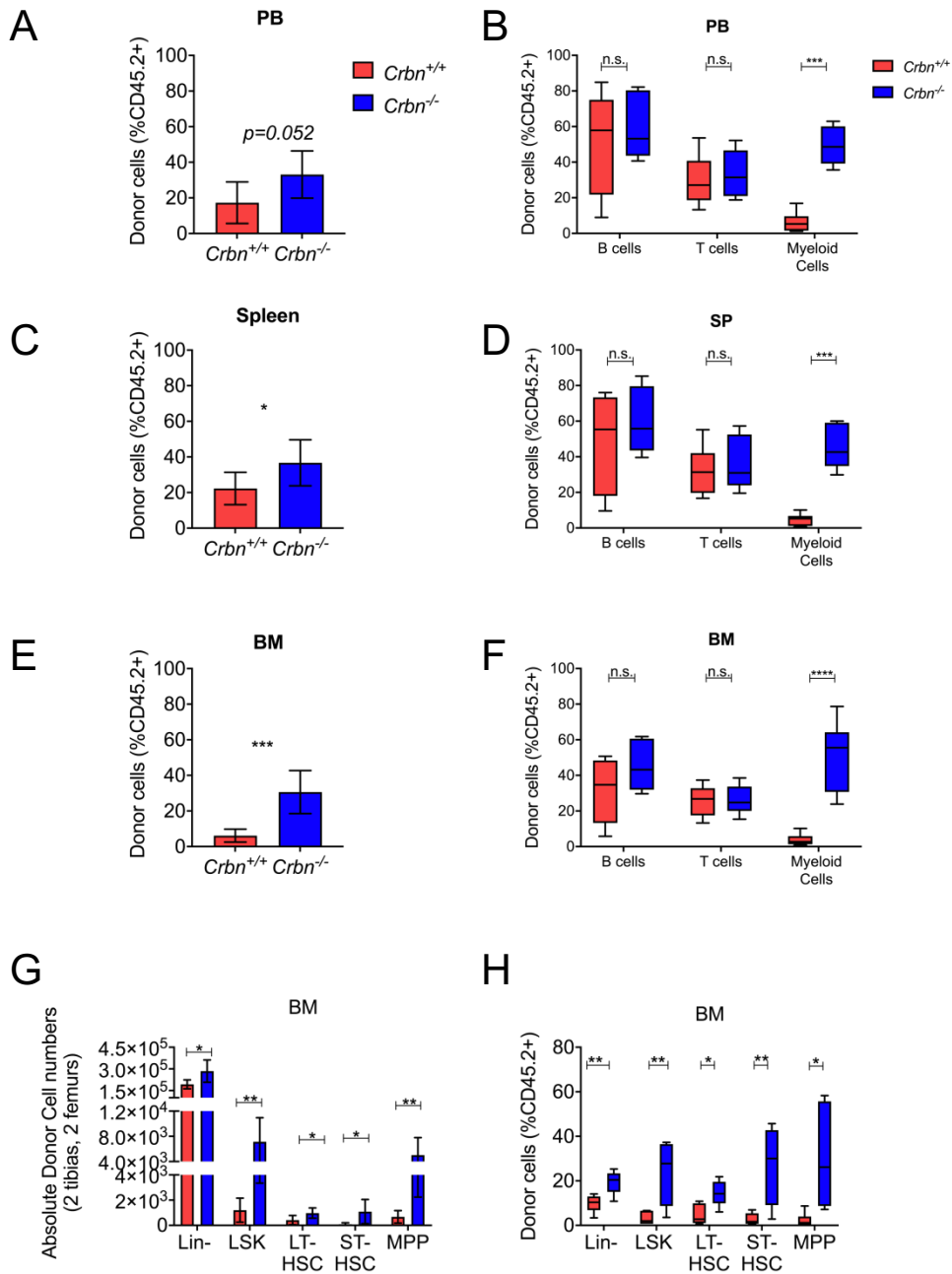


**Figure 30. Long-term reconstitution capacity is enhanced by CRBN ablation in HSCs.** Secondary recipients from Figure 29 were pulled per genotype and transplanted into tertiary CD45.1 recipients (n=15 per genotype). **(A, C, E)** PB, Sp and BM chimerism at endpoint (4 months). T cell, B-cell and myeloid chimerism at endpoint from PB **(B)**, Sp **(D)**, BM **(F)** at endpoint. HSPCs donor-derived absolute counts **(G)** and chimerism **(H)** measure by flow cytometric analysis. Multiple Student's t-test per population was performed and significance achieved at \* $p<0.05$ , \*\* $p<0.01$ , \*\*\* $p<0.001$ , \*\*\*\* $p<0.0001$

To further clarify these conflicting results, we examined HSC frequencies in *Crbn*<sup>-/-</sup> mice and evaluated the vasculature of mature adult animals. Femurs from *Crbn*<sup>-/-</sup> (n=5) and *Crbn*<sup>+/+</sup> (n=5) mice were harvested, formalin-fixed, decalcified, embedded, sectioned and then stained for the presence of CD34+ vascular endothelial cells. *Crbn*<sup>-/-</sup> bone marrow expressed a modest but significant increase in CD34+ vessels per field of view at 20X (Figure 31A). The hypoxic character of LT-HSCs is determined by their position within the BM so we next determined if CRBN-deficient HSC localize normally to the hypoxic bone marrow regions using Hypoxyprobe<sup>TM</sup> (pimonidazole hydrochloride) staining which detects cells under <5% of oxygen (O<sub>2</sub>). *Crbn*<sup>-/-</sup> (n=4) and *Crbn*<sup>+/+</sup> (n=4) mice were injected (IP) with pimonidazole HCl (60mg/kg) and bone marrow was harvested after 90 minutes and stained for anti-pimonidazole conjugated to FITC. Using flow cytometry, no significant differences in pimonidazole staining was observed among *Crbn*<sup>-/-</sup> and *Crbn*<sup>+/+</sup> HSPC populations (Figure 31B).

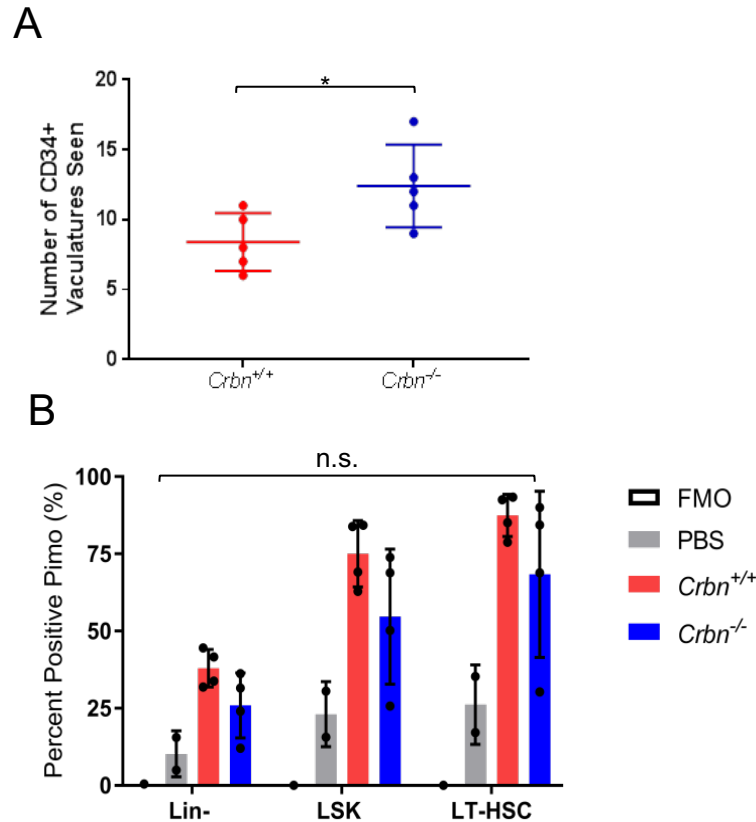


**Figure 31. CRBN deficiency modestly increases vasculature. (A)** Femurs from *Crbn*<sup>-/-</sup> (n=5) and *Crbn*<sup>+/+</sup> (n=5) littermates were harvested, formalin fixed (18 h), decalcified, sectioned and stained via immunohistochemistry (IHC) and analyzed for the presence of CD34+ vascular endothelial cells. The number of CD34+ vasculature seen per field of view at 20X per mouse per genotyped was determined and graphed. Multiple Student's t-test per population was performed and significance achieved at \**p*<0.05, \*\**p*<0.01, \*\*\**p*<0.001, \*\*\*\**p*<0.0001 **(B)** *Crbn*<sup>-/-</sup> and *Crbn*<sup>+/+</sup> were injected (i.p.) with PBS (n=1 per genotype) or pimonidazole (pimo). BM was harvest 90 minutes later and percent of pimo positive cells in Lin-, LSK and LT-HSC was assessed via flow cytometry and graphed. FMO= fluorescence minus one control. One-way ANOVA followed by Dunnett's multiple comparison was performed and significance achieved at \**p*<0.05, \*\**p*<0.01, \*\*\**p*<0.001, \*\*\*\**p*<0.0001

### CRBN reduces HSC's response to transcription and translation arrest

As indicated at steady state and in the fetal liver, *Crbn*<sup>-/-</sup> HSCs are reduced in frequency but more commonly in cell cycle (studied on in adult bone marrow). Cycling cells are selectively sensitive to the effects of 5-fluorouracil (5-FU), a pyrimidine analog

that interferes with DNA and RNA synthesis, relative to quiescent primitive multipotent progenitor cells. Next, *Crbn*<sup>-/-</sup> and *Crbn*<sup>+/+</sup> mice were exposed to weekly challenges of 5-FU (150mg/kg) and survival was monitored (Figure 32A). Lethality occurred in all *Crbn*<sup>-/-</sup> mice (10 of 10) following 5-FU challenge compared to only three *Crbn*<sup>+/+</sup> mice (3 of 10) ( $p < 0.001$ ) (Figure 32B). Despite having higher baseline WBCs, *Crbn*<sup>-/-</sup> mice had significantly less WBCs (Figure 32C) and all other mature populations (data not shown), after two doses of 5-FU. HSPC numbers after the 1<sup>st</sup> (Figure 32D) and 2<sup>nd</sup> (Figure 32E) 5-FU dose were significantly ( $p < 0.05$ ) lower in the *Crbn*<sup>-/-</sup> compared to *Crbn*<sup>+/+</sup> mice.

Since 5-FU primarily blocks DNA and RNA synthesis, but can also induce DNA damage, we administered two doses of 5-FU and monitored multi-lineage reconstitution in the PB overtime. Interestingly, WBC counts and HSPC numbers in *Crbn*<sup>-/-</sup> mice were fully restored to control levels 18 days post 2<sup>nd</sup> 5-FU (Figure 32F-G) strongly suggesting that CRBN deficiency was related to higher nucleic acid synthesis caused by greater proliferation and not from irreversible DNA-damage. Remarkably, despite their almost undetectable levels after the 2<sup>nd</sup> 5-FU challenge, *Crbn*<sup>-/-</sup> HSPC numbers were restored (trending decrease compared to *Crbn*<sup>+/+</sup> HSPC,  $p = 0.14$ ) demonstrating that *Crbn*<sup>-/-</sup> do indeed have a remarkable ability for differentiation and self-renewal in the mature adult bone marrow.

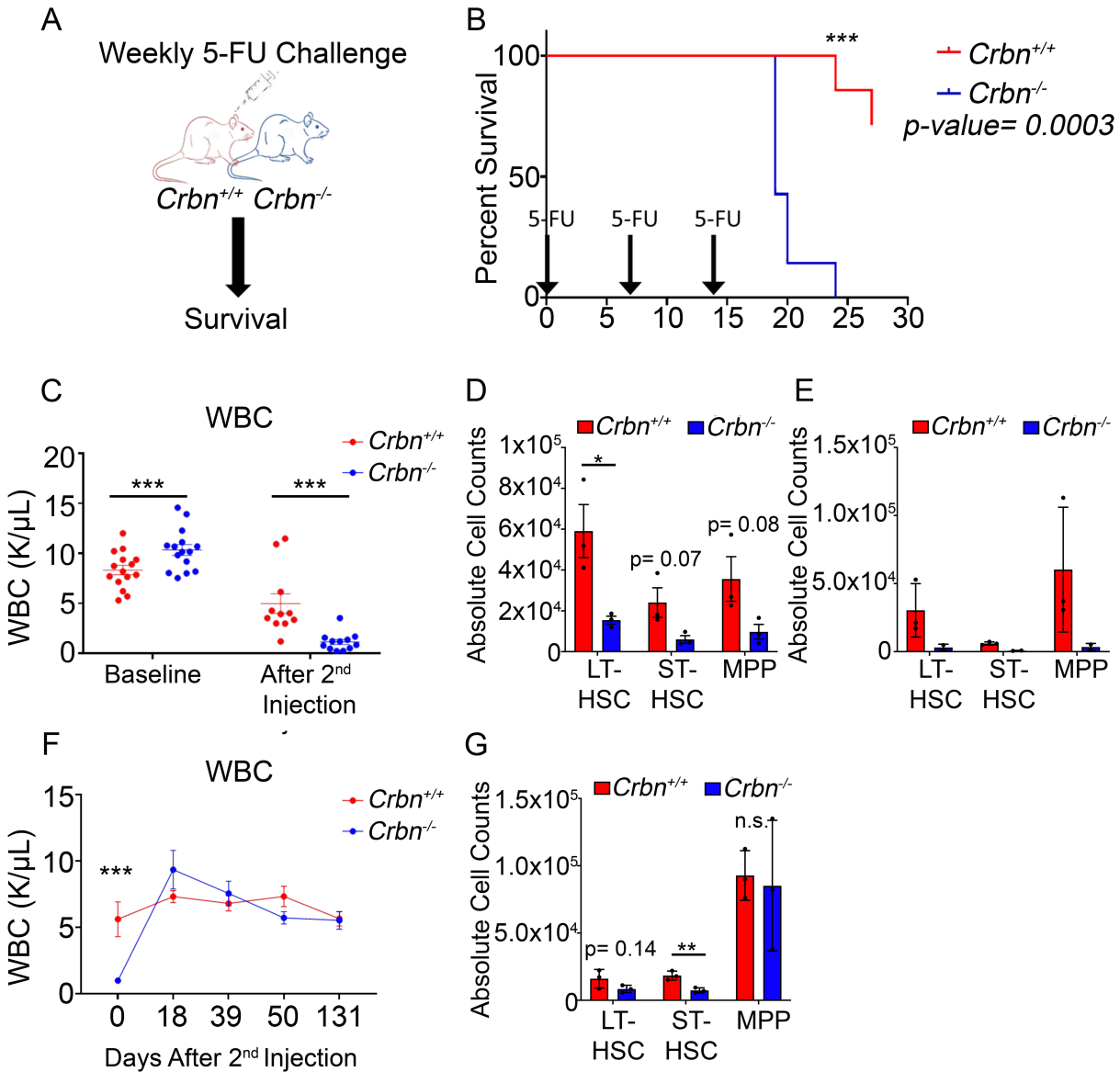


**Figure 32. Increased HSC proliferation sensitizes CRBN-deficient HSCs to 5-FU treatment (A)** Experimental design. *Crbn*<sup>-/-</sup> (n=10) and *Crbn*<sup>+/+</sup> (n=10) littermates were dosed with weekly challenges of 5-FU. **(B)** Survival overtime. P value was determined using Mantel-Cox Log-rant test. **(C-G)** *Crbn*<sup>-/-</sup> (n=15) and *Crbn*<sup>+/+</sup> (n=16) littermates were given 2 doses (1 dose per week) of 5-FU. Five days after each dose, BM from randomly selected 3-4 mice per genotype was harvested and HSPC absolute counts and complete blood counts were measured. **(C)** White blood cell counts (WBCs) at baseline and following 2<sup>nd</sup> Injection. HSPC absolute counts from 1 femur and 1 tibia after the 1<sup>st</sup> (n=3 per genotype) **(D)** and 2<sup>nd</sup> challenge (n=2-3 per genotype) **(E)**. **(F)** WBC counts measured over 131 days after 2<sup>nd</sup> 5-FU challenge (n=5-6 per genotype) via CBCs. **(G)** HSPC absolute counts (using Trumpp et al classification[66]) from 1 femur and 1 tibia (n=3 per genotype) eighteen days after 2<sup>nd</sup> 5-FU challenge. Multiple Student's t-test per population was performed and significance achieved at \**p*<0.05, \*\**p*<0.01, \*\*\**p*<0.001, \*\*\*\**p*<0.0001.

## Control of CXCR4 is associated with LT-HSC regulation

Detailed analysis of fetal and adult hematopoiesis has shown a critical role for the niche, localization, and homing. We found that *Crbn*<sup>-/-</sup> cell homing to adult bone marrow was normal. However, there is a critical role of CXCR4/CXCL12 in immature hematopoiesis in the adult bone marrow[87] and fetal liver[86]. CXCR4 is a G protein-coupled chemokine receptor that binds to classical chemokines and nonclassical activating ligands. Although *Cxcr4* germline deficient mice are perinatally lethal due to gross organ defects[148], there is a dramatic defect in definitive HSC development in the fetal liver due to changes in recruitment, survival and expansion in the fetal BM environment that was associated with diminished stemness, activation, and sensitization to 5-FU[86]. CXCR4 deficient fetal liver cells also showed an increase in cycling HSPC and granulocytes in peripheral blood. Re-expression of CXCR4 repaired the defect and normalized hematopoiesis suggesting that this does not induce stem cell exhaustion or depletion long-term. Moreover, CXCR4 haploinsufficient HSPCs had a competitive repopulating advantage. Therefore, CXCR4 and other adhesion factors important for niche localization, including VCAM-1, were examined in the LT-HSCs and other purified hematopoietic cell populations from adult *Crbn*<sup>-/-</sup> and *Crbn*<sup>+/+</sup> bone marrow. All *Crbn*<sup>-/-</sup> HSPCs (only LT-HSC shown) and Lin<sup>+</sup> had a significant decrease in *Cxcr4* mRNA expression (Figure 33A). CRBN deficiency also provoked loss of *Vcam1* mRNA expression in LT-HSC but no differences in other HSPC and mature populations (Figure 33A). These results were particularly interesting because VCAM-1 deletion has been shown to result in increased egress from the BM with elevated presence in the peripheral blood of immature lymphocyte [149]. Furthermore, thalidomide treatment in endothelial

cell line, HUVEC, resulted in downregulation of TNF $\alpha$ -induced expression of ICAM-1 (CD54), VCAM-1 (CD106) and E-selectin antigens[150] supporting the proposition that CRBN may regulate cell adhesion molecule expression on HSCs.

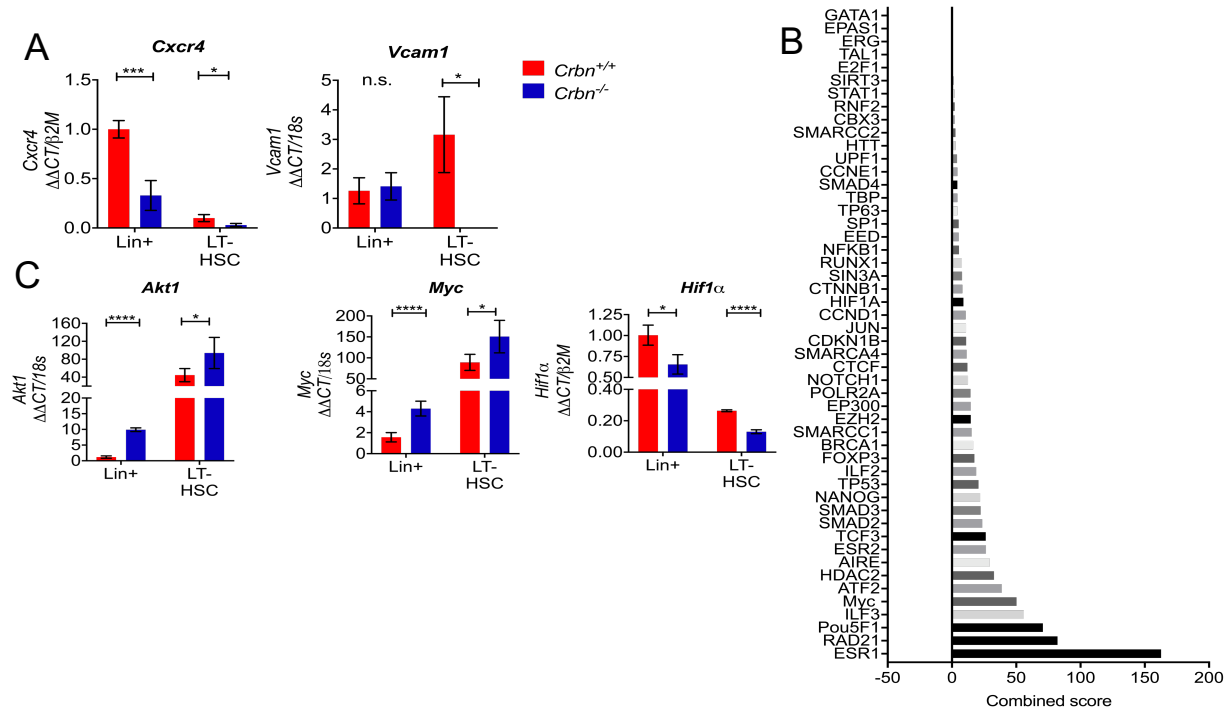


**Figure 33. CRBN deletion alters transcription factor profiles of HSPCs.** (A) Femurs and tibias were harvested from *Crbn*<sup>-/-</sup>(n=7) and *Crbn*<sup>+/+</sup>(n=7) mice. Following lineage depletion cells were stained with flow panel (Table13) and FACs-sorted into Lin<sup>+</sup>, Lin<sup>-</sup>, LSK, MPP, ST-HSC & LT-HSC. RNA was isolated and cDNA synthesized, and qRT-PCR performed to assess mRNA expression of adhesion-related genes *Cxcr4* and *Vcam1*. Gene expression was normalized to  $\Delta\Delta CT$  values obtained from control gene,  $\beta 2M$  and then normalized to *Crbn*<sup>+/+</sup> Lin<sup>+</sup> cells. (B) Dysregulated transcription factors determined by pathway analysis (EnrichR) of RNA-sequencing results from purified *Crbn*<sup>-/-</sup> or *Crbn*<sup>+/+</sup> LSKs. (C) mRNA expression of *Akt1*, *Myc* and *Hif1 $\alpha$*  from *Crbn*<sup>-/-</sup> and *Crbn*<sup>+/+</sup> Lin<sup>+</sup> and LT-HSC. Multiple Student's t-test per population was performed and significance achieved at \*p<0.05, \*\*p<0.01, \*\*\*p<0.001, \*\*\*\*p<0.0001.

Metabolic cues are often orchestrated by niche cells through secreted factors, hypoxia, or cell-to-cell interactions including CXCR4/CXCL12 and VCAM-1/ $\alpha\beta$ -Integrins axes[151-154]. Metabolically activated HSCs are poised to undergo lineage priming and differentiation which results in reduction in stem-related genes[152]. Metabolic status of

HSPCs was analyzed using pathway analysis generated from RNA-sequencing results of purified *Crbn*<sup>-/-</sup> and *Crbn*<sup>+/+</sup> LSKs. Key metabolic pathways, ESR1, MYC, ATF2, HIF1 $\alpha$ , HDAC2, TP53, EZH2, ESR2[155-161], were dysregulated between *Crbn*<sup>-/-</sup> and *Crbn*<sup>+/+</sup> LSKs (Figure 33B). Quantitative RT-PCR validation confirmed CRBN deficiency stimulates metabolic activity as indicated by increased *Akt1* (Lin+ p<0.0001, LT-HSC p<0.05) and *Myc* (Lin+ p<0.0001, LT-HSC p<0.05) mRNA expression accompanied by decreased *Hif1 $\alpha$*  (Lin+ p<0.05, LT-HSC p<0.0001) mRNA levels in *Crbn*<sup>-/-</sup> Lin+ and LT-HSC (Figure 33C). Collectively, the genetic signatures of *Crbn*<sup>-/-</sup> LT-HSC resemble that of activated HSC[152, 162].

### **CRBN loss in niche cells does not alter hematopoiesis**

As HSC extrinsic-induced alterations in niche interactions can influence cell cycle and therefore HSC maintenance, the impact of CRBN deletion in the bone marrow niche was examined using a transplantation model. Whole bone marrow from control congenic mice (CD45.1) was transplanted into lethally irradiated *Crbn*<sup>-/-</sup> (n=15) or *Crbn*<sup>+/+</sup> (n=13) mice (CD45.2) recipient mice. Peripheral blood chimerism and multi-lineage reconstitution were monitored over time (Figure 34A). There were no differences between *Crbn*<sup>-/-</sup> and *Crbn*<sup>+/+</sup> recipients in frequencies of donor derived cells in PB, Sp or BM (Figure 34B, E-F), mature blood cell output in peripheral blood (Figure 34C-D) or HSPC numbers in the bone marrow at endpoint (Figure 34G). These data show that the impact on HSPCs is likely to be driven by an intrinsic role for CRBN in hematopoiesis rather than the regulation of the bone marrow environment.



To test if the difference in response to 5-FU treatment is dependent on the bone marrow niche, we transplanted congenic control WBM cells into lethally irradiated *Crbn*<sup>-/-</sup> and *Crbn*<sup>+/+</sup> mice and administered 3 doses of 5-FU three months post BMT (Figure 35A). There were no observable differences in white blood cell output (Figure 35B) or survival (Figure 35C). However, both *Crbn*<sup>-/-</sup> and *Crbn*<sup>+/+</sup> succumbed to bone marrow failure, likely due to impaired niche function from the combined effects of irradiation and 5-FU.

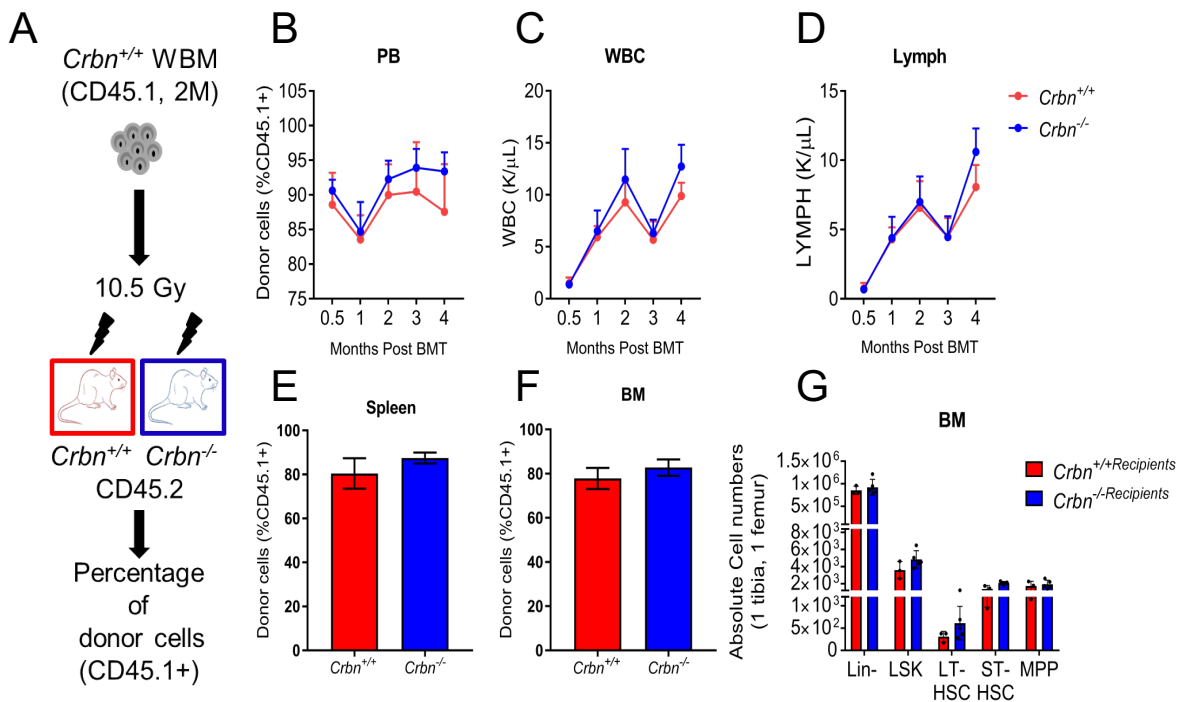


**Figure 34. CRBN deficiency in niche cells does not impact hematopoiesis. (A)** Experimental design. Wild-type whole bone marrow (WBM) ( $1 \times 10^6$ ) CD45.1 cells were transplanted into lethally irradiated *Crbn*<sup>-/-</sup> ( $n=15$ ) or *Crbn*<sup>+/+</sup> ( $n=13$ ) CD45.2 recipients. **(B-D)** Peripheral blood chimerism and complete blood counts (only WBC & Lymph shown) overtime by determined flow cytometric analyses. **(E)** Spleen and BM **(F)** chimerism and HSPC absolute cell counts **(G)** at endpoint ( $n=3-5$  per genotype). Multiple Student's t-test per population was performed and significance achieved at \* $p < 0.05$ , \*\* $p < 0.01$ , \*\*\* $p < 0.001$ , \*\*\*\* $p < 0.0001$ .

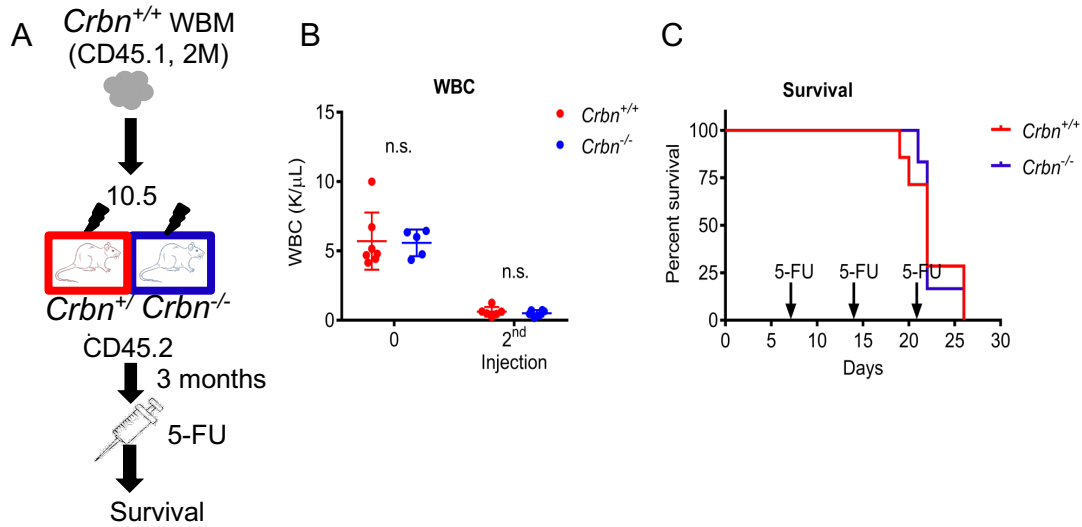


**Figure 35. CRBN deficiency in niche cells does not alter stress hematopoiesis. (A)** Experimental design. Randomly selected cohort from Figure 34; *Crbn*<sup>-/-</sup> (n=5) and *Crbn*<sup>+/+</sup> (n=7) were injected with 3 doses (1 per week) of 5-FU 3 months after initial bone marrow transplant (BMT). **(B)** Peripheral WBC counts were determined one day before 1<sup>st</sup> 5-FU dose and 1 week after 2<sup>nd</sup> 5-FU dose via flow cytometry. Multiple Student's t-test per population was performed and significance achieved at \*p<0.05, \*\*p<0.01, \*\*\*p<0.001, \*\*\*\*p<0.0001. **(C)** Survival overtime. P value was determined using Mantel-Cox Log-rant test.

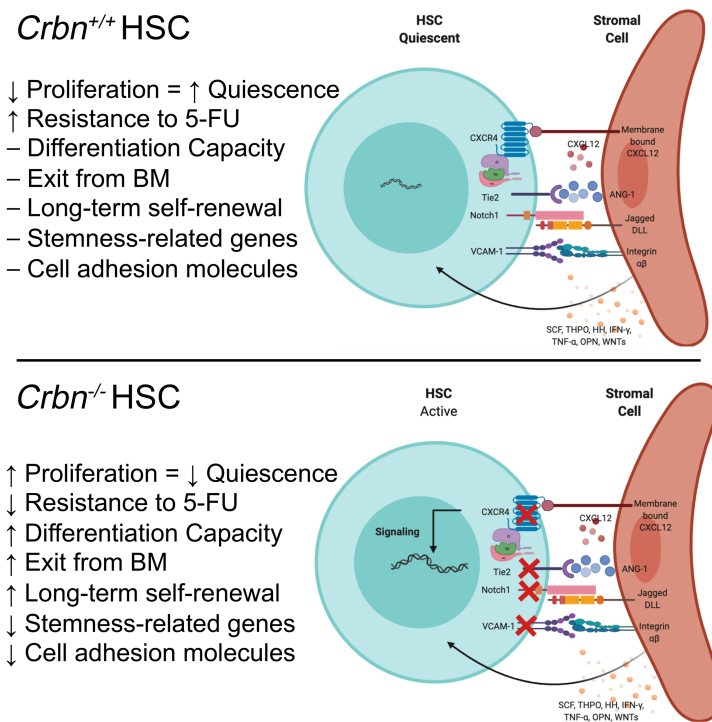


**Figure 36. Visual Abstract**

## Discussion:

Hematopoietic stem cells transplantation (HSCT) from an HLA matched allogeneic donor or from autologous bone marrow can restore the functional hematopoietic system and blood cell production[163]. As such, HSCT has become the gold standard for the treatment of many neoplastic and nonmalignant disorders. However, three major obstacles impede its widespread success: 1) disease relapse, 2) graft-versus-host-disease (GVHD) (in allogeneic HSCT), and 3) a shortage of HSC due to limited HLA-matched donors (in allogeneic HSCT) and unsuccessful *in vitro* expansion of HSC (in both allogeneic and autologous HSCT). Understanding the molecular mechanisms governing HSC cell fate and quiescence could facilitate successful *in vitro* expansion of HSCs and enable the application of HSCT for the treatment of various hematologic and genetic diseases.

Del5q MDS is a pathological disease that arises from hematopoietic stem cells harboring somatically-acquired chromosomal abnormalities[18]. These highly proliferative mutant clones give rise to abnormal immature myeloid cells that colonize the bone marrow and inhibit normal HSC function. BM hypercellularity and peripheral cytopenia is the resultant phenotype in these patients[164]. Primarily del(5q), but also non-del(5q), MDS patients are sensitive to lenalidomide (one of the IMiD® drugs) where it reduces the malignant stem cell population but increases erythropoiesis [43, 141, 165, 166]. Lenalidomide treatment in non-del(5q) MDS patients leads to an increase in erythropoietin (EPO) receptor signaling that stimulates erythropoiesis. In del(5q) MDS, the frequency of cytogenetic and erythroid response is higher due to multiple mechanism of action of lenalidomide treatment in these patients through synthetic lethality. The

del(5q) clonal disorder causes haploinsufficiency of many deleted genes including CK1 $\alpha$ [167]. Lenalidomide-dependent cereblon-mediated degradation of CK1 $\alpha$  induces lethality in the aberrant del(5q) clones [30] and restores effective erythropoiesis through eradication of the malignant clone while simultaneously increasing erythropoietin promoting activity in non-malignant clones. Furthermore, lenalidomide treatment provokes other hematologic responses such as an increase in CXCR4 expression on CD34+ HSPCs, increased differentiation of CD34+ HSPCs characterized by a decrease in CD34+ HSPCs and an increase circulating lymphocytes with increased effector function[141, 166]. These data suggest a regulatory role of cereblon in hematopoiesis perhaps via CXCR4/CXCL12 axis.

In a similar manner, in this study we have identified CRBN as a novel regulator of HSC maintenance. CRBN deficiency in HSC causes a loss of long-term HSCs in the bone marrow characterized by increased proliferation, improved repopulation capability in a non-competitive environment, white blood cell expansion in the periphery as well as a genetic signature that confers decreased dormancy.

Although we did not identify any birth defects in *Crbn*<sup>-/-</sup> mice, there was a consistent decrease in their weight (Figure 20B) that becomes more apparent at older ages (data not shown). CRBN deficiency alleviated high fat diet (HFD)-induced weight gain (data not shown) suggesting a metabolic regulatory function of CRBN. Indeed pathway analysis data comparing differentially expressed transcription factors between *Crbn*<sup>-/-</sup> to *Crbn*<sup>+/+</sup> LSKs highlights many metabolic regulators (ESR1, MYC, ATF2, HIF1 $\alpha$ , HDAC2, TP53, EZH2, ESR2[155-161]) as altered. Validation of expression levels of these crucial metabolic regulators should be confirmed on purified LT-HSC via single cell

transcriptional analysis or total seq for both mRNA and protein analysis. Though preliminary, a slight elevation in mRNA expression of *c-Myc* and *Akt1* observed was in *Crbn*<sup>-/-</sup> LT-HSC supporting the possibility that *Crbn*<sup>-/-</sup> HSC have altered metabolic function. Our laboratory recently investigated CRBN's role in regulating T cell function and showed that it acts to harness effector T cell metabolism. Metabolism induced through antigen engagement in CD8<sup>+</sup> T cells influences the quality and durability of the response and controls pathogen clearance and memory development. Interestingly, CRBN has the highest level of mRNA and protein expression in resting cells and then rapidly declines following T cell receptor (TCR) engagement. Moreover, its expression is highly induced later in the activation response which is consistent with its regulatory role (Hesterberg et al, *manuscript under review*). Our study along with our data suggests that CRBN expression may be required for maintaining a metabolically inactive state (dormancy in LT-HSC).

Previous studies have demonstrated the importance of low mitochondrial activity to the preservation of HSC quiescence and in the prevention of HSC exhaustion [152, 168-174]. *Crbn*<sup>-/-</sup> HSCs showed a modest but significant increase in BrdU staining coupled with enhanced differentiation capacity and sensitivity to 5-FU treatment suggesting that *Crbn*<sup>-/-</sup> HSCs are in a "primed" state, dubbed "G<sub>Alert</sub>" cycle state (neither quiescent nor activated) by Rodgers et al[98]. The G<sub>Alert</sub> state is described as a subdivision of G<sub>0</sub> cell cycle state that is characterized by a distinct transcriptional profile and an accelerated response to physiological stimuli[98, 175, 176]. Though further genetic and proteomic investigation of purified *Crbn*<sup>-/-</sup> and *Crbn*<sup>+/+</sup> LT-HSC is required, *Crbn*<sup>-/-</sup> HSC appear to be poised for activation.

Aggregate results suggest that HSC pools are replenished through symmetric cell division (SCD) and differentiate through asymmetric cell division (ACD). Cues that define these cell fates are under investigation but can be either cell-intrinsic (pre or post-mitosis) or niche-directed. Recent evidence suggests that cell intrinsic pre-mitosis determinants dictate HSC division[177, 178]. At each developmental stage (embryonic (E14.5), adult and aged) *Crbn*<sup>-/-</sup> LT-HSC frequencies and counts are significantly lower than controls even at older ages when LT-HSC expansion has been demonstrated [97, 143, 144, 177]. Hence, we propose that cell-intrinsic factors controlled by CRBN determine the type of HSC division, and therefore, the size of the HSC pool.

HSC retention in the bone marrow and development from fetal liver is controlled by cell autonomous and extrinsic factors. Cell-to-cell interactions between HSCs and niche cell are thought to be the primary mechanism of HSC retention in the bone marrow. In adult bone marrow, niche cells such osteoblasts, CAR cells, sympathetic neurons vascular endothelial cells, and sinusoidal endothelial cells (SECs) express a number of receptor molecules including, N-cadherin, VCAM-1, CD44, membrane-bound stem cell factor and secrete a number of ligands CXCL12, ANG1, THPO that collectively anchor HSCs in their dormant niches[86, 87, 162]. Additionally, HSCs express various receptors CXCR4, VCAM-1, VLA-4, TIE2, MPL, and NOTCH-1 that either directly interact with receptors on the niche cells or respond to factors secreted by them to control localization and dormancy during steady-state[99, 162, 179-183]. *Crbn*<sup>-/-</sup> HSC have a significant reduction in a number of these factors which may contribute to their phenotype in adult BM and fetal liver. Because the loss of HSC is observed at embryonic stages, we propose

that the production, retention and activation of HSC in adult bone marrow is contributing to the low numbers observed in *Crbn*<sup>-/-</sup> adult mice.

Despite their enhanced mature cell output in the peripheral blood and the increase in leukocyte infiltration at older ages, *Crbn*<sup>-/-</sup> mice neither exhibit bone marrow failure nor decreased survival from autoimmune-related conditions. Left unperturbed, no changes in long-term survival were observed between *Crbn*<sup>-/-</sup> and *Crbn*<sup>+/+</sup> littermates. While additional stress-hematopoiesis inducing methods such as exposure to mobilization factor, GM-CSF, or inflammatory endotoxin, lipopolysaccharides (LPS), will determine if CRBN deficient HSCs have impaired response to stress or injury, their ability to restore mature and HSPC numbers after limited 5-FU exposure and non-competitive transplantation suggest CRBN deficient maintain effective response to non-DNA damaging injury.

In conclusion, our results show that CRBN is an emerging regulator of HSC that may have therapeutic implications in hematological malignancies including the modulation of cell-adhesion mediated drug resistance, differentiation/activation of drug-resistant malignant blast cells/tumor-initiating quiescent cells rendering them more susceptible to chemotherapy and increasing the persistence of HSC in recipients who have received HSCT.

## Experimental Procedures

### Animal Husbandry

Germline *Crbn* heterozygous mice (*Crbn*<sup>+/-</sup>) were obtained from Dr. Anjali Rajadhyaksha (Cornell University). Mice were genotyped using methods described by Rajadhyaksha Lab and all genotyping primers can be found below [122]. C57BL/6 and littermates of *Crbn*<sup>-/-</sup> mice were used as *Crbn*<sup>+/+</sup> controls. Congenic mice, B6.SJL-*Ptprc*<sup>a</sup> *Pepc*<sup>b</sup>/BoyJ (CD45.1), were ordered from Jackson Lab (Cat# 002014). All animals were maintained under specific pathogen-free conditions and fed with standard diet. Use of these mice was governed by a research protocol approved by the Institutional Animal Care and Use Committee and all mice were bred and maintained at the H. Lee Moffitt Cancer Center and Research Institute (IACUC protocols IS00006028 and IS00004986).

**Table 10. Cereblon Genotyping Primers**

Mouse strain	Primer	Sequence 5'- 3'
<i>Crbn</i> <sup>+/+</sup>	<i>Loxf</i> (Wild-Type forward primer)	AGGAGCACTGAACGGCTTACAG
<i>Crbn</i> <sup>-/-</sup>	<i>F</i> (knockout forward primer)	TTGTTTCAGAACTGCTGGGATGTG
<i>Crbn</i> <sup>+/+</sup> <i>Crbn</i> <sup>-/-</sup>	<i>Lox R</i> (common reverse primer)	CGCATGCTGACTGATCACAGC

### Flow Cytometry Analysis for BM Populations

Mouse BM cells were harvested for flow cytometric analysis using a previously described protocol[184-187]. Briefly, BM cells were collected from tibias and femurs, lysed using RBC lysis buffer (# 00-4300-54, eBioscience) and incubated with antibodies for 1 hour on ice. Viability was determined using DAPI (Invitrogen Corp., Carlsbad, CA) unless otherwise stated. Mouse peripheral blood was collected from the submandibular vein and subjected to the same RBC lysis and staining procedure as BM. Flow cytometry was run



on a FACS LSRII cytometer (BD Biosciences, San Jose, CA) and analyzed with FlowJo software v10.5.0 (FlowJo LLC, Ashland, Oregon). HSPCs from BM were determined after antibody (clones, commercial sources, instrument settings, fluorochromes and filters are described in Table 11-12. Total LSK, HSC, and MPP measurements were extrapolated based on the total BM counts and an established surface marker profile. To analyze mature populations, mouse BM and peripheral blood samples were incubated with antibody cocktail listed in Table 11-12. To evaluate donor and recipient populations in BM transplantation assays, BM, Sp and peripheral blood cells were stained with PE or BV711 conjugated anti-CD45.1 (clone A20, TONBO Bioscience/ Biolegend) and APC/Cy7-conjugated anti-CD45.2 (clone 104, TONBO Biosciences). Total LSK, HSC, and MPP measurements were extrapolated based on the total BM counts and an established surface marker profile.

### **Bone Marrow Colony Assays**

BM cells ( $1 \times 10^5$  or  $5 \times 10^4$ ) were suspended in 100- $\mu$ l RPMI, which was added to 1.5-ml Methocult medium (# 03444, Stem Cell Technologies) with or without cytokines (# 03231, Stem Cell Technologies) and vigorously vortexed for 30 sec. When bubbles disappeared 20 min later, Methocult medium was dispensed into 35 mm culture dishes and incubated at 37°C and 5% CO<sub>2</sub>. Colonies were observed and counted after incubation for 7 days.

### **Apoptosis, BrdU & Hypoxia Assays**

To examine apoptosis, BM from *Crbn*<sup>-/-</sup> (n=5) and *Crbn*<sup>+/+</sup> (n=4) were harvested and incubate with CellEvent™ Caspase-3/7 (#C10423, Invitrogen Carlsbad, CA) for 30

minutes and then stained with HSPC panel (Table 13). Percentage of hematologic cells positive for caspase 3/7 was assessed via flow cytometry.

For BrdU incorporation assay, BrdU (100 mg/kg body weight; BD Biosciences) was injected intraperitoneally into mice for 16 to 18 h before analysis. BrdU incorporation was determined by flow cytometric analysis using the BrdU Flow Kit (BD Biosciences) according to the manufacturer's instructions.

To investigate hypoxia in the bone marrow, *Crbn*<sup>-/-</sup> and *Crbn*<sup>+/+</sup> mice were intraperitoneally injected with pimonidazole HCl solution (Hypoxyprobe™, #HP2-200Kit, Burlington MA) at a dosage of 60mg/kg body weight or PBS. Ninety minutes later, BM was harvested and stained with HSPCs panel then fixed and permeabilize with Cytofix/cytoperm (# 88-8824-00, eBioscience), then stained with anti-pimonidazole, FITC-conjugated IgG1 mouse monoclonal antibody (clone 4.3.11.3) and analyzed by flow cytometry.

### **BM homing assay**

Lin<sup>-</sup> cells were purified from either *Crbn*<sup>+/+</sup> or *Crbn*<sup>-/-</sup> mice and were labeled with carboxyfluorescein succinimideylester (CFSE). CFSE-labeled Lin<sup>-</sup> (1x10<sup>6</sup>) cells were transplanted into lethally irradiated (550 cGy, 500 cGy, ~3 h apart) recipients. Recipients were sacrificed 16 h later and CFSE<sup>+</sup> bone marrow populations were quantified by flow cytometric analysis to determine the percentage of homed cells.

### **Competitive and non-competitive transplant**

Donor BM cells were harvested from either *Crbn*<sup>+/+</sup> or *Crbn*<sup>-/-</sup> C57BL/6j-*Ptprc*<sup>b</sup> (CD45.2<sup>+</sup>) mice and mixed 1:1 with B6.SJL-*Ptprc*<sup>a</sup> (CD45.1<sup>+</sup>) BM cells. Adult recipient mice (7-12

weeks) were lethally irradiated (550 cGy, 500 cGy, ~ 3 h apart) on the day of transplantation. Recipients received  $1.0 \times 10^6$  cells/mouse (i.v.). Peripheral chimerism, and hematopoietic reconstitution were monitored for indicated times from the submandibular vein to evaluate donor cell engraftment. BM, Spleen and blood (cardiac puncture) chimerism were analyzed via flow cytometry at indicated endpoints.

For non-competitive transplant, BM from

### ***In vivo* 5-FU challenge**

For serial 5-FU treatments, *Crbn*<sup>+/+</sup> (n=15) and *Crbn*<sup>-/-</sup> mice (n=16) (8–13 weeks) were intraperitoneally injected with a single dose (150 mg/kg body weight) of 5-FU weekly, survival was monitored daily and CBCs weekly. Smaller cohort of mice (n=3) were then euthanized at indicated time points, and bone marrow cells were isolated and counted. The proportions of HSPCs were analyzed by flow cytometry and then multiplied by the total number of bone marrow cells to calculate the absolute number of HSPCs.

### **Fetal Liver harvest and culture**

Six to 8-week-old *Crbn*<sup>+/+</sup> or *Crbn*<sup>-/-</sup> breeding pairs were mated at night. The next morning plugged dams were separated. Fourteen days following the time plug was observed (E14.5), pregnant dams were humanely euthanized by CO<sub>2</sub> inhalation. Fetal livers from embryos were dissected out under dissection microscope and placed in ice-cold condition mouse medium[188]. FL were passed through 40-micron cell strainer (#22-363-547, Fisher Scientific, Hampton, NH) using the plunger from a 3mL syringe (#309657, Becton, Dickinson and Company). Once single-cell suspension was attained cells were lysed with

RBC lysis buffer (eBioscience) washed and stained for HSPC panel (Table 13) and analyzed via flow cytometry.

### **RNA-sequencing & pathway analysis**

Bone marrow (femurs, tibia & iliac crest) from *Crbn*<sup>-/-</sup> (n=16) and *Crbn*<sup>+/+</sup> (n=16) were harvested and pooled into groups of four per genotype (mixed genders, distributed equally per group). Following BM processing outlined above, samples were stained with Lineage cocktail, Sca-1 and c-Kit antibodies and LSKs (5x10<sup>5</sup>cells/group) were FAC sorted using BD Aria. Following two washes, pellets were lysed with RLT Plus buffer (RNeasy Micro Kit, #74034, Qiagen, Germantown, MD). Total RNA was then harvested using RNeasy Micro Plus Kit following a modified manufacturer's protocol with additional on-column DNase treatment (RNase-Free DNase Set, #79254, Qiagen) prior to elution. RNA-seq libraries were prepared using the Ovation® SoLo RNA-Seq System (#0501, NuGen, Redwood City, CA) following the manufacturer's protocol. Approximately 50M pairs of 75-base reads per sample were generated on the Illumina NextSeq 500 sequencer. RNA sequence data were aligned to the mouse reference genome mm10 using Tophat2 (PMC2672628). Aligned sequences were assigned to exons using the HTseq package (PMC4287950) against RefSeq gene to generate initial gene counts. Normalization, expression modeling, and differential expression between *Crbn*<sup>+/+</sup> and *Crbn*<sup>-/-</sup> LSKs were performed using DESeq2 (PMC4302049). RNAseq quality control was performed to examine read count metrics, alignment fraction, chromosomal alignment counts, expression distribution measures using RSeqQC (PMID:22743226), and with principal components analysis and

hierarchical clustering. Differentially expressed genes were subjected to pathway analysis using Enrichr (<https://amp.pharm.mssm.edu/Enrichr/>)

### qRT-PCR analysis

Total RNA was extracted using RNeasy Micro Plus Kit (#74034, Qiagen) and used as templates to synthesize cDNA using iScript cDNA synthesis kit (#1708890, Bio-Rad Laboratories) according to the manufacturer's instructions. cDNA was added to Taqman PCR mix (Life Technologies) in a 12- $\mu$ L final volume containing forward and reverse primers. Amplification cycles (n=40) were performed using 7900HT Real-time PCR System (Applied Biosystems). Primers were purchased from Life Technologies, Carlsbad, CA. See Table 14 for list of TaqMan primers used. Data were normalized to the reference gene 18S ribosomal RNA (18S) or  $\beta$ 2 microglobulin (B2M) by a relative quantification using the  $\Delta\Delta$ Ct method and was measured relative to *Crbn*<sup>+/+</sup> Lin<sup>+</sup> cells or *Crbn*<sup>+/+</sup> LSK (in the instances where the genes were not expressed by Lin<sup>+</sup> cells).

**Table 11. List of Taqman Primers**

Gene	TaqMan RefSeq
<i>Crbn</i>	Mm01182416_m1
<i>Akt1</i>	Mm01331626_m1
<i>Myc</i>	Mm00487804_m1
<i>Hif1<math>\alpha</math></i>	Mm00468869_m1
<i>Gata1</i>	Mm01352636_m1
<i>Notch1</i>	Mm00627185_m1
<i>Tek</i>	Mm00443243_m1
<i>Mpl</i>	Mm00440310_m1
<i>Vcam1</i>	Mm01320970_m1
<i>Cxcr4</i>	Mm01996749_s1

## Statistical Analyses

Statistical analyses were conducted using GraphPad Prism Software (GraphPad Software, Inc, La Jolla, CA). Differences between groups were compared using the unpaired two-tailed multiple Student's t-test corrected for multiple comparisons using Holm-Sidak method. Equal variance is assumed between groups. One-way ANOVA followed by Dunnett's multiple comparison was performed when comparing multiple groups. Survival statistics were measured using Mantel-Cox Log-rank test. Statistical significance was established at \*\*\*\* P <0.0001, \*\*\* P<0.001, \*\* P <0.01, \* P<0.05. All data represented as mean with standard deviation bars representing  $\pm$  standard deviation. The number of animals used for biological replicates is listed in figure legends. Technical replicate experiments (primarily qRT-PCR analysis) are representative of 1-2 independent experiments and contain 3-5 replicates. Group sizes were based on prior experience with similar studies.

**Table 12. Flow cytometry instrument settings**

Laser			Detector Spectral Range (nm)	Optical Filters		Fluorochrome
Wavelength (nm)	Power (nm)	Type		Long Pass (nm)	Band Pass (nm)	
488	50	DPSS	685-735	685	710/50	PerCP- Cy5.5
			505-525	505	515/20	FITC, BB515
			483-493	--	488/10	SSC
405	100	DPSS	755-810	755	780/60	BV785
			685-735	670	710/50	BV711
			650-670	630	660/20	BV650

**Table 12 (cont.)**

Laser			Detector Spectral Range (nm)	Optical Filters		Fluorochrome
Wavelength (nm)	Power (nm)	Type		Long Pass (nm)	Band Pass (nm)	
			600-620	590	610/20	BV605
			570-607*	570	585/42	BV570
			505-525	505	515/20	BV510
			425-475	--	450/50	BV421
640	100	DPSS	750-810	740	780/60	APC-H7/Cy7
			685-735	685	710/50	AF700
			663-677	--	670/14	AF647, APC
532	150	DPSS	760-800	740	780/40	PE-Cy7
			690-735*	690	710/50	PE-Cy5.5
			640-680	640	660/40	PE-Cy5
			600-620	595	610/20	PE-CF594
			562-588	--	575/26	PE
355	20	DPSS	790-850	770	820/60	BUV805
			500-530	450	515/30	BUV496
			365-393	--	379/28	BUV395

Instrument Configuration. This panel was developed and optimized for use on BDLsRII flow cytometry instrument with the listed optical configuration.

**Table 13. Flow cytometry antibodies and panel design**

Antibody						Staining Conditions			
Specificity	Fluorochrome	Clone	Vendor	Catalog Number	Vol/Test (µL)	Vol (µL)	T (C)	t (min)	Step
<b>Mature Populations</b>									
CD45	PE/CF594	30-F11	BD	562420	1	100	4	60	EC
CD3	BV711	145-2C11	BL	100349	1	100	4	60	EC
	or FITC		BD	553061					
B220	PerCP/Cy5.5	RA3-6B2	BL	103236	1	100	4	60	EC
CD41	BV605	MWReg30	BL	133921	1	100	4	60	EC
F4/80	BUV395	T45-2342	BD	565614	1	100	4	60	EC
CD11b	APC	M1/70	BL	101212	1	100	4	60	EC
Ter119	BV510	TER-119	BL	116237	1	100	4	60	EC
CD71	PE/Cy7	RI7217	BL	113812	1	100	4	60	EC
DAPI			TF	D3571	1	100	4	60	EC
<b>Lineage Cocktail</b>									
CD3	Biotin	145-2C11	BL	100304	1	100	4	60	EC
CD4	Biotin	RM4-5	eBio	13-0042-85	1	100	4	60	EC
CD8	Biotin	53-6.7	BL	100704	1	100	4	60	EC
CD11b	Biotin	M1/70	BD	553309	1	100	4	60	EC
CD19	Biotin	6D5	BL	115504	1	100	4	60	EC
CD127	Biotin	B12-1	BD	555288	1	100	4	60	EC



Antibody						Staining Conditions			
Specificity	Fluorochrome	Clone	Vendor	Catalog Number	Vol/Test (μL)	Vol (μL)	T (C)	t (min)	Step
B220	Biotin	RA3-6B2	BL	103204	1	100	4	60	EC
Gr-1	Biotin	RB6-8C5	BD	553125	1	100	4	60	EC
Ter119	Biotin	TER-119	BL	116204	1	100	4	60	EC
<b>Stem and Progenitor Populations</b>									
CD45	PE/CF594	30-F11	BD	562420		100	4	60	EC
Streptavidin	APC-Cy7		BL	405208	1	100	4	60	EC
c-Kit	APC	2B8	BL	105812	1	100	4	60	EC
Sca-1	PE-Cy7	D7	BL	108114	1	100	4	60	EC
CD34	PE	RAM34	BD	551387	4	100	4	60	EC
CD135	BV421	A2F10	BL	135314	1	100	4	60	EC
CD150	PerCP/Cy5.5	TC15-12F 12.2	BL	115922	1	100	4	60	EC
CD 48	BV 605	HM48-1	BL	103441	1	100	4	60	EC
Ghost Dye Viability Dye	BV510		Tonbo	TB-13-087 0-T500	1	100	4	60	EC
<b>Congenetic Markers</b>									
CD45.1	PE or BV711	A20	Tonbo BL	TB-50-045 3-U100 110739	1	100	4	60	EC
CD45.2	APC/Cy7	104	Tonbo	TB-25-045 4-U100	1	100	4	60	EC

Commercial reagents used in the final panel (Abbreviations: BL, BioLegend; BD, Becton-Dickinson; eBio, Affymetrix eBioscience; Tonbo, Tonbo Biosciences; TF, Thermo Fischer Scientific; EC, extracellular staining.

## CHAPTER FOUR

### SUMMARY, FUTURE PERCEPTIVES AND CLINICAL IMPLICATIONS

The successful use of IMiD®s in hematological cancers, as well as the development of PROTACs has brought CRBN to the forefront of various fields, including oncology and medicinal chemistry. Differences in IMiD® effects on mouse and human cells have been reported, suggesting differential regulation of CRBN by IMiD®s[15, 100]. In these studies (Chapter 2), we have determined that the non-conserved Ile391 in the thalidomide binding domain of mouse CRBN thalidomide-binding domain (TBD) does not alter its binding affinity with immunomodulatory drugs and that mouse CRBN can trigger CRBN-dependent degradation of BRD4, confirming that the CRBN/DDB1/Cu14A/Rbx1 complex is indeed functional in mouse cells. However, our work also established a critical difference between substrate recruitment of mouse and human CRBN, highlighting the impact this difference will have on the development and testing of novel IMiD®s and PROTACs. Because mouse CRBN is incapable of degrading the IMiD®-associated (in human cells) neo-substrates IKAROS, AIOLOS, and CK1 $\alpha$ , and potentially other unidentified targets that contain  $\beta$ -hairpin-loop tertiary structure that the form van der Waal interactions with V388, careful consideration of appropriate preclinical models must be taken to accurately assess potential/unexpected drug effects in humans.

The development of homo-PROTACs that degrade cereblon has provided a useful tool to study the endogenous function of cereblon across different cell types and diseases[57]. Preliminary studies conducted in our lab using a novel cereblon degrader

demonstrated a potential to expand human T cells *in vitro*, to improve effector function in tumor-infiltrating lymphocyte (TIL) therapy and to sensitize tumor cells to chemotherapy. Additionally, our cereblon degrader was functional in mouse T cells *in vitro* and showed promising pharmacodynamics, pharmacokinetics properties and target engagement when orally administered to mice.

Furthermore, homo-PROTAC cereblon degraders will serve as valuable tools in the exploration of the effects of acute versus chronic deletion of CRBN in HSC and in the identification of key endogenous players (e.g. substrates) in CRBN-mediated regulation of HSC cell fate. For example, oral administration of a CRBN degrader over short or extended periods followed by lineage output monitoring via flow cytometric analysis of peripheral blood, bone marrow and spleen will provide additional evidence that indeed CRBN ablation increases differentiation capacity and thereafter a subsequent loss in HSPCs. Additionally, the use of a cereblon degrader may distinguish between species-dependent IMiD®-mediated or endogenous protein regulation, which could provide critical information in preclinical drug design. Using these new agents, it may be possible to appreciate the physiological roles for CRBN in protein regulation since it is evident that it plays a fundamental role in both IMiD®-mediated and endogenous intracellular protein regulation.

Our work has also highlighted a novel therapeutic vulnerability due to CRBN's regulation of HSC cell fate in hematological malignant cells (Chapter 3). Chemical depletion of cereblon could target quiescent and drug resistant minimal residual disease (MRD) and leukemia initiating cells (LIC) by suppressing quiescence and stimulating susceptibility to chemotherapy. Furthermore, since we observe a decrease in mRNA

expression of *Cxcr4*, *Vcam-1* and *Tek* (gene encodes Tie2) in stem cells that lack CRBN, CRBN ablation has the potential to target cell adhesion-mediated drug resistance facilitated by CXCR4/CXCL12, VCAM-1/VLA-4 and TIE2/ANG-1 interactions[189]. Our studies presented here as well as in previous works[58, 142], highlight a potential role for CRBN-mediated regulation of metabolism. Future assessment of CRBN's role in regulating metabolic activity of hematopoietic and immune cells may highlight CRBN as a potential novel therapeutic target for metabolic disorders such as cutaneous lupus erythematosus (CLE), rheumatoid arthritis, multiple sclerosis and diabetes. Through modulation of CRBN expression/function it may be possible to inhibit aberrantly regulated metabolic pathways in cells that rely on an overactive metabolism for survival. Indeed non-malignant diseases such as cutaneous lupus, a condition whereby immune cells attack the body's own tissues as due to impaired immunosurveillance, are now being effectively treated with IMiDs [190-192]. This clinical activity has been difficult to comprehend given the potentiating effects of IMiDs on T cells, a cell population that is hyperactivated in these autoimmune diseases. In a trial of 59 patients receiving allogeneic stem cell transplantation, the potentiation of T cells was evident from an increased severity of GVHD in a thalidomide-treated cohort compared to a group receiving placebo [193]. However, thalidomide was developed in 1953 where it was widely released to the public based on rodent models that led to the belief that the drug is nontoxic to humans. After the teratogenic effects were discovered by a German pediatrician and geneticist linking it to the induction of congenital abnormalities when used in pregnancy [194, 195], the drug gained traction for profound clinical activity in a patient with erythema nodosum leprosum (ENL)[196]. As a severe inflammatory condition

associated with leprosy, this clinical activity led to the subsequent research of thalidomide in other inflammatory conditions including sarcoidosis, cutaneous lupus, inflammatory bowel diseases, ankylosing spondylitis and rheumatoid arthritis. Mechanistically, responses of IMiD®s in inflammatory conditions has been linked to the suppression of TNF $\alpha$  mRNA and NF $\kappa$ B DNA binding [197] as well as IL-6 and IL-12 [198]. However, our research demonstrating the direct functions of CRBN on hematopoiesis generates rationale for development of a pure agonist – to degrade neo-substrates, and pure antagonist – to suppress CRBN. While these two mechanisms are occurring simultaneously in the current IMiD® compounds, separation of the activity may induce distinct clinical outcomes.

Finally, the continued investigation of regulators of HSC cell fate will enhance our understanding of stem cell biology and could positively impact the use of hematopoietic stem cell transplantation (HSCT) and other HSC-based clinical applications. HSC expansion *ex vivo* and *in vivo* is dependent on the balance among various cell fates including quiescence, self-renewal, differentiation, apoptosis, and migration. Previous attempts to obtain higher numbers of transplantable HSC, in both allogeneic and autologous HSCT, to achieve rapid and sustainable engraftment have had limited success[199-202]. Since CRBN deficient HSC show enhanced long-term self-renewal capacity in non-competitive transplantation, a “block” in HSC aging phenotypes and increased differentiation potential, the modulation of CRBN expression could provide a mechanism to enhance the persistence of HSCs following transplantation. Moreover, the increased proliferative state of *Crbn*<sup>-/-</sup> HSC may enhance targeted genome editing techniques in HSCs and/or improve the ability to expand such manipulated HSCs *ex vivo*.

In conclusion, our work has highlighted important aspects of the biochemical properties and cell biological functions CRBN. Our studies strongly support the need for continuing the elucidation of these biochemical properties and cell biological functions in the context of both the normal function of CRBN, as well as its altered activity in response to IMiD® therapies. Our studies presented here along with such future studies will provide important contributions to the preclinical development of PROTAC compounds. Ultimately, understanding the integrated constituents required for HSC cell fate decisions will have a profound impact on HSC-based therapeutic approaches, and for additional discoveries of regulatory components of HSC fate.

## REFERENCES

1. Shi, Q. and L. Chen, *Cereblon: A Protein Crucial to the Multiple Functions of Immunomodulatory Drugs as well as Cell Metabolism and Disease Generation*. Journal of immunology research, 2017. **2017**: p. 9130608-9130608.
2. Sievers, F. and D.G. Higgins, *Clustal Omega, accurate alignment of very large numbers of sequences*. Methods Mol Biol, 2014. **1079**: p. 105-16.
3. Abruzzese, M.P., et al., *The homeobox transcription factor MEIS2 is a regulator of cancer cell survival and IMiDs activity in Multiple Myeloma: modulation by Bromodomain and Extra-Terminal (BET) protein inhibitors*. Cell Death & Disease, 2019. **10**(4): p. 324.
4. A Akuffo, A., et al., *Controversy regarding the functional conservation of cereblon CUL4-type E3 ligase substrate receptor*. Integrative Cancer Science and Therapeutics, 2018. **5**(4).
5. Ward, S.P., *Thalidomide and congenital abnormalities*. Br Med J, 1962. **2**(5305): p. 646-7.
6. Diggle, G.E., *Thalidomide: 40 years on*. Int J Clin Pract, 2001. **55**(9): p. 627-31.
7. Peltzman, S., *An Evaluation of Consumer Protection Legislation: The 1962 Drug Amendments*. Journal of Political Economy, 1973. **81**(5): p. 1049-1091.
8. D'Amato, R.J., et al., *Thalidomide is an inhibitor of angiogenesis*. Proc Natl Acad Sci U S A, 1994. **91**(9): p. 4082-5.
9. Haslett, P.A., et al., *Thalidomide costimulates primary human T lymphocytes, preferentially inducing proliferation, cytokine production, and cytotoxic responses in the CD8+ subset*. J Exp Med, 1998. **187**(11): p. 1885-92.
10. Singhal, S., et al., *Antitumor activity of thalidomide in refractory multiple myeloma*. N Engl J Med, 1999. **341**(21): p. 1565-71.
11. Thomas, D.A., *Pilot studies of thalidomide in acute myelogenous leukemia, myelodysplastic syndromes, and myeloproliferative disorders*. Seminars in Hematology, 2000. **37**: p. 26-34.
12. Zeldis, J.B., et al., *S.T.E.P.S.: a comprehensive program for controlling and monitoring access to thalidomide*. Clin Ther, 1999. **21**(2): p. 319-30.
13. Fischer, E.S., et al., *Structure of the DDB1-CRBN E3 ubiquitin ligase in complex with thalidomide*. Nature, 2014. **512**(7512): p. 49-53.
14. Kronke, J., et al., *Lenalidomide causes selective degradation of IKZF1 and IKZF3 in multiple myeloma cells*. Science, 2014. **343**(6168): p. 301-5.
15. Petzold, G., E.S. Fischer, and N.H. Thoma, *Structural basis of lenalidomide-induced CK1alpha degradation by the CRL4(CRBN) ubiquitin ligase*. Nature, 2016. **532**(7597): p. 127-30.
16. Iyer, C.G., et al., *WHO co-ordinated short-term double-blind trial with thalidomide in the treatment of acute lepra reactions in male lepromatous patients*. Bull World Health Organ, 1971. **45**(6): p. 719-32.



17. Sampaio, E.P., et al., *Thalidomide selectively inhibits tumor necrosis factor alpha production by stimulated human monocytes*. J Exp Med, 1991. **173**(3): p. 699-703.
18. List, A., et al., *Efficacy of lenalidomide in myelodysplastic syndromes*. N Engl J Med, 2005. **352**(6): p. 549-57.
19. Brimnes, M.K., I.M. Svane, and H.E. Johnsen, *Impaired functionality and phenotypic profile of dendritic cells from patients with multiple myeloma*. Clin Exp Immunol, 2006. **144**(1): p. 76-84.
20. Brown, R.D., et al., *Dendritic cells from patients with myeloma are numerically normal but functionally defective as they fail to up-regulate CD80 (B7-1) expression after huCD40LT stimulation because of inhibition by transforming growth factor-beta1 and interleukin-10*. Blood, 2001. **98**(10): p. 2992-8.
21. Maecker, B., et al., *Viral antigen-specific CD8+ T-cell responses are impaired in multiple myeloma*. Br J Haematol, 2003. **121**(6): p. 842-8.
22. Quach, H., et al., *Mechanism of action of immunomodulatory drugs (IMiDs) in multiple myeloma*. Leukemia, 2010. **24**(1): p. 22-32.
23. Urashima, M., et al., *Transforming growth factor-beta1: differential effects on multiple myeloma versus normal B cells*. Blood, 1996. **87**(5): p. 1928-38.
24. Bharti, A.C., et al., *Nuclear factor-kappaB and STAT3 are constitutively active in CD138+ cells derived from multiple myeloma patients, and suppression of these transcription factors leads to apoptosis*. Blood, 2004. **103**(8): p. 3175-84.
25. Hideshima, T., et al., *The role of tumor necrosis factor alpha in the pathophysiology of human multiple myeloma: therapeutic applications*. Oncogene, 2001. **20**(33): p. 4519-4527.
26. Qian, S., et al., *Therapeutic effects of thalidomide in myeloma are associated with the expression of fibroblast growth factor receptor 3*. Therapeutics and clinical risk management, 2005. **1**(3): p. 231-241.
27. Zhang, Z.-L., Z.-S. Liu, and Q. Sun, *Effects of thalidomide on angiogenesis and tumor growth and metastasis of human hepatocellular carcinoma in nude mice*. World journal of gastroenterology, 2005. **11**(2): p. 216-220.
28. Ito, T., et al., *Identification of a primary target of thalidomide teratogenicity*. Science, 2010. **327**(5971): p. 1345-50.
29. Lupas, A.N., H. Zhu, and M. Korycinski, *The Thalidomide-Binding Domain of Cereblon Defines the CULT Domain Family and Is a New Member of the beta-Tent Fold*. PLOS Computational Biology, 2015. **11**(1): p. e1004023.
30. Krönke, J., et al., *Lenalidomide induces ubiquitination and degradation of CK1alpha in del(5q) MDS*. Nature, 2015. **523**(7559): p. 183-188.
31. Petzold, G., E.S. Fischer, and N.H. Thoma, *Structural basis of lenalidomide-induced CK1alpha degradation by the CRL4 ubiquitin ligase*. Nature, 2016.
32. Gandhi, A.K., et al., *Measuring cereblon as a biomarker of response or resistance to lenalidomide and pomalidomide requires use of standardized reagents and understanding of gene complexity*. Br J Haematol, 2014. **164**(2): p. 233-44.
33. O'Brien, S., et al., *Ikaros imposes a barrier to CD8+ T cell differentiation by restricting autocrine IL-2 production*. J Immunol, 2014. **192**(11): p. 5118-29.

34. Thomas, R.M., et al., *Ikaros enforces the costimulatory requirement for IL2 gene expression and is required for anergy induction in CD4+ T lymphocytes*. J Immunol, 2007. **179**(11): p. 7305-15.
35. Kronke, J., et al., *Lenalidomide induces ubiquitination and degradation of CK1alpha in del(5q) MDS*. Nature, 2015. **523**(7559): p. 183-8.
36. Manni, S., et al., *Inactivation of CK1 $\alpha$  in multiple myeloma empowers drug cytotoxicity by affecting AKT and  $\beta$ -catenin survival signaling pathways*. Oncotarget, 2017. **8**(9): p. 14604-14619.
37. Fratta, I.D., E.B. Sigg, and K. Maiorana, *Teratogenic effects of thalidomide in rabbits, rats, hamsters, and mice*. Toxicology and Applied Pharmacology, 1965. **7**(2): p. 268-286.
38. Lu, J., et al., *Metabolism of Thalidomide in Liver Microsomes of Mice, Rabbits, and Humans*. Journal of Pharmacology and Experimental Therapeutics, 2004. **310**(2): p. 571-577.
39. Schumacher, H.J., et al., *Thalidomide: disposition in rhesus monkey and studies of its hydrolysis in tissues of this and other species*. J Pharmacol Exp Ther, 1970. **173**(2): p. 265-9.
40. Woollam, D.H., *Thalidomide disaster considered as an experiment in mammalian teratology*. British medical journal, 1962. **2**(5299): p. 236-237.
41. Kim, J.H. and A.R. Scialli, *Thalidomide: The Tragedy of Birth Defects and the Effective Treatment of Disease*. Toxicological Sciences, 2011. **122**(1): p. 1-6.
42. Ito, T. and H. Handa, *Recent topics in IMiDs and cereblon*. Rinsho Ketsueki, 2017. **58**(10): p. 2067-2073.
43. Wei, S., et al., *Lenalidomide promotes p53 degradation by inhibiting MDM2 auto-ubiquitination in myelodysplastic syndrome with chromosome 5q deletion*. Oncogene, 2013. **32**(9): p. 1110-1120.
44. Carpio, C., et al., *Avadomide monotherapy in relapsed/refractory DLBCL: Safety, efficacy, and a predictive gene classifier*. Blood, 2020.
45. Bjorklund, C.C., et al., *Iberdomide (CC-220) is a potent cereblon E3 ligase modulator with antitumor and immunostimulatory activities in lenalidomide- and pomalidomide-resistant multiple myeloma cells with dysregulated CRBN*. Leukemia, 2019.
46. Sakamoto, K.M., et al., *Protacs: chimeric molecules that target proteins to the Skp1-Cullin-F box complex for ubiquitination and degradation*. Proc Natl Acad Sci U S A, 2001. **98**(15): p. 8554-9.
47. Crews, C.M., *Targeting the undruggable proteome: the small molecules of my dreams*. Chemistry & biology, 2010. **17**(6): p. 551-555.
48. Gu, S., et al., *PROTACs: An Emerging Targeting Technique for Protein Degradation in Drug Discovery*. BioEssays, 2018. **40**(4): p. 1700247.
49. Petterson, M. and C.M. Crews, *PROteolysis TArgeting Chimeras (PROTACs) — Past, present and future*. Drug Discovery Today: Technologies, 2019. **31**: p. 15-27.
50. Sakamoto, K.M., et al., *Development of Protacs to target cancer-promoting proteins for ubiquitination and degradation*. Mol Cell Proteomics, 2003. **2**(12): p. 1350-8.

51. Winter, G.E., et al., *DRUG DEVELOPMENT. Phthalimide conjugation as a strategy for in vivo target protein degradation*. Science, 2015. **348**(6241): p. 1376-81.
52. Lu, J., et al., *Hijacking the E3 Ubiquitin Ligase Cereblon to Efficiently Target BRD4*. Chem Biol, 2015. **22**(6): p. 755-63.
53. Zhou, B., et al., *Discovery of a Small-Molecule Degradator of Bromodomain and Extra-Terminal (BET) Proteins with Picomolar Cellular Potencies and Capable of Achieving Tumor Regression*. J Med Chem, 2018. **61**(2): p. 462-481.
54. Buhimschi, A.D., et al., *Targeting the C481S Ibrutinib-Resistance Mutation in Bruton's Tyrosine Kinase Using PROTAC-Mediated Degradation*. Biochemistry, 2018. **57**(26): p. 3564-3575.
55. Sun, Y., et al., *PROTAC-induced BTK degradation as a novel therapy for mutated BTK C481S induced ibrutinib-resistant B-cell malignancies*. Cell Res, 2018. **28**(7): p. 779-781.
56. Zhu, Y.X., et al., *Cereblon expression is required for the antimyeloma activity of lenalidomide and pomalidomide*. Blood, 2011. **118**(18): p. 4771-9.
57. Steinebach, C., et al., *Homo-PROTACs for the Chemical Knockdown of Cereblon*. ACS Chemical Biology, 2018. **13**(9): p. 2771-2782.
58. Lee, K.M., et al., *Functional modulation of AMP-activated protein kinase by cereblon*. Biochim Biophys Acta, 2011. **1813**(3): p. 448-55.
59. Xu, Q., et al., *Expression of the cereblon binding protein argonaute 2 plays an important role for multiple myeloma cell growth and survival*. BMC Cancer, 2016. **16**: p. 297.
60. Nguyen, T.V., et al., *Glutamine Triggers Acetylation-Dependent Degradation of Glutamine Synthetase via the Thalidomide Receptor Cereblon*. Mol Cell, 2016. **61**(6): p. 809-20.
61. Eichner, R., et al., *Immunomodulatory drugs disrupt the cereblon-CD147-MCT1 axis to exert antitumor activity and teratogenicity*. Nat Med, 2016. **22**(7): p. 735-43.
62. Weissman, I.L., *Stem cells: units of development, units of regeneration, and units in evolution*. Cell, 2000. **100**(1): p. 157-68.
63. Spangrude, G.J., S. Heimfeld, and I.L. Weissman, *Purification and characterization of mouse hematopoietic stem cells*. Science, 1988. **241**(4861): p. 58-62.
64. Baum, C.M., et al., *Isolation of a candidate human hematopoietic stem-cell population*. Proceedings of the National Academy of Sciences of the United States of America, 1992. **89**(7): p. 2804-2808.
65. Bhatia, M., et al., *Purification of primitive human hematopoietic cells capable of repopulating immune-deficient mice*. Proc Natl Acad Sci U S A, 1997. **94**(10): p. 5320-5.
66. Cabezas-Wallscheid, N., et al., *Identification of regulatory networks in HSCs and their immediate progeny via integrated proteome, transcriptome, and DNA methylome analysis*. Cell Stem Cell, 2014. **15**(4): p. 507-522.
67. Cheng, H., Z. Zheng, and T. Cheng, *New paradigms on hematopoietic stem cell differentiation*. Protein & Cell, 2020. **11**(1): p. 34-44.

68. Liu, L., et al., *Homing and Long-Term Engraftment of Long- and Short-Term Renewal Hematopoietic Stem Cells*. PLOS ONE, 2012. **7**(2): p. e31300.
69. Velten, L., et al., *Human haematopoietic stem cell lineage commitment is a continuous process*. Nat Cell Biol, 2017. **19**(4): p. 271-281.
70. Sanjuan-Pla, A., et al., *Platelet-biased stem cells reside at the apex of the haematopoietic stem-cell hierarchy*. Nature, 2013. **502**(7470): p. 232-6.
71. Yamamoto, R., et al., *Clonal analysis unveils self-renewing lineage-restricted progenitors generated directly from hematopoietic stem cells*. Cell, 2013. **154**(5): p. 1112-1126.
72. Notta, F., et al., *Distinct routes of lineage development reshape the human blood hierarchy across ontogeny*. Science, 2016. **351**(6269): p. aab2116.
73. de Bruijn, M.F., et al., *Definitive hematopoietic stem cells first develop within the major arterial regions of the mouse embryo*. Embo j, 2000. **19**(11): p. 2465-74.
74. Umeda, K., et al., *Development of primitive and definitive hematopoiesis from nonhuman primate embryonic stem cells in vitro*. Development, 2004. **131**(8): p. 1869-1879.
75. Zambidis, E.T., et al., *Hematopoietic differentiation of human embryonic stem cells progresses through sequential hematoendothelial, primitive, and definitive stages resembling human yolk sac development*. Blood, 2005. **106**(3): p. 860-870.
76. Zhao, M. and L. Li, *Dissecting the bone marrow HSC niches*. Cell Research, 2016. **26**(9): p. 975-976.
77. Lo Celso, C., et al., *Live-animal tracking of individual haematopoietic stem/progenitor cells in their niche*. Nature, 2009. **457**(7225): p. 92-96.
78. Pinho, S. and P.S. Frenette, *Haematopoietic stem cell activity and interactions with the niche*. Nature Reviews Molecular Cell Biology, 2019. **20**(5): p. 303-320.
79. Zhang, J., et al., *Identification of the haematopoietic stem cell niche and control of the niche size*. Nature, 2003. **425**(6960): p. 836-41.
80. Calvi, L.M., et al., *Osteoblastic cells regulate the haematopoietic stem cell niche*. Nature, 2003. **425**(6960): p. 841-6.
81. Guerrouahen, B.S., I. Al-Hijji, and A.R. Tabrizi, *Osteoblastic and vascular endothelial niches, their control on normal hematopoietic stem cells, and their consequences on the development of leukemia*. Stem Cells Int, 2011. **2011**: p. 375857.
82. Morrison, S.J. and D.T. Scadden, *The bone marrow niche for haematopoietic stem cells*. Nature, 2014. **505**(7483): p. 327-334.
83. Xie, Y., et al., *Detection of functional haematopoietic stem cell niche using real-time imaging*. Nature, 2009. **457**(7225): p. 97-101.
84. Kunisaki, Y., et al., *Arteriolar niches maintain haematopoietic stem cell quiescence*. Nature, 2013. **502**(7473): p. 637-43.
85. Mendelson, A. and P.S. Frenette, *Hematopoietic stem cell niche maintenance during homeostasis and regeneration*. Nature Medicine, 2014. **20**(8): p. 833-846.
86. Nie, Y., Y.-C. Han, and Y.-R. Zou, *CXCR4 is required for the quiescence of primitive hematopoietic cells*. The Journal of experimental medicine, 2008. **205**(4): p. 777-783.



87. Sugiyama, T., et al., *Maintenance of the hematopoietic stem cell pool by CXCL12-CXCR4 chemokine signaling in bone marrow stromal cell niches*. Immunity, 2006. **25**(6): p. 977-88.
88. Zhang, Y., et al., *CXCR4/CXCL12 axis counteracts hematopoietic stem cell exhaustion through selective protection against oxidative stress*. Sci Rep, 2016. **6**: p. 37827.
89. Tzeng, Y.S., et al., *Loss of Cxcl12/Sdf-1 in adult mice decreases the quiescent state of hematopoietic stem/progenitor cells and alters the pattern of hematopoietic regeneration after myelosuppression*. Blood, 2011. **117**(2): p. 429-39.
90. Gomei, Y., et al., *Functional differences between two Tie2 ligands, angiopoietin-1 and -2, in regulation of adult bone marrow hematopoietic stem cells*. Exp Hematol, 2010. **38**(2): p. 82-9.
91. Arai, F., et al., *Tie2/Angiopoietin-1 Signaling Regulates Hematopoietic Stem Cell Quiescence in the Bone Marrow Niche*. Cell, 2004. **118**(2): p. 149-161.
92. Kumano, K., et al., *Notch1 but Not Notch2 Is Essential for Generating Hematopoietic Stem Cells from Endothelial Cells*. Immunity, 2003. **18**(5): p. 699-711.
93. Lampreia, F.P., J.G. Carmelo, and F. Anjos-Afonso, *Notch Signaling in the Regulation of Hematopoietic Stem Cell*. Current stem cell reports, 2017. **3**(3): p. 202-209.
94. Duncan, A.W., et al., *Integration of Notch and Wnt signaling in hematopoietic stem cell maintenance*. Nat Immunol, 2005. **6**(3): p. 314-22.
95. Baumann, K., *Stem cells: Keeping alert*. Nature Reviews Molecular Cell Biology, 2014. **15**(7): p. 428-429.
96. Bigarella, C.L., R. Liang, and S. Ghaffari, *Stem cells and the impact of ROS signaling*. Development, 2014. **141**(22): p. 4206-4218.
97. Mohrin, M., et al., *Hematopoietic stem cell quiescence promotes error-prone DNA repair and mutagenesis*. Cell Stem Cell, 2010. **7**(2): p. 174-85.
98. Rodgers, J.T., et al., *mTORC1 controls the adaptive transition of quiescent stem cells from G0 to GAlert*. Nature, 2014. **510**(7505): p. 393-396.
99. Wilson, A., et al., *c-Myc controls the balance between hematopoietic stem cell self-renewal and differentiation*. Genes & development, 2004. **18**(22): p. 2747-2763.
100. Akuffo, A.A., et al., *Ligand-mediated protein degradation reveals functional conservation among sequence variants of the CUL4-type E3 ligase substrate receptor cereblon*. J Biol Chem, 2018. **293**(16): p. 6187-6200.
101. Bjorklund, C.C., et al., *Rate of CRL4(CRBN) substrate Ikaros and Aiolos degradation underlies differential activity of lenalidomide and pomalidomide in multiple myeloma cells by regulation of c-Myc and IRF4*. Blood Cancer J, 2015. **5**: p. e354.
102. Robak, T., J.Z. Blonski, and P. Robak, *Antibody therapy alone and in combination with targeted drugs in chronic lymphocytic leukemia*. Semin Oncol, 2016. **43**(2): p. 280-90.
103. Arora, M., S. Gowda, and J. Tuscano, *A comprehensive review of lenalidomide in B-cell non-Hodgkin lymphoma*. Ther Adv Hematol, 2016. **7**(4): p. 209-21.

104. Gopalakrishnan, R., et al., *Immunomodulatory drugs target IKZF1-IRF4-MYC axis in primary effusion lymphoma in a cereblon-dependent manner and display synergistic cytotoxicity with BRD4 inhibitors*. *Oncogene*, 2016. **35**(14): p. 1797-810.
105. Fionda, C., et al., *The IMiDs targets IKZF-1/3 and IRF4 as novel negative regulators of NK cell-activating ligands expression in multiple myeloma*. *Oncotarget*, 2015. **6**(27): p. 23609-30.
106. Fang, J., et al., *A calcium- and calpain-dependent pathway determines the response to lenalidomide in myelodysplastic syndromes*. *Nat Med*, 2016. **22**(7): p. 727-34.
107. Hagner, P.R., et al., *CC-122, a pleiotropic pathway modifier, mimics an interferon response and has antitumor activity in DLBCL*. *Blood*, 2015. **126**(6): p. 779-89.
108. Gandhi, A.K., et al., *Immunomodulatory agents lenalidomide and pomalidomide co-stimulate T cells by inducing degradation of T cell repressors Ikaros and Aiolos via modulation of the E3 ubiquitin ligase complex CRL4(CRBN.)*. *Br J Haematol*, 2014. **164**(6): p. 811-21.
109. Chesi, M., et al., *Drug response in a genetically engineered mouse model of multiple myeloma is predictive of clinical efficacy*. *Blood*, 2012. **120**(2): p. 376-85.
110. Fratta, I.D., E.B. Sigg, and K. Maiorana, *Teratogenic Effects of Thalidomide in Rabbits, Rats, Hamsters, and Mice*. *Toxicol Appl Pharmacol*, 1965. **7**: p. 268-86.
111. Sakamoto, K.M., *Protacs for treatment of cancer*. *Pediatr Res*, 2010. **67**(5): p. 505-8.
112. Chamberlain, P.P., et al., *Structure of the human Cereblon-DDB1-lenalidomide complex reveals basis for responsiveness to thalidomide analogs*. *Nat Struct Mol Biol*, 2014. **21**(9): p. 803-9.
113. Sherman, W., H.S. Beard, and R. Farid, *Use of an induced fit receptor structure in virtual screening*. *Chem Biol Drug Des*, 2006. **67**(1): p. 83-4.
114. Sabel, C.E., J.M. Neureuther, and S. Siemann, *A spectrophotometric method for the determination of zinc, copper, and cobalt ions in metalloproteins using Zincon*. *Anal Biochem*, 2010. **397**(2): p. 218-26.
115. Lindner, S. and J. Kronke, *The molecular mechanism of thalidomide analogs in hematologic malignancies*. *J Mol Med (Berl)*, 2016.
116. Lopez-Girona, A., et al., *Cereblon is a direct protein target for immunomodulatory and antiproliferative activities of lenalidomide and pomalidomide*. *Leukemia*, 2012. **26**(11): p. 2326-35.
117. Otahal, P., et al., *Lenalidomide enhances antitumor functions of chimeric antigen receptor modified T cells*. *Oncoimmunology*, 2016. **5**(4): p. e1115940.
118. McDaniel, J.M., et al., *Reversal of T-cell tolerance in myelodysplastic syndrome through lenalidomide immune modulation*. *Leukemia*, 2012. **26**(6): p. 1425-9.
119. Wang, R., et al., *The transcription factor Myc controls metabolic reprogramming upon T lymphocyte activation*. *Immunity*, 2011. **35**(6): p. 871-82.
120. Sun, Y., et al., *BET bromodomain inhibition suppresses graft-versus-host disease after allogeneic bone marrow transplantation in mice*. *Blood*, 2015. **125**(17): p. 2724-8.

121. Mailloux, A.W., et al., *Expansion of effector memory regulatory T cells represents a novel prognostic factor in lower risk myelodysplastic syndrome*. J Immunol, 2012. **189**(6): p. 3198-208.
122. Rajadhyaksha, A.M., et al., *Behavioral characterization of cereblon forebrain-specific conditional null mice: a model for human non-syndromic intellectual disability*. Behav Brain Res, 2012. **226**(2): p. 428-34.
123. Min, Y., et al., *Cereblon negatively regulates TLR4 signaling through the attenuation of ubiquitination of TRAF6*. Cell Death Dis, 2016. **7**(7): p. e2313.
124. Hartmann, M.D., et al., *Thalidomide mimics uridine binding to an aromatic cage in cereblon*. J Struct Biol, 2014. **188**(3): p. 225-32.
125. Saenz, D.T., et al., *Novel BET protein proteolysis targeting chimera (BET-PROTAC) exerts superior lethal activity than bromodomain inhibitor (BETi) against post-myeloproliferative neoplasm (MPN) secondary (s) AML cells*. Leukemia, 2017.
126. Zhou, B., et al., *Discovery of a Small-Molecule Degradator of Bromodomain and Extra-Terminal (BET) Proteins with Picomolar Cellular Potencies and Capable of Achieving Tumor Regression*. J Med Chem, 2017.
127. Schneekloth, J.S., Jr., et al., *Chemical genetic control of protein levels: selective in vivo targeted degradation*. J Am Chem Soc, 2004. **126**(12): p. 3748-54.
128. Bargagna-Mohan, P., et al., *Use of PROTACS as molecular probes of angiogenesis*. Bioorganic & Medicinal Chemistry Letters, 2005. **15**(11): p. 2724-2727.
129. Wang, X., et al., *New strategy for renal fibrosis: Targeting Smad3 proteins for ubiquitination and degradation*. Biochem Pharmacol, 2016. **116**: p. 200-9.
130. Zengerle, M., K.H. Chan, and A. Ciulli, *Selective Small Molecule Induced Degradation of the BET Bromodomain Protein BRD4*. ACS Chem Biol, 2015. **10**(8): p. 1770-7.
131. Lebraud, H., et al., *Protein Degradation by In-Cell Self-Assembly of Proteolysis Targeting Chimeras*. ACS Cent Sci, 2016. **2**(12): p. 927-934.
132. Raina, K., et al., *PROTAC-induced BET protein degradation as a therapy for castration-resistant prostate cancer*. Proc Natl Acad Sci U S A, 2016. **113**(26): p. 7124-9.
133. Jo, S., et al., *Identification and functional characterization of cereblon as a binding protein for large-conductance calcium-activated potassium channel in rat brain*. J Neurochem, 2005. **94**(5): p. 1212-24.
134. Kang, J.A., et al., *Epigenetic regulation of Kcna3-encoding Kv1.3 potassium channel by cereblon contributes to regulation of CD4(+) T-cell activation*. Proc Natl Acad Sci U S A, 2016. **113**(31): p. 8771-6.
135. Eichner, R., et al., *Immunomodulatory drugs disrupt the cereblon-CD147-MCT1 axis to exert antitumor activity and teratogenicity*. Nature Medicine, 2016. **22**: p. 735.
136. Martin, M.P., et al., *A novel approach to the discovery of small-molecule ligands of CDK2*. Chembiochem, 2012. **13**(14): p. 2128-36.
137. Bernstein, F.C., et al., *The Protein Data Bank. A computer-based archival file for macromolecular structures*. Eur J Biochem, 1977. **80**(2): p. 319-24.

138. Berman, H.M., et al., *The Protein Data Bank*. Nucleic Acids Res, 2000. **28**(1): p. 235-42.
139. Sastry, G.M., et al., *Protein and ligand preparation: parameters, protocols, and influence on virtual screening enrichments*. J Comput Aided Mol Des, 2013. **27**(3): p. 221-34.
140. Yamada, T., C.S. Park, and H.D. Lacorazza, *Genetic control of quiescence in hematopoietic stem cells*. Cell cycle (Georgetown, Tex.), 2013. **12**(15): p. 2376-2383.
141. Ximeri, M., et al., *Effect of lenalidomide therapy on hematopoiesis of patients with myelodysplastic syndrome associated with chromosome 5q deletion*. Haematologica, 2010. **95**(3): p. 406-14.
142. Lee, K.M., et al., *Disruption of the cereblon gene enhances hepatic AMPK activity and prevents high-fat diet-induced obesity and insulin resistance in mice*. Diabetes, 2013. **62**(6): p. 1855-1864.
143. Sudo, K., et al., *Age-associated characteristics of murine hematopoietic stem cells*. J Exp Med, 2000. **192**(9): p. 1273-80.
144. de Haan, G., W. Nijhof, and G. Van Zant, *Mouse strain-dependent changes in frequency and proliferation of hematopoietic stem cells during aging: correlation between lifespan and cycling activity*. Blood, 1997. **89**(5): p. 1543-50.
145. Hamilton, M.L., et al., *Does oxidative damage to DNA increase with age?* Proc Natl Acad Sci U S A, 2001. **98**(18): p. 10469-74.
146. Porto, M.L., et al., *Reactive oxygen species contribute to dysfunction of bone marrow hematopoietic stem cells in aged C57BL/6 J mice*. Journal of biomedical science, 2015. **22**: p. 97-97.
147. Han, T., et al., *Identification of novel genes and networks governing hematopoietic stem cell development*. EMBO reports, 2016. **17**(12): p. 1814-1828.
148. Ma, Q., et al., *Impaired B-lymphopoiesis, myelopoiesis, and derailed cerebellar neuron migration in CXCR4- and SDF-1-deficient mice*. Proceedings of the National Academy of Sciences of the United States of America, 1998. **95**(16): p. 9448-9453.
149. Ulyanova, T., et al., *VCAM-1 expression in adult hematopoietic and nonhematopoietic cells is controlled by tissue-inductive signals and reflects their developmental origin*. Blood, 2005. **106**(1): p. 86-94.
150. Geitz, H., S. Handt, and K. Zwingenberger, *Thalidomide selectively modulates the density of cell surface molecules involved in the adhesion cascade*. Immunopharmacology, 1996. **31**(2): p. 213-221.
151. Suda, T., K. Takubo, and Gregg L. Semenza, *Metabolic Regulation of Hematopoietic Stem Cells in the Hypoxic Niche*. Cell Stem Cell, 2011. **9**(4): p. 298-310.
152. Cabezas-Wallscheid, N., et al., *Transition out of HSC Dormancy By a Continuous Upregulation of Metabolism Is Controlled Via Dietary Vitamin A/ Retinoic Acid Signaling*. Blood, 2016. **128**(22): p. LBA-4-LBA-4.
153. Ito, K., M. Bonora, and K. Ito, *Metabolism as master of hematopoietic stem cell fate*. International Journal of Hematology, 2019. **109**(1): p. 18-27.



154. Shyh-Chang, N. and H.H. Ng, *The metabolic programming of stem cells*. Genes Dev, 2017. **31**(4): p. 336-346.
155. Khristi, V., et al., *Disruption of ESR1 alters the expression of genes regulating hepatic lipid and carbohydrate metabolism in male rats*. Mol Cell Endocrinol, 2019. **490**: p. 47-56.
156. Lacroix, M., et al., *Metabolic functions of the tumor suppressor p53: Implications in normal physiology, metabolic disorders, and cancer*. Molecular Metabolism, 2019.
157. Maekawa, T., W. Jin, and S. Ishii, *The role of ATF-2 family transcription factors in adipocyte differentiation: antiobesity effects of p38 inhibitors*. Mol Cell Biol, 2010. **30**(3): p. 613-25.
158. Manente, A.G., et al., *Estrogen receptor  $\beta$  activation impairs mitochondrial oxidative metabolism and affects malignant mesothelioma cell growth in vitro and in vivo*. Oncogenesis, 2013. **2**(9): p. e72-e72.
159. Mihaylova, M.M. and R.J. Shaw, *Metabolic reprogramming by class I and II histone deacetylases*. Trends in endocrinology and metabolism: TEM, 2013. **24**(1): p. 48-57.
160. Pang, B., et al., *EZH2 promotes metabolic reprogramming in glioblastomas through epigenetic repression of EAF2-HIF1 $\alpha$  signaling*. Oncotarget, 2016. **7**(29): p. 45134-45143.
161. Seong, H.-A., R. Manoharan, and H. Ha, *Smad proteins differentially regulate obesity-induced glucose and lipid abnormalities and inflammation via class-specific control of AMPK-related kinase MPK38/MELK activity*. Cell Death & Disease, 2018. **9**(5): p. 471.
162. Trumpp, A., M. Essers, and A. Wilson, *Awakening dormant haematopoietic stem cells*. Nat Rev Immunol, 2010. **10**(3): p. 201-9.
163. Norkin, M. and J.R. Wingard, *Recent advances in hematopoietic stem cell transplantation*. F1000Res, 2017. **6**: p. 870.
164. Valent, P. and H.-P. Horny, *Minimal diagnostic criteria for myelodysplastic syndromes and separation from ICUS and IDUS: update and open questions*. European Journal of Clinical Investigation, 2009. **39**(7): p. 548-553.
165. Kotla, V., et al., *Mechanism of action of lenalidomide in hematological malignancies*. Journal of Hematology & Oncology, 2009. **2**(1): p. 36.
166. Talati, C., D. Sallman, and A. List, *Lenalidomide: Myelodysplastic syndromes with del(5q) and beyond*. Seminars in Hematology, 2017. **54**(3): p. 159-166.
167. Schneider, R.K., et al., *Role of casein kinase 1A1 in the biology and targeted therapy of del(5q) MDS*. Cancer cell, 2014. **26**(4): p. 509-520.
168. Cho, I.J., et al., *Mechanisms, Hallmarks, and Implications of Stem Cell Quiescence*. Stem cell reports, 2019. **12**(6): p. 1190-1200.
169. Filippi, M.-D. and S. Ghaffari, *Mitochondria in the maintenance of hematopoietic stem cells: new perspectives and opportunities*. Blood, 2019. **133**(18): p. 1943-1952.
170. Ito, K. and T. Suda, *Metabolic requirements for the maintenance of self-renewing stem cells*. Nat Rev Mol Cell Biol, 2014. **15**(4): p. 243-56.

171. Jang, Y.Y. and S.J. Sharkis, *A low level of reactive oxygen species selects for primitive hematopoietic stem cells that may reside in the low-oxygenic niche.* Blood, 2007. **110**(8): p. 3056-63.
172. Ludin, A., et al., *Reactive oxygen species regulate hematopoietic stem cell self-renewal, migration and development, as well as their bone marrow microenvironment.* Antioxidants & redox signaling, 2014. **21**(11): p. 1605-1619.
173. Ryu, J.M., et al., *Regulation of Stem Cell Fate by ROS-mediated Alteration of Metabolism.* International journal of stem cells, 2015. **8**(1): p. 24-35.
174. Simsek, T., et al., *The distinct metabolic profile of hematopoietic stem cells reflects their location in a hypoxic niche.* Cell Stem Cell, 2010. **7**(3): p. 380-90.
175. Cheung, T.H. and T.A. Rando, *Molecular regulation of stem cell quiescence.* Nature reviews. Molecular cell biology, 2013. **14**(6): p. 329-340.
176. Lee, G., et al., *Fully reduced HMGB1 accelerates the regeneration of multiple tissues by transitioning stem cells to GAlert.* Proc Natl Acad Sci U S A, 2018. **115**(19): p. E4463-e4472.
177. Florian, M.C., et al., *Aging alters the epigenetic asymmetry of HSC division.* PLOS Biology, 2018. **16**(9): p. e2003389.
178. Zimdahl, B., et al., *Lis1 regulates asymmetric division in hematopoietic stem cells and in leukemia.* Nature genetics, 2014. **46**(3): p. 245-252.
179. He, N., et al., *Bone marrow vascular niche: home for hematopoietic stem cells.* Bone Marrow Res, 2014. **2014**: p. 128436.
180. Kumar, S. and H. Geiger, *HSC Niche Biology and HSC Expansion Ex Vivo.* Trends Mol Med, 2017. **23**(9): p. 799-819.
181. Levesque, J.-P. and I.G. Winkler, *Cell Adhesion Molecules in Normal and Malignant Hematopoiesis: from Bench to Bedside.* Current Stem Cell Reports, 2016. **2**(4): p. 356-367.
182. Liu, Y.F., et al., *ICAM-1 Deficiency in the Bone Marrow Niche Impairs Quiescence and Repopulation of Hematopoietic Stem Cells.* Stem Cell Reports, 2018. **11**(1): p. 258-273.
183. Orkin, S.H. and L.I. Zon, *Hematopoiesis: an evolving paradigm for stem cell biology.* Cell, 2008. **132**(4): p. 631-44.
184. Cabezas-Wallscheid, N., et al., *Vitamin A-Retinoic Acid Signaling Regulates Hematopoietic Stem Cell Dormancy.* Cell, 2017. **169**(5): p. 807-823 e19.
185. Park, D.S., et al., *Clonal hematopoiesis of indeterminate potential and its impact on patient trajectories after stem cell transplantation.* PLoS Comput Biol, 2019. **15**(4): p. e1006913.
186. Muench, D.E. and H.L. Grimes, *Transcriptional Control of Stem and Progenitor Potential.* Curr Stem Cell Rep, 2015. **1**(3): p. 139-150.
187. Muench, D.E., et al., *SKI controls MDS-associated chronic TGF- $\beta$  signaling, aberrant splicing, and stem cell fitness.* Blood, 2018. **132**(21): p. e24-e34.
188. Yue, L., et al., *HDAC11 deficiency disrupts oncogene-induced hematopoiesis in myeloproliferative neoplasms.* Blood, 2020. **135**(3): p. 191-207.
189. Kim, Y.-R. and K.-S. Eom, *Simultaneous Inhibition of CXCR4 and VLA-4 Exhibits Combinatorial Effect in Overcoming Stroma-Mediated Chemotherapy Resistance in Mantle Cell Lymphoma Cells.* Immune network, 2014. **14**(6): p. 296-306.

190. Yin, Y., et al., *Normalization of CD4<sup>+</sup> T cell metabolism reverses lupus*. Science Translational Medicine, 2015. **7**(274): p. 274ra18-274ra18.
191. Kindle, S.A., et al., *Lenalidomide treatment of cutaneous lupus erythematosus: the Mayo Clinic experience*. Int J Dermatol, 2016. **55**(8): p. e431-9.
192. Pelle, M.T. and V.P. Werth, *Thalidomide in cutaneous lupus erythematosus*. Am J Clin Dermatol, 2003. **4**(6): p. 379-87.
193. Chao, N.J., et al., *Paradoxical effect of thalidomide prophylaxis on chronic graft-vs.-host disease*. Biol Blood Marrow Transplant, 1996. **2**(2): p. 86-92.
194. Lenz, W., et al., *THALIDOMIDE AND CONGENITAL ABNORMALITIES*. The Lancet, 1962. **279**(7219): p. 45-46.
195. McBride, W.G., *THALIDOMIDE AND CONGENITAL ABNORMALITIES*. The Lancet, 1961. **278**(7216): p. 1358.
196. Sampaio, E.P., et al., *The influence of thalidomide on the clinical and immunologic manifestation of erythema nodosum leprosum*. J Infect Dis, 1993. **168**(2): p. 408-14.
197. Barnes, P.J. and M. Karin, *Nuclear factor-kappaB: a pivotal transcription factor in chronic inflammatory diseases*. N Engl J Med, 1997. **336**(15): p. 1066-71.
198. Bauditz, J., S. Wedel, and H. Lochs, *Thalidomide reduces tumour necrosis factor alpha and interleukin 12 production in patients with chronic active Crohn's disease*. Gut, 2002. **50**(2): p. 196-200.
199. Nakamura-Ishizu, A., H. Takizawa, and T. Suda, *The analysis, roles and regulation of quiescence in hematopoietic stem cells*. Development, 2014. **141**(24): p. 4656-66.
200. Riddell, J., et al., *Reprogramming committed murine blood cells to induced hematopoietic stem cells with defined factors*. Cell, 2014. **157**(3): p. 549-64.
201. Daley, G.Q., *Deriving blood stem cells from pluripotent stem cells for research and therapy*. Best Pract Res Clin Haematol, 2014. **27**(3-4): p. 293-7.
202. Xie, J. and C. Zhang, *Ex vivo expansion of hematopoietic stem cells*. Science China Life Sciences, 2015. **58**(9): p. 839-853.

**APPENDIX A**  
**INSTITUTION REVIEW BOARD**



RESEARCH INTEGRITY AND COMPLIANCE  
Institutional Review Boards, FWA No. 00001669  
12901 Bruce B. Downs Blvd., MDC035 • Tampa, FL 33612-4799  
(813) 974-5638 • FAX (813) 974-7091

3/12/2014

Dana Rollison, Ph.D.  
H Lee Moffitt Cancer Center  
12902 Magnolia Drive  
Tampa, FL 33612

RE: **Expedited Approval for Initial Review**  
IRB#: Pro00016372  
Title: Prospective Study of Cutaneous Viral Infections and Non-Melanoma Skin Cancer -  
MCC# 17755

**Study Approval Period: 3/10/2014 to 3/10/2015**

Dear Dr. Rollison:

On 3/10/2014, the Institutional Review Board (IRB) reviewed and **APPROVED** the above application and all documents outlined below.

**Approved Item(s):**  
**Protocol Document(s):**  
[Protocol \(version 1, 01/31/2014\)](#)

**Consent/Assent Document(s)\*:**  
[Informed Consent \(version 1, 02/26/2014\) - clean.pdf](#)

\*Please use only the official IRB stamped informed consent/assent document(s) found under the "Attachments" tab. Please note, these consent/assent document(s) are only valid during the approval period indicated at the top of the form(s).

It was the determination of the IRB that your study qualified for expedited review which includes activities that (1) present no more than minimal risk to human subjects, and (2) involve only procedures listed in one or more of the categories outlined below. The IRB may review research through the expedited review procedure authorized by 45CFR46.110 and 21 CFR 56.110. The research proposed in this study is categorized under the following expedited review category:

(2) Collection of blood samples by finger stick, heel stick, ear stick, or venipuncture as follows:  
(a) from healthy, nonpregnant adults who weigh at least 110 pounds. For these subjects, the amounts drawn may not exceed 550 ml in an 8 week period and collection may not occur more frequently than 2 times per week; or (b) from other adults and children, considering the age, weight, and health of the subjects, the collection procedure, the amount of blood to be collected, and the frequency with which it will be collected. For these subjects, the amount drawn may not exceed the lesser of 50 ml or 3 ml per kg in an 8 week period and collection may not occur more frequently than 2 times per week.

(3) Prospective collection of biological specimens for research purposes by noninvasive means.

(7) Research on individual or group characteristics or behavior (including, but not limited to, research on perception, cognition, motivation, identity, language, communication, cultural beliefs or practices, and social behavior) or research employing survey, interview, oral history, focus group, program evaluation, human factors evaluation, or quality assurance methodologies.

As the principal investigator of this study, it is your responsibility to conduct this study in accordance with IRB policies and procedures and as approved by the IRB. Any changes to the approved research must be submitted to the IRB for review and approval by an amendment.

We appreciate your dedication to the ethical conduct of human subject research at the University of South Florida and your continued commitment to human research protections. If you have any questions regarding this matter, please call 813-974-5638.

Sincerely,



E. Verena Jorgensen, M.D., Chairperson  
USF Institutional Review Board


## APPENDIX B

### INSTITUTIONAL ANIMAL CARE & USE COMMITTEE APPROVAL



#### MEMORANDUM

TO: Gary Reuther,

FROM:   
Farah Moulvi, MSPH, IACUC Coordinator  
Institutional Animal Care & Use Committee  
Research Integrity & Compliance

DATE: 1/28/2020

PROJECT TITLE: Blockade in mesenchymal stromal self-renewal as a novel mediator of the profibrotic marrow phenotype  
Preclinical development of HDAC inhibitor therapy for myelofibrosis  
In vivo testing of TGF-Beta inhibitors in mouse models of myelofibrosis  
Identifying novel therapies for MPNs  
HDAC11 a novel therapeutic target for myeloproliferative neoplasms (MPN) through metabolic alterations  
Immune modulation through cereblon suppression  
Overcoming the inefficacy of ruxolitinib in myeloproliferative neoplasm patients by targeting the SHP2 tyrosine phosphatase

FUNDING SOURCE: Non-Profit (Private Foundations, H. Lee Moffitt Cancer Center, etc.), For Profit (Industry Sponsored) or Other

Miles for Moffitt grant (Moffitt Cancer Center), Incyte Corporation, Celgene Corporation

IACUC PROTOCOL #: R IS00006028

PROTOCOL STATUS: **Amendment APPROVED**

The Institutional Animal Care and Use Committee (IACUC) received your Modification concerning the above referenced IACUC protocol.

On 1/28/2020 the IACUC reviewed and approved your Modification for the following:

**Modification: Amendment Request for IACUC Study 2.1.1**

**Added: New or Additional Protocol Title**

**Modification: Amendment - Update Title 2.2.1**


**Overcoming the inefficacy of ruxolitinib in myeloproliferative neoplasm patients by targeting the SHP2 tyrosine phosphatase**



RESEARCH INTEGRITY & COMPLIANCE  
INSTITUTIONAL ANIMAL CARE & USE COMMITTEE

MEMORANDUM

TO: Pearlie Epling-Burnette, PharmD, PhD

FROM:   
Farah Moulvi, MSPH, IACUC Coordinator  
Institutional Animal Care & Use Committee  
Research Integrity & Compliance

DATE: 1/21/2020

PROJECT TITLE: Immunological modulation through cereblon suppression-Breeding Protocol  
Preclinical development of HDAC6 inhibitor therapy for myelofibrosis  
Cereblon suppression offers novel approach for anti-tumor immunity

FUNDING SOURCE: Non-Profit (Private Foundations, H. Lee Moffitt Cancer Center, etc.), For  
Profit (Industry Sponsored) or Other  
Celgene Corporation

IACUC PROTOCOL #: M IS00004986

PROTOCOL STATUS: **Procedural Change APPROVED**

The Institutional Animal Care and Use Committee (IACUC) received your Modification concerning the above referenced IACUC protocol.

On **1/21/2020** the IACUC reviewed and approved your Modification for the following:

Modifications: Study Identification 1.1.3 (Principal Investigator)

Gary Reuther

Old Value: Pearlie Epling-Burnette

Modifications: Study Identification 1.1.6 (List Secondary Study Contact)

Added: Aya Elmarsafawi

Added: Rebecca Hesterberg

Removed: Shiun Chang

**changing the primary PI from Dr. Burnette to Dr. Gary Reuther**

INSTITUTIONAL ANIMAL CARE AND USE COMMITTEE  
PHS No. A4100-01, AAALAC No. 000434, USDA No. 58-R-0015



## APPENDIX C

### COPYRIGHT PERMISSION OF PREVIOUSLY PUBLISHED MATERIALS

**Journal of biological chemistry**  
 Publication type: e-Journal

ISSN: 1083-351X  
 Publication Year: 1905 - Present  
 Publisher: AMERICAN SOCIETY FOR BIOCHEMISTRY AND MOLECULAR BI

Language: English  
 Country: United States of America  
 URL: <http://www.jbc.org/>

[View all details](#)

Request Details Additional Details

Journal of Biological Chemistry permissions policies: • If you are an author of the content for which you are seeking permission, or if you are not an author but are requesting permission to copy, distribute, transmit and adapt the work for noncommercial purposes (e.g. reproduction of a figure for educational purposes such as schoolwork, or appending a reprinted article to a PhD dissertation), you do not need to seek permission using the options listed below, as long as any reuse includes the credit line in the reuse policies listed above. • Parties who are not authors on the article who wish to reuse content for commercial purposes such as reproducing a figure in a book, journal, or coursepack published by a commercial publisher, do need permission and should request permission by completing the form below. For more information please see Journal of Biological Chemistry: <http://www.jbc.org/site/misc/edpolicy.xhtml#copyright>

Type of Use (TOU)  [+ Create Project](#)

3/3/2020

RightsLink - Your Account



RightsLink®

[My Orders](#) [My Library](#) [My Profile](#)

Welcome a.a.akuffo@gmail.com [Log out](#) | [Help](#)

[My Orders](#) > [Orders](#) > [All Orders](#)

#### My Orders

[Orders](#) [Billing History](#) [Payable Invoices](#)

#### SEARCH

Order Number:

Date Range: From  To  [Go](#)

**View:**  All  On Hold  Response Required  Pending  Completed  Canceled  Denied  Credited

Results: 1-5 of 5

Order Date	Article Title	Publication	Type Of Use	Price	Order Status	Expiration Date	Order Number
3-Mar-2020	Haematopoietic stem cell activity and interactions with the niche	Nature Reviews Molecular Cell Biology	Thesis/Dissertation	0.00 \$	Completed		<a href="#">4781531283750</a>
3-Mar-2020	Awakening dormant haematopoietic stem cells	Nature Reviews Immunology	Thesis/Dissertation	0.00 \$	Completed		<a href="#">4781530776493</a>
3-Mar-2020	Hematopoietic stem cell niche maintenance during homeostasis and regeneration	Nature Medicine	Thesis/Dissertation	0.00 \$	Completed		<a href="#">4781530245259</a>
3-Mar-2020	Emergency granulopoiesis	Nature Reviews Immunology	Thesis/Dissertation	0.00 \$	Completed		<a href="#">4781521080373</a>
3-Mar-2020	xPharm: The Comprehensive Pharmacology Reference	Elsevier Books	reuse in a thesis/dissertation	0.00 \$	Completed		<a href="#">4781510878865</a>



## ABOUT THE AUTHOR

Afua Adutwumwa Akuffo was born and raised in Ghana. In kindergarten, Afua aspired to become a physician. In junior high, Afua attended a program at Stanford School of Medicine where she shadowed medical students and partook in a study on Lyme disease. Following this eye-opening experience, Afua became interested in scientific research as career objective.

When a friend unexpectedly passed from sudden cardiovascular disease, Afua began to study the heart. By her senior year of high school, Afua knew a lot about heartaches but not the typical heartaches many teenagers knew. In college, through studying the immune system, with its intricate networks, Afua found her calling; cancer research with a focus in immunotherapy.

Afua graduated from college with honors and transitioned to Washington University School of Medicine where she studied regenerative therapies in glioblastoma and narcolepsy and embarked on her journey to fight cancer at the bench and bedside.

With the goal of becoming a translational scientist, Afua's journey led her to Moffitt Cancer Center where she has facilitated and executed several collaborative projects in diverse disciplines that resulted in 6 publications, pharmaceutical and institutional research grants and a patent application.

Upon graduation Afua is transitioning onto the path to becoming a Medical Science Liaison: a role that will allow her to bridge her clinical and research interests.

END PAGE